INVESTIGATION OF DYNAMIC BEHAVIOR OF POWER SYSTEM INSTALLED WITH STATCOM

BY

MUHAMMAD FAREED KANDLAWALA

A Thesis Presented to the
DEANSHIP OF GRADUATE STUDIES

KING FAHD UNIVERSITY OF PETROLEUM & MINERALS
DHAHRAN, SAUDI ARABIA

In Partial Fulfillment of the
Requirements for the Degree of

MASTER OF SCIENCE

In

ELECTRICAL ENGINEERING

December 2001

KING FAHD UNIVERSITY OF PETROLEUM AND MINERALS

DHAHRAN 31261, SAUDI ARABIA

DEANSHIP OF GRADUATE STUDIES

This thesis, written by

MUHAMMAD FAREED KANDLAWALA

under the direction of his Thesis Advisor and approved by his Thesis Committee, has been presented to and accepted by the Dean of Graduate Studies, in partial fulfillment of the requirements for the degree of

MASTER OF SCIENCE IN ELECTRICAL ENGINEERING

Thesis Committee

A. H. Rahim

Dr. ABUHAMED M. ABDURRAHIM (Chairman)

Dr. YOUSSEF ABDEL – MAGID (Member)

Dr. IBRAHIM O. HABIBALLAH (Member)

Dr. SAMIR A. AL – BAIYAT
(Department Chairman)

Dr. OSAMA AHMED JANNADI
(Dean of Graduate Studies)

13/1/2002

Date

Dedicated

to

My Beloved Grand Mother, Aba, Maa

and

Brothers, Sisters

Acknowledgements

In the name of Allah, Most Gracious, Most Merciful. Read! In the name of your Lord and Cherisher, Who has Created (all that exists). He has created man from a clot (a piece of thick coagulated blood). Read! And your Lord is the Most Generous. Who has taught (the writing) by the pen. Taught man that which he knew not. Nay! Verily, man does transgress (in disbelief and evil deed). Because he considers himself self-sufficient. Surely, unto your Lord is the return.

(Surah 96. Al-'Alaq. The Holy Quran)

All praise be to Allah the Lord of the worlds, for having guided me at every stage of my life. I seek His mercy, favor and forgiveness. I feel privileged to glorify His name in the sincerest way through this small accomplishment.

I would like to pay a high tribute to my thesis advisor Dr. Abuhamed Abdur-Rahim for his invaluable guidance and helpful ideas throughout this thesis work. His appreciation and words of encouragement gave a new life to my efforts in hard times. I am also indebted to him for his valuable time, efforts and his continuous support and inspiration. I am also grateful for the aid he provided me in the programming. At the later stages, he helped me a lot in writing my thesis.

I would also like to express my deep appreciation to my committee members, Dr. Youssef L. Abdel Magid and Dr. Ibrahim Omar Habiballah, for their constant help and encouragement.

I am thankful to Dr. Sameer A. Al-Baiyat, Chairman Electrical Engineering Department for establishing an excellent graduate research laboratory in our department.

I am thankful to King Fahd University of Petroleum & Minerals for supporting my M.S. studies and this research work.

I am thankful to my friend Wasif naeem for his helpful suggestions. I am also thankful to my friends Abdul Shakoor, Muhammed Kamil, Muhammed saleem, Ajmal, Ahmar, Salman Khan, Khateeb-ur-Rehman, Shafayat, Faisal Ali Shah, Faisal Abdul Razzak, Abdul Hameed, Tariq waheed qureshi and Zahid Qamar for their support and guidance. Thanks are also due to my friends Saad, Moin, Munir, Hassan Riyaz, Anas Waqar, Khurram Razzak, Mir Asif, Arshad, Muffazal, Kashif, Mehmood, Moin, Atif, Rafay, Rais, Junaid, Saif, Hamid, Zeeshan Jeelani and Asif. Thanks are also due to all those who cared for me during the days when i was on bed rest because of leg fracture.

Last, but not least, thanks are due to my parents, family members and my fiancee for their emotional and moral support, patience, encouragement and prayers.

Contents

List of Tables

List of Figures

Nomenclature

English Symbols

X	Transmission line reactance
H	Inertia constant
M	Inertia coefficient, $M = 2H$
D	Damping coefficient
K_p, K_d, K_i	Gains of PID controller
p.u.	Per unit quantities
pf	Power factor
P_e	Electrical power output from the machine
eq	Internal voltage across x_q
V_t	Machine terminal voltage
P_m	Mechanical power output to the machine

Greek Symbols

ψ	Phase angle of the mid-bus voltage
e'_q	Internal voltage on q-axis proportional to field flux linkage
E_{fd}	Generator field voltage
δ	Angle between q-axis and the infinite busbar
T'_{do}	Open-circuit field time constant
K'_A	Exciter gain
T'_A	Exciter time constant
x_q	Quadrature axis reactance
x_d	Direct axis reactance
x'_d	Direct axis transient reactance
w_o	Radian frequency
i_d, i_q	Armature current, direct and quadrature axis component
v_d, v_q	Armature voltage, direct and quadrature axis component
V_b	Infinite busbar voltage
V_m	STATCOM bus voltage or mid-bus voltage
$\dot{g}$	Derivative of g

Abbreviations

AC	Alternating current
DC	Direct current

FACTS	Flexible AC transmission system
SVC	Static Var compenstor
TCSC	Thyristor controlled series capacitor
TCPAR	Thyristor controlled phase angle regulator
STATCOM	Static synchronous compensator
STATCON	Static condensor
SSSC	Static synchronous series compensator
UPFC	Unified power flow controller
PID	Proportional-integral-derivative
PWM	Pulse width modulation
PSS	Power system stabilizer
GTO	Gate turn-off thyristor
IGBT	Insulated Gate bipolar transistor
MTO	Metal-oxide semiconductor turn-off thyristor
IGCT	Insulated Gate commutated thyristor
VSC	Voltage-sourced converter
SMIB	Single-machine infinite-bus

THESIS ABSTRACT

Name: Muhammad Fareed Kandlawala

Title: Investigation of Dynamic Behavior of Power System Installed With STATCOM

Degree: Master of science

Major Field: Electrical Engineering

Date of Degree: December 2001

A Static synchronous compensator(STATCOM) is one of the new generation flexible AC transmission system (FACTS) devices with a promising feature of applications in power system. STATCOMs are used to stabilize the system by exchanging reactive power with the power system. In this thesis, dynamic behavior of the single machine infinite bus power system with STATCOM has been investigated. Both an approximate and a detailed mathematical model are used for damping control of a power system. The effect of PID controllers in damping enhancement has been investigated.It was observed that proportional and derivative control is superior to other combinations of PID. The simultaneous control of electromehanical transient damping and STATCOM voltage variation was found to be difficult. A robust STATCOM controller design is presented. Method of multiplicative uncertainty has been employed to model the variations of the operating points in the system. The design is carried out applying robustness criteria for stability and performance. A loop-shaping technique has been employed to select a suitable open-loop transfer function, from which the robust controller is constructed. The proposed controller has been tested through a number of disturbances including three-phase faults. The robust controller designed has been demonstrated to provide extremely good damping characteristics over a good range of operating conditions.

Keywords: Power System, FACTS, STATCOM, Loop-shaping method, H_∞ Control, PID Controller, Robust Controller

Master of Science Degree

King Fahd University of Petroleum & Minerals, Dhahran.
December 2001

خلاصة الرسالة

الإسم:	محمد فريد كاند لاوالا
العنوان:	بحث السلوك النشيط لنظام طاقة رُكِب مع Statcom
الدرجة:	الماجستير في العلوم
التخصص الرئيسي:	الهندسة الكهربائية
تاريخ التخرج:	كانون أول "ديسمبر" ٢٠٠١

يعد المعادل المتزامن الثابت STATCOM أحد أنظمة الجيل الجديد في إرسال التيار المتردد (FACT) والتي تبشر بتطبيقات متعددة. تستخدم STATCOMs في تثبيت النظام عن طريق تبادل الطاقة الترجعية مع نظام الطاقة. في هذه الرسالة تم بحث السلوك النشيط لنظام طاقة لماكينة أحاديه ذات ناقل لا متناهي. تم إستخدام نموذج رياضي مفصل وآخر تقريبي للتحكم بالمضائله لنظام الطاقة. تم بحث أثر مضبطات PID في تحسين المضائلة. لوحظ أن التحكم المقتبس والمتناسب كانت أفضل من باقي إتحادات PID الأخرى. وجد أن الضبط المتزامن لمضائلة كهروميكانيكيه عابره وتغيرات الفولتيه ل STATCOM هي عملية صعبة. تم تقديم تصميم لمضبط STATCOM ذو ثبات قوي. من أجل محاكاة التغيرات في نقاط التشغيل في النظام، تم إستخدام طريقة الشك المضاعف. نفذ التصميم بإستخدام معايير ثبات قوية للإستقرار والأداء. تم تطبيق تقنية تشكيل العقد لإنتقاء دالة النقل المناسبة و التي تم من خلالها بناء مضبط ذو ثبات عالي. تم عرض كيفية استخدام هذا المضبط ذو الثبات العالي لإعطاء ميزات مضائلة جيدة جداً على تشكيله واسعة من ظروف التشغيل.

الكلمات الرئيسية: نظام طاقة، FACTS ، STATCOM ، طرق تشكيل العقدة، ضبط H ∞ ، مضبطPID ، مضبط ذو ثبات قوي.

درجة الماجستير في العلوم

جامعة الملك فهد للبترول والمعادن

كانون اول "ديسمبر" ٢٠٠١

Chapter 1

Introduction

1.1 Introduction

An AC power system is a complex network of synchronous generators, transmission lines and loads. The transmission lines can be represented mostly as reactive networks composed of series inductors and shunt capacitors. The total series inductance, which is proportional to the length of the line, determines primarily the maximum transmissible power at a given voltage. The shunt capacitance influences the voltage profile and thereby the power transmission along the line.

The transmitted power over a given line is determined by the line impedance, the magnitude of, and phase angle between the end voltages, or in other words, the forcing voltage acting across the transmission line.

The basic operating requirements of an AC power system are that the synchronous generators must remain in synchronism and the voltages must be kept close to their rated values. The capability of a power system to meet these requirements in the face of possible disturbances such as line faults, generator and line outages and load switching etc. is characterized by its transient, dynamic and voltage stability. The stability requirements usually determine the maximum transmittable power at a stipulated system security level.

Since the 1970s, energy cost, environmental restrictions, right-of-way difficulties together with other legislative, social and cost problems have delayed the construction of both generations facilities, and in particular, new transmission lines. In this time period, there have also been profound changes in the industrial structure, often with significant geographic shifts of highly populated areas. In the last few years, there has been a worldwide movement of deregulation, which, in order to facilitate the development of competitive electric energy markets, stipulates "unbundling" the power generation from transmission and mandates open access to transmission services [1].

The economic, social, and legislative developments had fueled the review of traditional power transmission theory, and the creation of new concepts that allow full utilization of existing power generation and transmission facilities without compromising system availability and security.

In the late 1980s, the Electric Power Research Institute (EPRI) in the USA formulated the vision of the Flexible AC Transmission System (FACTS) in which various power electronics based controllers regulate power flow and transmission voltage and, through rapid control action, mitigate dynamic disturbances[1].

N.G.Hingorani [2, 3, 4, 5] proposed the concept of FACTS devices that involves the applications of high power electronic controllers in AC transmission networks that enable fast and reliable control of power flows and voltages.

FACTS technology is not a single high power controller but rather a collection of controllers that can be applied individually or collectively to control the interrelated parameters. The main objectives of FACTS are:

- Regulation of power flows in prescribed transmission routes.
- Secure loading of lines near their thermal limits.
- Prevention of cascading outages by contributing to emergency control.
- Damping of oscillations which can threaten security or limit the usable line capacity and improve system stability in general.

Table 1.1 shows that the FACTS controllers can be broadly classified into two classes:

- Shunt connected controllers providing voltage control
- Series connected controllers providing power flow control

The simplified expression for power flow in a lossless transmission line is given by,

$$P = \frac{V_S V_R \sin(\delta_{SR} + \phi)}{X} \tag{1.1}$$

Name	Type	Main Function	Controller Used	Comments
SVC	Shunt	Voltage Control	Thyristor	Variable Impedance Device
TCSC	Series	Power Flow Control	Thyristor	Variable Impedance Device
TCPAR	Series and Series	Power Flow Control	Thyrisotr	Phase Control
STATCOM	Shunt	Voltage Control	GTO	Variable Voltage Source
SSSC	Series	Power Flow Control	GTO	Variable Voltage Source
UPFC	Shunt and Series	Voltage and Power Flow Control	GTO	Variable Voltage Source

Table 1.1: FACTS Controllers

where V_S and V_R are sending and receiving end bus voltages, X is the series reactance of the line δ_{SR} is the phase difference in the bus angles, ϕ is the phase angle shift introduced by a phase angle regulator (phase shifting transformer).

It is obvious from Eq. (1.1) that the control of voltage, series reactance and phase angle (ϕ)have effect on the power flow. While the control over the voltage and series reactance can be used to increase the power limit. The control over ϕ can be used to regulate power flow in the loops.

1.2 Static synchronous compensator(STATCOM)

The new generations of FACTS controllers are based on voltage source converter, which use turn-off devices like GTOs. These controllers require lower ratings of passive elements (inductors and capacitors) and the voltage source characteristics present several advantages over conventional variable impedance controllers.

The general arrangement of an STATCOM device is shown in Fig. 1.1. The solid-state synchronous voltage source, implemented by a voltage source converter,

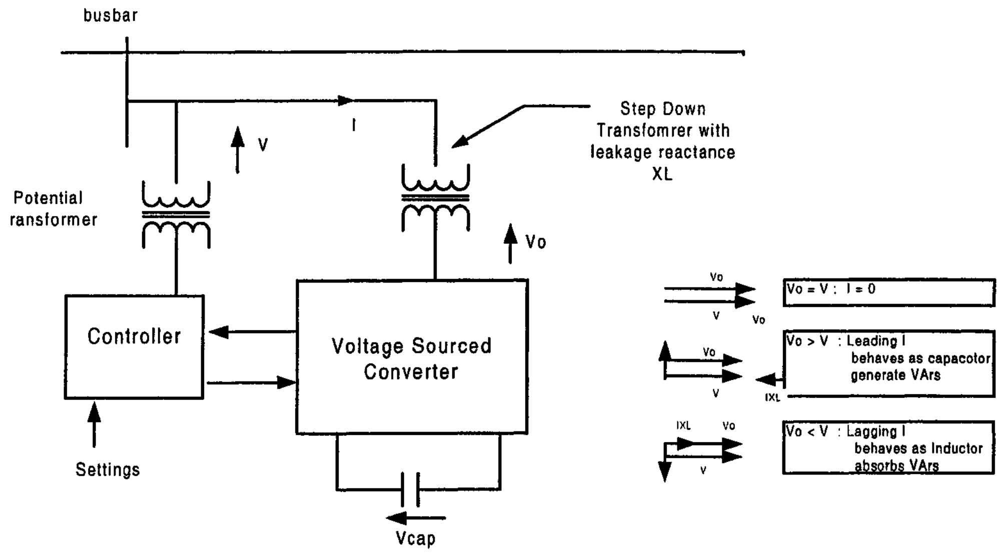

Figure 1.1: The general arrangement of STATCOM.

is operated as a shunt connected static VAR compensator (SVC). This arrangement of SVC exhibits operation and performance characteristics similar to that of an ideal rotating synchronous condenser and for this reason was called Static synchronous condenser (STATCON)[7]. Other names of the device are static synchronous compensator (STATCOM) and advanced static VAR compensator (ASVC). Recent literature uses the name STATCOM instead of STATCON.

The voltage sourced converter produces a set of three phase voltages that are in phase with the corresponding bus voltage. The reactive power is varied by varying the magnitude of the converter output voltages. A small phase difference exists in steady state, depending on reactive power output, so that real power can be drawn from the lines to compensate for the losses. The current on the DC side is mainly a ripple of magnitude much smaller than the AC line currents. As no real energy exchange, except to compensate for the losses, takes place in steady state, the DC voltage can be maintained by a capacitor. The major advantages of the STATCOM over the SVC are [6, 7]

- The STATCOM can supply required reactive current even at low values of bus voltage, whereas the reactive current capability of SVC at its susceptance limit decreases linearly with decrease in bus voltage. The STATCOM is therefore, superior to SVC in maintaining system voltage.

- With proper choice of device ratings and thermal design, STATCOM can have a short time overload capability. This is not possible in an SVC because there is an inherent susceptance limit support.

- Significant size reduction can be achieved because of reduced number of passive component and their small size.

- STATCOM can allow for real power modulation if it has energy storage at its DC terminals.

- The ability of STATCOM to produce full capacitive output current at low system voltage also make it highly effective in improving the transient (first swing) stability.

- The transient stability margin obtained with the STATCOM is significantly greater than that attainable with the SVC of identical rating. This means that the transmittable power can be increased if the shunt compensation is provided by the STATCOM rather than SVC, or in other words, for the same stability margin, the rating of STATCOM can be decreased below that of the SVC.

1.3 Literature Review

1.3.1 Basic concept

The technical concept of the voltage-sourced advanced static VAR generator (ASVG) employing gate turnoff (GTO) thyristors was given in an article published in 1988 [8].The article gives an overview of the electrical and mechanical configurations of $\pm$ 100 MVAR prototype ASVG and the details of the test performed on it.

In 1994, Laszlo Gyugyi gave the basic concept of STATCOM using voltage-sourced converter [6]. In his paper, he described the basic operation of STATCOM and the functional control scheme to control the STATCOM used for both reactive and real power compensation.

Analysis of 6 and 12 pulse STATCOM is given in [8]. A study of conditions leading to circuit resonance is carried out together with possible method of avoiding such problems. Study of multilevel topologies of STATCOM has been presented in [7, 9].

1.3.2 Modeling, analysis and control design

Schauder and Mehta [10] proposed a vector control scheme for control of reactive current using STATCOM. They described two controller structures for the STATCOM one of which involves both magnitude (using PWM strategy) and phase control of inverter, and the other structure uses only phase angle control. For the latter controller structure the system is not amenable to linear output feedback control in all operating regions. Authors proposed a nonlinear state feedback controller to overcome this problem.

Design of the voltage controller and the analysis of its dynamic behavior using eigenvalue analysis and its simulation are presented in [11]. The paper concentrates on the application of STATCOM for the reactive power compensation of a long transmission line by regulating the voltage at its mid point. It has been found that the plant transfer function is of the minimum phase type. Eigenvalue analysis using linearized model was carried out to design a compensator in cascade with an integral controller to overcome this problem.

A comparative study for dynamic operation of different models of STATCOM and their performance is given in [12].

Averaged modeling and nonlinear control of advanced static VAR compensator (ASVC) was given in [13]. The generalized averaged method has been used to get time invariant continues nonlinear model of the system. It was shown that for this system a PI controller with constant parameters is not robust enough because of the variation of the pole zero frequency with the operating point. A nonlinear controller based on linearization via feedback associated with a proportional controller has been chosen. The internal stability has been investigated and it is guaranteed on the whole STATCOM operating range.

Design of a nonlinear controller for STATCOM based on the differential algebra theory is presented in [14]. The controller designed by this method allows linearizing the compensator and controlling directly the capacitor voltage and output reactive power of the STATCOM. Such a control enables to stabilize the compensation system and thus helps to improve largely the transient performance of the global system.

Y. Ni [15] proposed a nonlinear PID controller on STATCOM with differential tracker for damping the inter-area oscillations.The simulation results showed good performance of the suggested differential tracker under large disturbances.

A rule-based controller for STATCOM was proposed in [16]. The paper analyzes the synchronizing and damping torque induced on the shaft of the generator by STATCOM in a single machine infinite bus (SMIB) system. It was found that the induced damping torque always decreases with the strengthening of the voltage control. Moreover, a fixed-parameter PI damping controller can be invalid or even provide the system with negative damping for certain system parameters and load conditions. Based on the synchronizing and damping torque coefficient calculation, a rule based controller, which employs bang-bang, fuzzy logic or fixed-parameter PI control strategy according to operation state of the system is designed to compromise the conflict between the control objectives.

Design of dynamic controller for SVC and STATCOM is the topic of very recent articles [17, 18] for steady state, transient stability and eigen value studies.

The thyristor controlled STATCOM with new double firing phase control which makes it possible to control the active and the reactive power directly and independently without any sacrifice of the harmonic characteristic is presented in [19]. The 12-pulse configuration is used for reducing the harmonics further.

In [20] the author described a technique to control the harmonic output of a STATCOM using a PWM scheme with a minimal number of additional switchings. A neural network algorithm was developed to define the switching instants. The technique seems to offer a better alternative to other conventional methods.

Fuzzy logic controllers are also used for STATCOM in interconnected system to improve the dynamic behavior of the system [21].

An optimal robust control procedure for SVC was presented in [22]. Variation of system operation conditions are represented by an unstructured uncertainty model. Structure singular value (μ) optimization together with model reduction techniques are used to design a low order controller which provides fast and stable voltage regulation under all system conditions.The effectiveness of the procedure was shown on a weak radial system with multiple SVCs. The H_∞ controller out-performs the classical PI control.

The problem of interaction between dynamic loads and FACTS controllers has been investigated in [23]. Authors show that while an accurate modeling of loads in power system is a difficult task and often uncertain because of the non-deterministic characteristic of the loads, but proper FACTS regulations can improve the overall robustness of the system. Two methods have been presented, one based on eigenvalue sensitivity and residue technique, which takes into account the uncertain characteristics of dynamic load to compute the most efficient phase compensation for low frequency oscillation damping. The second approach is based on designing a robust controller by linear matrix inequalities techniques for guaranteeing a certain degree of stability and performance of the FACTS controller.

A Supplementary control of SVC and STATCOM using H_∞ control is proposed for improving the damping of synchronous machines oscillations in [24]. The power system considered for the simulation was a 2-generator 4-bus system.The dynamic response of the synchronous machines subjected to a three-phase fault are given to demonstrate the effectiveness of the supplementary control of SVC and STATCOM. Results indicate both SVC and STATCOM can provide smoother voltage profiles as well as better damping characteristic under disturbance conditions.

A robust nonlinear controller is proposed for STATCOM voltage control in [25]. Direct feedback linearization technique was employed to transform the nonlinear model into a linear one. The Riccati equation approach is then used to design the robust controller for the linearized model.Simulation studies show that in addition to the true system parameters, the bounds of the plant unknown time-varying parameters are also needed for the design, and the overall system was found to be asymptotically stable for all admissible uncertainties.

In [26], author pointed out that the mid-point location, which was described as the best location for the SVC, is also a possible best location of the modern FACTS devices such as STATCOM for voltage support. For the system considered, he showed that it doubled the power transfer of the line and facilitated independent control of the reactive power at both ends of the transmission line.

1.3.3 Application of STATCOM for stability improvement

In [27], authors demonstrated that a distributed STATCON (D-STATCON), applied in a distribution system, could be either used to greatly increase the load or distance served by the voltage-limited lines compared with existing conventional means. Use of D-STATCOM appears to be particularly advantageous for lumped loads, where its rapid response and broad voltage control capacity can be fully exercised.

The use of FACTS controller generates significant harmonics in the power system. These harmonics can be eliminated by the multiple inverter connection and the use of zig-zag transformers [28]. The paper outlines the experimental arrangements and early results for a 24-pulse STATCOM.

A comparative study between the conventional SVC and STATCOM for effectiveness in damping power oscillations is given in [29].Comparative study of two damping controllers, power system stabilizers (PSS) and STATCOM for damping enhancement of generator oscillations occurring in a system subject to disturbances by employing PID controller was presented in [30, 31]. The simulation results show that proposed STATCOM controller renders better damping performance over the PSS and SVC.

In references [32, 33], authors investigated the application of STATCOM for dynamic stability of the third nuclear power plant in Taiwan power system. Simulation and analytical results show the effectiveness of the designed damping controller in terms of dynamic stability enhancement and power flow increment.

A comprehensive study was undertaken to investigate how STATCOM could be used with fixed-speed wind turbines, which use induction generator to improve both steady state and dynamic impact of a wind farm on the network[34]. An optimal power flow model based on loss minimization was developed. The simulation results show the improvement of steady state stability limit, prevention of damaging over-voltages and mitigation of the voltage fluctuations at blade passing frequency, which may occur if the rotor of a number of wind turbines fall into synchronism.

From the above cited literature,it is clear that a good amount of work have been done on different aspects of design, control and application of SVC and STATCOM for power system damping and oscillation enhancements. However STATCOM are relatively new power applications and not all aspects of their dynamic performance are fully explored.

1.4 Objectives and scope of the thesis

The application of FACTS controllers creates new challenges for power engineers, not only in hardware implementation, but also in design of control systems, planning and analysis. In particular the effectiveness of these controllers will depends on the development of adequate and dependable control strategies. Due to the fast response of such controllers, study of a wide spectrum of transient behaviour, including network dynamics, generator rotor low frequency oscillations and torsional oscillations, etc. are necessary.

Motivated by these observations, the objective of this thesis are

- Dynamic modeling and analysis of STATCOM for a single-machine infinite-bus power system.
- Evaluation of existing control design techniques for STATCOM devices. Study the applicability of PID (proportional-integral-derivative) type in dynamic performance enhancement.
- Design of STATCOM controller which will be dependable for a good range of operating conditions (robustness of controllers) etc.

1.5 Outline of the thesis

The chapter-wise summary of the work reported is as follows.

Chapter 2 covers the basic concept of STATCOM and the mathematical modeling of the single machine infinite-bus power system installed with STATCOM. Two models have been investigated: an approximate model and a detailed model.

Chapter 3 addressed the design of various PID controllers for the approximate as well as detailed model. The simulations studies are carried out using MATLAB and SIMULINK program.

The basic concepts of robust control,an overview of the robust stability criteria, necessary and sufficient conditions for the design of the robust controller, etc. have been presented in chapter 4. A detailed overview of the robust controller design through loop-shaping technique is also presented.

Chapter 5 presents the simulation results for both the models with the proposed robust controller.

Conclusions and suggestions for future work are presented in chapter 6.

Chapter 2

Dynamic model of a single machine system with STATCOM

2.1 Introduction

Static synchronous compensator is a second generation FACTS device used for shunt reactive power compensation. It is based on voltage sourced converters (VSC) and used self-commutating power semiconductor devices such as GTO. Fig. 2.1 shows the basic six-pulse STATCOM. The output voltage contains substantial harmonics and therefore higher pulse numbers are usually used by combining a number of six-pulse VSCs appropriately. Alternatively, harmonics can be reduced by pulse width modulation (PWM) switching strategies. Two models of the synchronous generator connected to an infinite bus with a STATCOM at the mid bus have been presented in this chapter. These are

- A third order model for generator and current controlled STATCOM model
- A detailed 5th order model for generator and STATCOM models

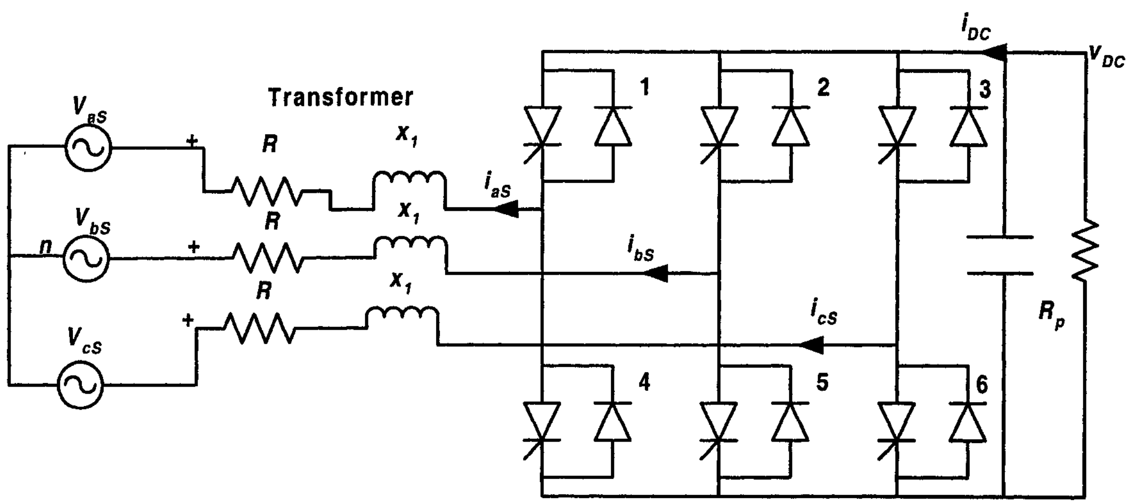

Figure 2.1: Six pulse STATCOM.

2.2 Basic concepts of voltage sourced converter

The voltage sourced converter is the building block of STATCOM, Unified power flow controller (UPFC), inter line power flow controller(IPFC) and other FACTS devices. Conventionally a thyristor device has only the turn-on control, its turn-off depends on the current coming to zero according to circuit and system conditions. Devices such as the GTO, IGBT, MTO, IGCT, etc. have turn-on and turn-off capability. These devices (referred to as turn-off devices) are more expensive and have higher losses than the thyristors without turn-off capability. However, turn-off devices enables converter concepts that can have significant overall system cost and performance advantages. Converter applicable to the FACTS Controllers would be of the self-commutating type. There are two basic categories of self-commutating converters [35]:

- Current-sourced converters in which direct current always has one polarity and power reversal takes place through reversal of the DC voltage polarity.
- Voltage-sourced converters in which DC voltage always has one polarity and power reversal takes place through reversal of the DC current polarity.

Conventional thyristor-based converters, being without turn-off capability, can only be current sourced converters, whereas turn-off device-base converters can be of either type.

For reasons of economics and performance, voltage-sources converters are often preferred over current-sourced converters for FACTS applications.

Since direct current (DC) in a voltage-sourced converter flows in either direction, the converter valves have to be bidirectional, and also, since DC voltage does not reverse, the turn-off devices need not to have reverse voltage capability. Such turn-off devices are known as asymmetric turn-off devices. Thus, a voltage-sources converter valve is made up of an asymmetric turn-off device such as GTO with a parallel diode connected in reverse as shown in Fig. 2.2. For higher power converters, provision of separate diodes is advantageous. There would be several turn-off device-diodes units in series for high voltage applications.

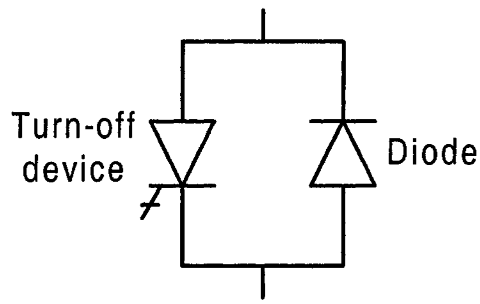

Figure 2.2: Valve for a voltage sourced converter.

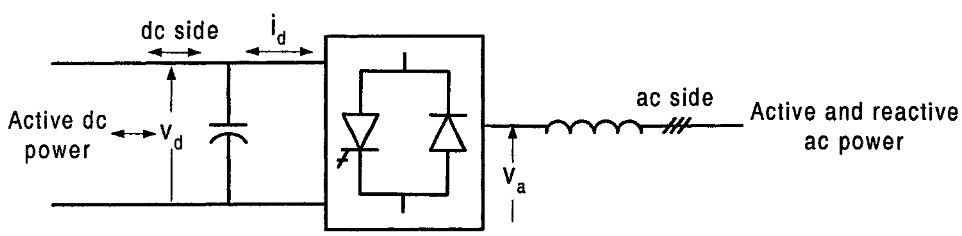

Figure 2.3: Voltage sourced converter concept.

Fig. 2.3 shows the basic functioning of a voltage-sources converter. On the DC side, voltage is unipolar and is supported by a capacitor. This capacitor is large enough to at least handle a sustained charge/discharge current that accompanies the switching sequence of the converter valves and shifts in phase angle of the switching valves without significant change in the DC voltage. It is also shown on the DC side that the DC current flow in either direction and that it can exchange DC power with the connected system in either direction. Shown on the AC side is the generated AC voltage connected to the AC system via an inductor. Being an AC voltage source with low internal impedance, a series inductive interface with the AC system (usually

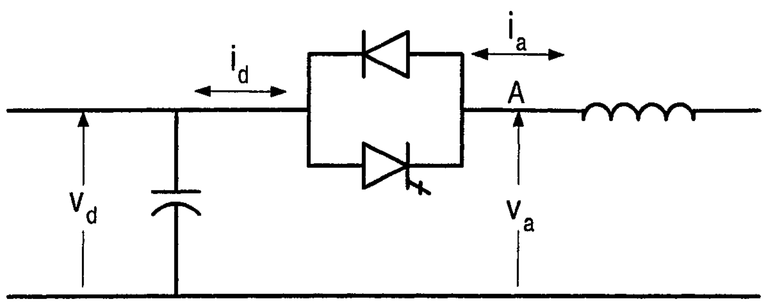

Figure 2.4: single valve operation of voltage sourced converter.

through a series inductor and /or a transformer) is essential to ensure that the DC capacitor is not discharged rapidly into a capacitive load such as a transmission line.

Basically a voltage-sourced converter which generates AC voltage from a DC voltage is, for historical reason, often referred to as an inverter, even though it has the capability to transfer power in either direction. With a voltage-sourced converter, the magnitude, the phase angle and the frequency of the output voltage can be controlled [35].

Fig. 2.4 shows a diagram of a single-valve operation, V_d assumed to be constant, supported by large capacitor, with the positive polarity side connected to the anode side of the turn-off devices. When turn-off device is turned on, the positive DC terminal is connected to the AC terminal 'A' and the AC voltage would jump to $+V_d$. If the current happens to flow from $+V_d$ to A (through device), the power would flow from the DC side to AC side (inverter action). However, if the current happens to flow from A to $+V_d$ it will flow through diode even if the device is so called turned on, and the power would flow from the AC side to the DC side (rectifier action). Thus, a valve with the combination of turn-off device and diode can handle power flow in either direction with the turn-off device with the turn-off device handling inverter action, and the diode handling rectifier action. This valve combination and its capability to act as a rectifier or as an inverter with the instantaneous current flow in positive (AC to DC side) or negative direction respectively, is basic to voltage-sourced converter concepts [35].

2.3 Mathematical models

A single-machine infinite-bus system (SMIB)with a STATCOM connected through a step-down transformer is shown in Fig. 2.5, and its equivalent circuit is shown in Fig. 2.6.

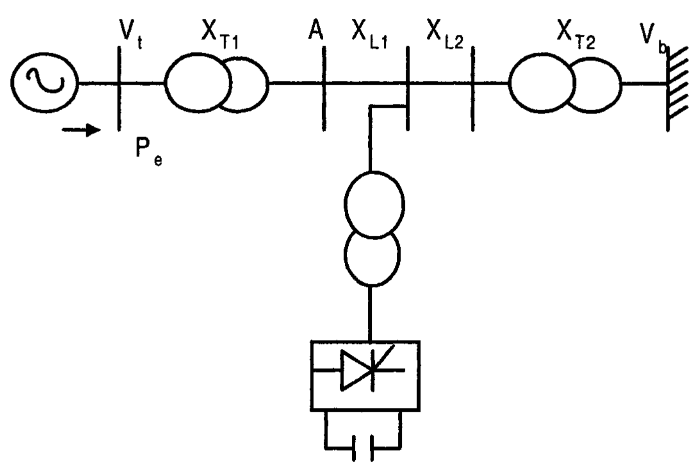

Figure 2.5: A SMIB system with STATCOM.

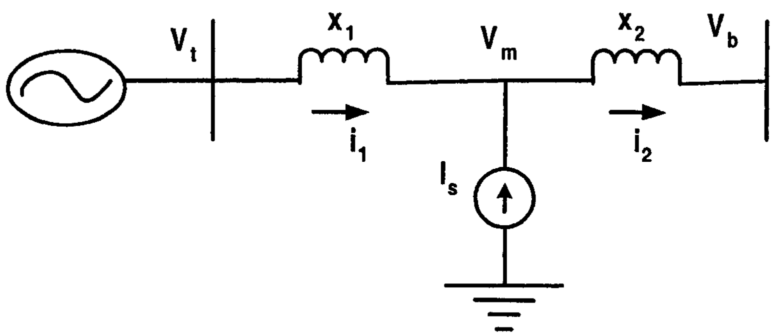

Figure 2.6: Equivalent circuit diagram of the system of Fig. 2.5

The Following assumptions have been made for building the dynamic model of the system [16]

- No detailed exciter and governor dynamics models.
- e_q , the voltage behind transient reactance x'_d , is considered to be constant.
- The mechanical power input to the system is also constant
- STATCOM is modeled as a controllable reactive current source with time delay.
- Inductive current generated by the STATCOM is assumed to be constant.

The electromechanical swing equation for the generator is broken up into

$$\begin{aligned} \dot{\delta} &= \omega_b \omega \\ \dot{\omega} &= \frac{1}{M}\left[P_m - P_e - D\omega\right] \end{aligned} \tag{2.1}$$

The dynamics of the current controller can be written as

$$\dot{I_S} = \frac{1}{T}[-I_S + Ku] \quad (2.2)$$

where

$$P_e = \frac{e_q{}'V_m}{x_d{}' + X_1}\sin\theta + \frac{V_m^2}{2}\frac{x_d{}' - x_q}{(x_d{}' + X_1)(x_q + X_1)}\sin 2\theta \quad (2.3)$$

$$V_{md} = \frac{(X_1 + x_q)V\sin\delta + I_S X_2 \sin\theta(X_1 + x_q)}{X_1 + X_2 + x_q} \quad (2.4)$$

$$V_{mq} = \frac{(X_1 + x_d{}')V\cos\delta + e_q{}'X_2 + I_S X_2\cos\theta(X_1 + x_d{}')}{X_1 + X_2 + x_d{}'} \quad (2.5)$$

$$V_m = V_{md} + jV_{mq} \quad (2.6)$$

δ is the load angle in radian, ω is relative speed, M is the inertia constant in seconds, D is the damping constant,P_e is delivered electrical power, I_s, u, K and T are the output current, controller output, gain and time constant of STATCOM, respectively. V_m in Eq. (2.3) is the terminal voltage of the STATCOM, x_d' and x_q are the direct and quadrature reactance of the generator, respectively. X_1 and X_2 are the sum of the reactance of the transformer and transmission line as shown in Fig.2.6. θ is the phase difference between quadrature axis of the generator and is written as

$$\theta = \tan^{-1}\left(\frac{V_{md}}{V_{mq}}\right) \quad (2.7)$$

where V_{md} and V_{mq} are the direct and quadrature axis components of V_m, respectively. By linearizing equations (2.1 -2.7) around an equilibrium point, one gets

$$\Delta V_m = K_{V_m\delta}\Delta\delta + K_{V_m I_S}\Delta I_S \tag{2.8}$$

$$\Delta P_e = K_{P_e\delta}\Delta\delta + K_{P_e I_S}\Delta I_S \tag{2.9}$$

here,

$$K_{V_m\delta} = \frac{\partial V_m}{\partial\delta} \tag{2.10}$$

$$K_{V_m I_S} = \frac{\partial V_m}{\partial I_S} \tag{2.11}$$

$$K_{P_e\delta} = \frac{\partial P_e}{\partial\delta} \tag{2.12}$$

$$K_{P_e I_S} = \frac{\partial P_e}{\partial I_S} \tag{2.13}$$

The STATCOM current controller output is expressed as

$$\Delta u = -C_u\Delta V_m + C_\omega\Delta\omega \tag{2.14}$$

where, C_u and C_ω are the control transfer functions in the voltage and damping control loop respectively. The entire linearized system can be described by the block diagram shown in Fig. 2.7. Detailed derivation of the system of equations is given in appendix A.

The remote signal $\Delta\omega$ is not readily available to STATCOM, however, it can be synthesized by locally measurable variables such as terminal voltage of the STATCOM and current through transmission lines[36].

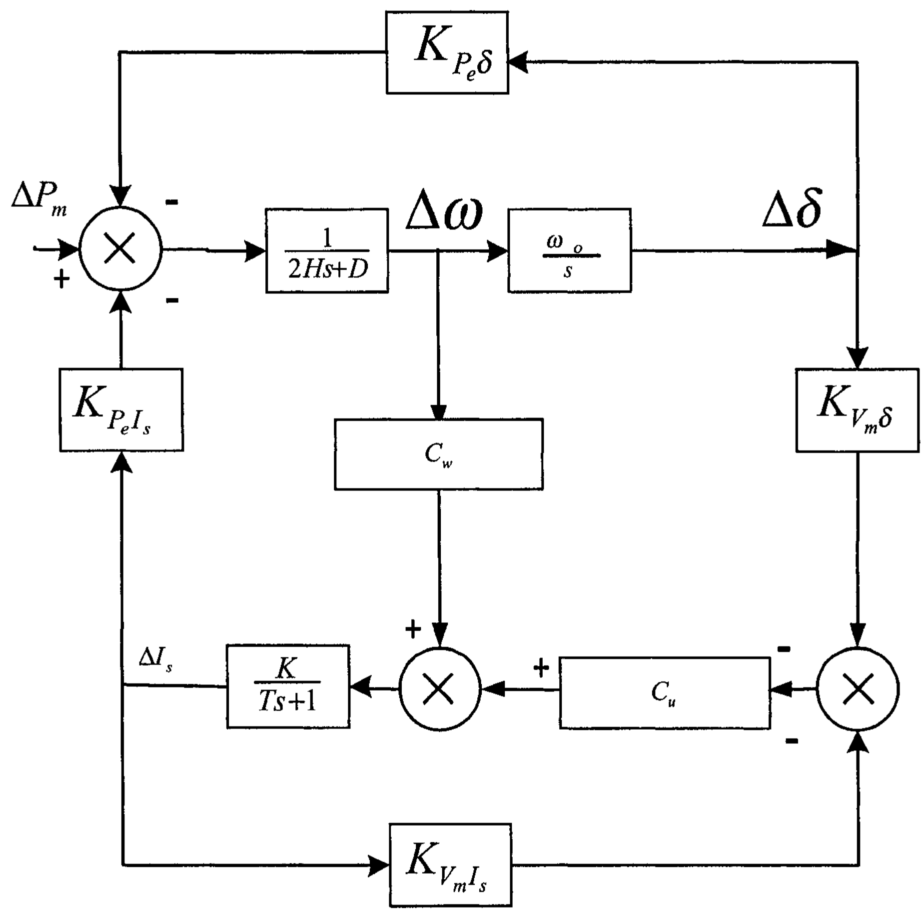

Figure 2.7: Block diagram of the linearized system.

2.4 Detailed Model of the Power System With STATCOM Controller

In the detailed model of the power system with STATCOM, in addition to the swing equation of the generator, the field and excitation system dynamics are considered. The STATCOM is modeled as a voltage sourced converter behind a step down transformer. Fig.2.8 shows a SMIB power system installed with STATCOM which consists of a step down transformer (SDT) with a leakage reactance X_{SDT}, a three phase GTO-based voltage sources converter(VSC) and a DC-capacitor. The VSC generates a controllable AC-voltage source $v_o(t) = V_o sin(\omega t - \psi)$ behind the leakage reactance. The voltage difference between the STATCOM-bus AC voltage V_L and V_o produces active and reactive power exchange between the STATCOM and the power system, which can be controlled by adjusting the magnitude V_o and the phase ψ. The voltage current relationship in the STATCOM are expressed as [37],

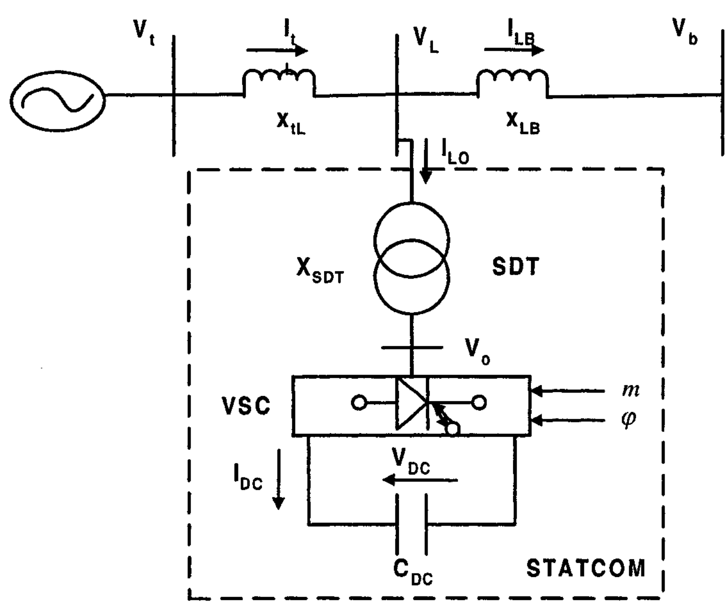

Figure 2.8: STATCOM installed in a single machine infinite bus power system.

$$\begin{aligned}
\bar{I}_{Lo} &= \bar{I}_{Lod} + j\bar{I}_{Loq} \\
V_o &= cV_{DC}(\cos\psi + j\sin\psi) = cV_{DC}\angle\psi \\
\frac{dV_{DC}}{dt} &= \frac{I_{DC}}{C_{DC}} = \frac{c}{C_{DC}}(I_{Lod}\cos\psi + I_{Loq}\sin\psi)
\end{aligned} \tag{2.15}$$

where, for the PWM inverter,

$$\begin{aligned}
c &= mk; \\
k &= \frac{\text{AC Voltage}}{\text{DC Voltage}}; \\
m &= \text{modulation ratio defined by PWM;} \\
\psi &= \text{phase angle, defined by PWM}
\end{aligned}$$

From Eq. (2.15), it can be seen that the magnitude of the STATCOM voltage V_{DC} depends on c, hence c is termed as magnitude control of the STATCOM. The complete derivation for the dynamic model of SMIB with STATCOM is given in Appendix A.

The nonlinear model of the power system of Fig. 2.8 is given as:

$$\begin{aligned}
\dot{\delta} &= \omega_b\omega \\
\dot{\omega} &= \frac{1}{M}[P_m - P_e - D\omega] \\
\dot{eq}' &= \frac{1}{T_{do'}}[E_{fd} - eq' - (x_d - x_d')I_{tLd}] \\
\dot{E}_{fd} &= -\frac{1}{T_A}(E_{fd} - E_{fdo}) + \frac{K_A}{T_A}(V_{to} - V_t) \\
\dot{V}_{dc} &= \frac{c}{C_{DC}}[I_{lod}\cos\psi + I_{loq}\sin\psi]
\end{aligned} \tag{2.16}$$

where,

$$
\begin{aligned}
P_e &= v_d I_{tLd} + v_q I_{tLq} = eq^{'} I_{tLd} + (x_d - x_d^{'}) I_{tLd} I_{tLq} \\
V_t &= \sqrt{v_d^2 + v_q^2} = \sqrt{(eq' - x_d^{'} I_{tLd})^2 + x_q^{'} I_{tLq}^2} \\
I_{tLd} &= \frac{\left(1 + \frac{X_{LB}}{X_{SDT}}\right) eq^{'} - \frac{X_{LB}}{X_{SDT}} c V_{DC} \sin\psi - V_B \cos\delta}{X_{tL} + X_{LB} + \frac{X_{tL}}{X_{SDT}} + \left(1 + \frac{X_{LB}}{X_{SDT}}\right) x_d^{'}} \\
I_{tLq} &= \frac{\frac{X_{LB}}{X_{SDT}} c V_{DC} \cos\psi + V_B \sin\delta}{X_{tL} + X_{LB} + \frac{X_{tL}}{X_{SDT}} + \left(1 + \frac{X_{LB}}{X_{SDT}}\right) x_q} \\
\overline{I}_{lod} &= \frac{eq'}{X_{SDT}} - \frac{(x_d' + X_{tL}) I_{tlq}}{X_{SDT}} - \frac{c V_{DC} Sin\psi}{X_{SDT}} \\
\overline{I}_{loq} &= \frac{c V_{DC} cos\psi}{X_{SDT}} - \frac{(x_q' + X_{tL}) I_{tlq}}{X_{SDT}}
\end{aligned}
$$

By linearizing equations for I_{tld} , I_{tlq} I_{tlod} , I_{loq} and then substituting in Eq. 2.16, the linearized system equation can be written as

$$
\begin{aligned}
\dot{\Delta\delta} &= \omega_b \Delta\omega \\
\dot{\Delta\omega} &= \frac{(-\Delta P_e - D\Delta\omega)}{M} \\
\dot{\Delta eq'} &= \frac{(-\Delta eq + D\Delta E_{fd})}{T_{do}^{'}} \\
\Delta\dot{E}_{fd} &= -\frac{1}{T_A}(\Delta E_{fd} - K_A \Delta V_t) \\
\Delta\dot{V}_{DC} &= \frac{1}{C_{DC}}[(I_{lod_0} cos\psi_0 + I_{loq_0})\Delta c + c_0(-I_{lod_0} sin\psi_0 + I_{loq_0} cos\psi_0)\Delta\psi + \\
& \quad c_0(cos\psi_0 \Delta I_{lod} + sin\psi_0 \Delta I_{lod})]
\end{aligned} \tag{2.17}
$$

where,

$$\Delta P_e = K_1 \Delta\delta + K_1 \Delta eq^{'} + K_{pDC} \Delta V_{DC} + K_{pc} \Delta c + K_{p\psi} \Delta\psi \tag{2.18}$$

$$\Delta eq = K_4 \Delta\delta + K_3 \Delta eq^{'} + K_{qDC} \Delta V_{DC} + K_{qc} \Delta c + K_{q\psi} \Delta\psi \tag{2.19}$$

$$\Delta V_t = K_5 \Delta\delta + K_6 \Delta eq^{'} + K_{vDC} \Delta V_{DC} + K_{vc} \Delta c + K_{v\psi} \Delta\psi \tag{2.20}$$

Arranging the state equations in a matrix form gives,

$$\begin{bmatrix} \dot{\Delta\delta} \\ \dot{\Delta\omega} \\ \Delta\dot{eq}' \\ \Delta\dot{E}_{fd} \\ \Delta\dot{V}_{DC} \end{bmatrix} = \begin{bmatrix} 0 & \omega_b & 0 & 0 & 0 \\ -k_1/M & -D/M & -k_2/M & 0 & -k_{pdc}/M \\ -k_4/T_{do'} & 0 & -k_3/T_{do'} & 1/T_{do'} & -k_{qdc}/T_{do'} \\ -k_A k_5/T_A & 0 & -k_A k_6/T_A & -1/T_A & -k_A K_{vDC}/T_A \\ K_7 & 0 & K_8 0 & K_9 & 0 \end{bmatrix} \begin{bmatrix} \Delta\delta \\ \Delta\omega \\ \Delta eq' \\ \Delta E_{fd} \\ \Delta V_{DC} \end{bmatrix} +$$

$$+ \begin{bmatrix} 0 & 0 \\ -k_{pc}/M & -k_{p\psi}/M \\ -k_{qc}/T_{do'} & -k_{q\psi}/T_{do'} \\ -k_A k_{vc}/T_A & -k_A k_{V\psi}/T_A \\ K_{dc} & K_{d\psi} \end{bmatrix} \begin{bmatrix} \Delta c \\ \Delta\psi \end{bmatrix} \tag{2.21}$$

Fig. 2.9 shows the block diagram for the system, here s represents the laplace transform (the derivatives) of the states. The five states are $\Delta\delta$, $\Delta\omega$, $\Delta eq'$, ΔE_{fd} and ΔV_{DC}. Δc and $\Delta\psi$ are the control inputs. The details of the derivation of the equations (2.18 - 2.21) are given in Appendix B.

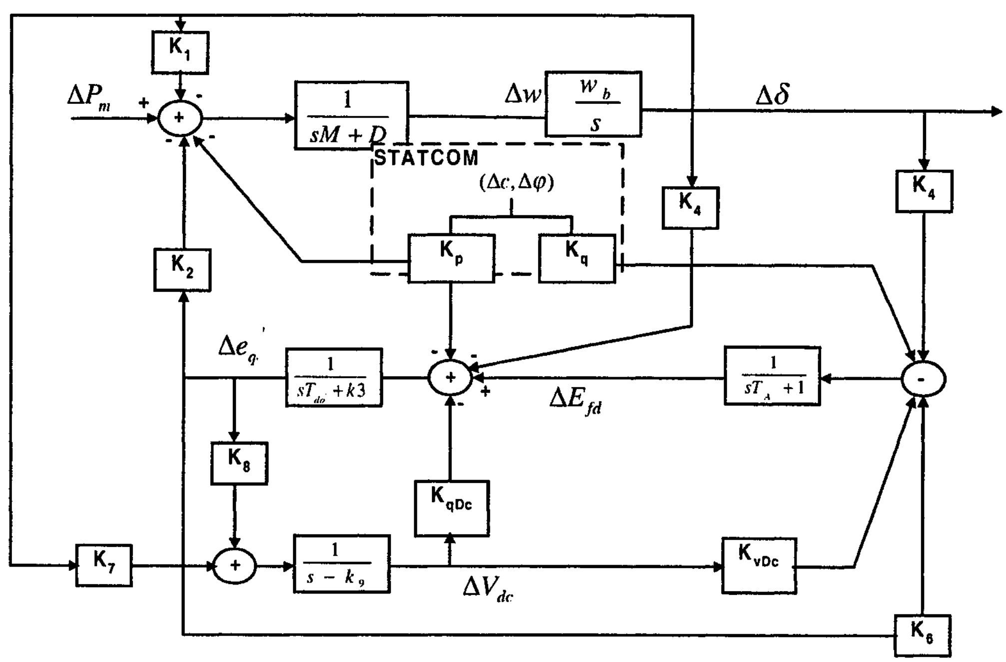

Figure 2.9: Block diagram of the linearized system installed with STATCOM.

Chapter 3

Design of PID Controller

The dynamic behaviour of the power system models installed with STATCOM, presented in chapter 2, has been investigated in this chapter for different PID controllers used.

3.1 Introduction to PID controller

A basic feedback system is given in Fig. 3.1.

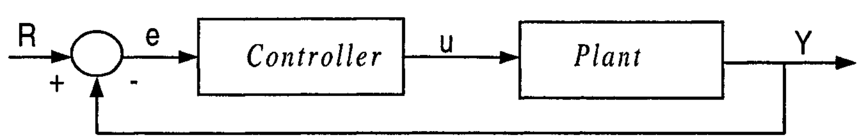

Figure 3.1: A basic feedback system .

The transfer function of a PID controller is

$$G_c(s) = K_p + \frac{K_I}{s} + K_d s \tag{3.1}$$

where,

K_p = Proportional gain

K_I = Integral gain

K_d = Derivative gain

The variable e represents the tracking error, the difference between the desired input value R and the actual output Y. This error signal is fed to controller, and the output of the controller is given as

$$u = K_p e + K_I \int edt + K_d \frac{de}{dt} \tag{3.2}$$

The proportional controller K_p will effect the steady state error and rise time. An integral control K_I controls the transient response and the steady state error. Inclusion of K_d has the effect of including anticipation in the system and making it faster. The effect of each of controllers K_p, K_d and K_I on a closed-loop system are summarized in the table [38].

CL Response	Rise Time	Overshoot	Settling Time	S-S Error
K_p	Decrease	Increase	Small change	Decrease
K_I	Decrease	Increase	Increase	Eliminate
K_d	Small change	decrease	decrease	Small change

Table 3.1: Characteristics of PID controller in close loop system

There is a degree of dependence of these factors on each other. In fact, changing one of these variables K_p, K_d and K_I can change the effect of the other two. For this reason, the table should only be used as a reference for choosing of K_p, K_d and K_I [38].

3.2 PID controller for Simplified STATCOM Model

The block diagram of the simplified model with PID controller in the speed and the voltage loop is given in Fig. 3.2. Because of difficulties with simulation on MATLAB, the derivative functions was approximated as

$$f(s) = \frac{K_d s + a}{s + b} \tag{3.3}$$

with a and b are selected as 0.1 and 1 respectively.

The dynamic behavior of the generator-STATCOM system was studied considering the following three controller configurations [39]:

- Controller in speed loop only
- Controller in voltage loop only
- Controller in combined voltage-speed loop

Different combinations of proportional, integral and derivative (PID) controls were tried in both the speed and the voltage loops. System data is given in Appendix C. A 100 % input torque pulse for 5ms is applied to simulate the disturbance. The uncontrolled system response is oscillatory. The following section presents the simulation results with the above scenarios.

3.2.1 PID control in the speed loop only

The gains of the PID controller were tuned and the effect of each of the proportional, derivative and integral controllers in the speed loop has been studied. The voltage

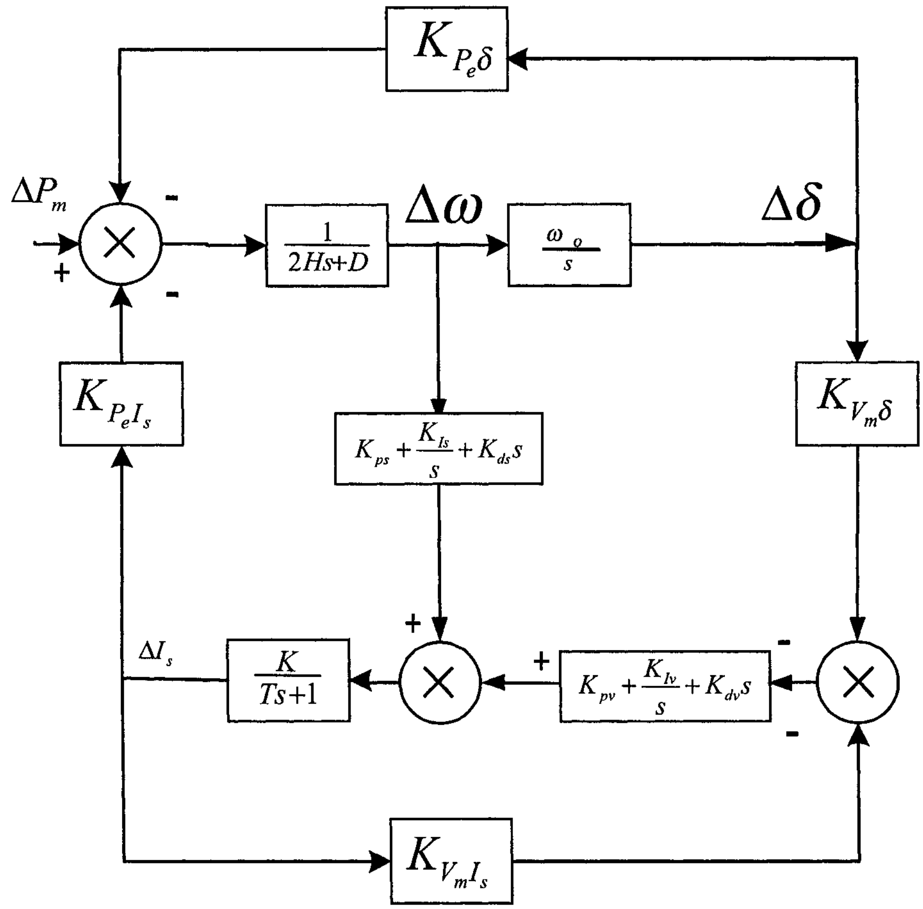

Figure 3.2: Block diagram for simplified model with PID controllers.

loop has been disabled during this study by keeping it open.

The gains of the proportional controller (K_{ps}) was varied between 0 - 150 for the 100 % torque pulse disturbance considered. It was observed that by increasing the value of K_{ps}, the system damping improves. But the increase in damping is at the cost of bus voltage excursion. Large gains, while provide enough electro-mechanical transient damping, gives large voltage variations. Satisfactory results in terms of system damping, the bus voltage and the controller current variations has been observed for a gain around 100.

The impact of proportional plus derivative controller was then examined by holding the gain K_{ps} to 100. It was observed that a slight improvement in the damping can be obtained with PD controller for K_{ds} of upto 10. Increasing the gain of further results in overshoot of the bus-voltage.

A PID controller for K_{ps} =100, K_{ds} = 10 and variable gain K_{Is} was simulated next. It was observed that inclusion of the integral controller results in oscillatory response.

Simulation results for the 100 % torque pulse disturbance with and without PID controller are given in Figures 3.3 - 3.5. Fig. 3.3 shows the rotor angle variation of the generator for the following cases. a)without stabilizing control, b) with proportional control alone, c) with proportional-derivative (PD) control and d) with proportional-integral-derivative (PID) control. Figures 3.4 and 3.5 show the corresponding variations of the mid-bus voltage and controller current outputs. A gain of K_{Is}=500 was employed in the PID control. The response with integral control is worse compared to that with PD. Comparison of the three responses indicate that PD is superior in terms of damping control. The voltage variations, however, are worsened.

This study indicated that PD control is suitable in the speed loop of the STATCOM alone for the particular system model considered.

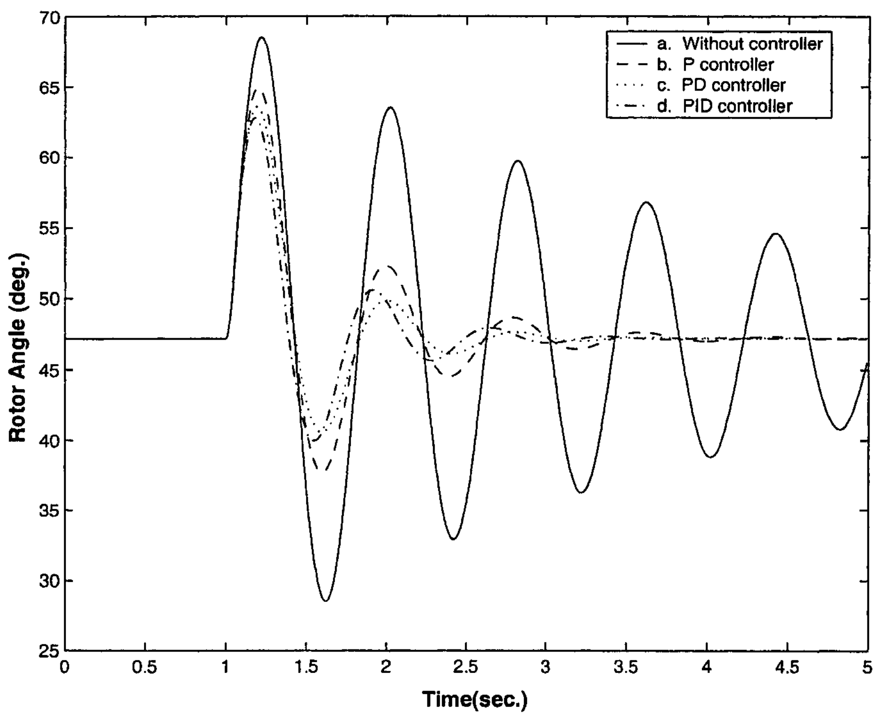

Figure 3.3: Comparative analysis of rotor angle(speed loop only)with PID controllers.

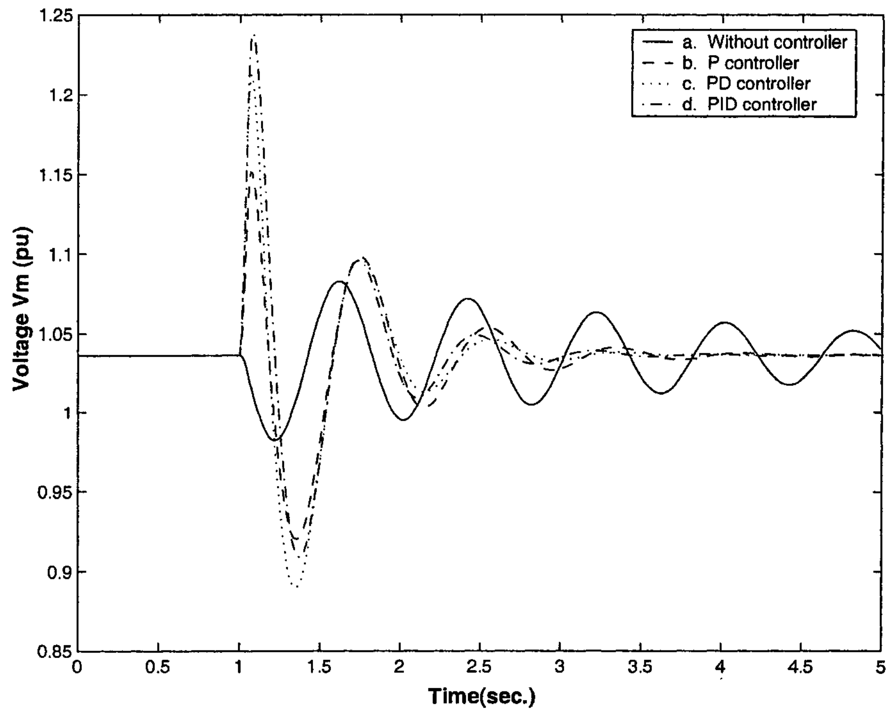

Figure 3.4: STATCOM bus voltage corresponding to Fig. 3.3.

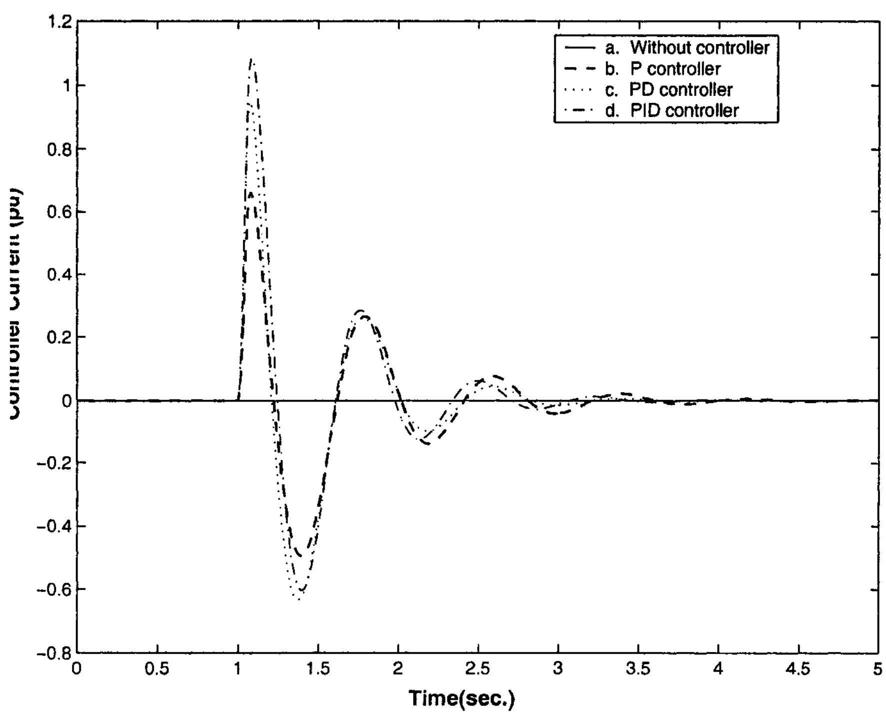

Figure 3.5: Controller current output corresponding to Fig. 3.3.

3.2.2 PID control in the voltage loop only

The transient response with PID controller on voltage loop alone are shown in Figures 3.6 - 3.7. Fig. 3.6 gives the variation of mid-bus voltage for 100 % input torque pulse for 5 ms. The response without any control is shown by curve a . With proportional, derivative or combinations of PD, the voltage response is completely oscillatory. However, the oscillation in voltage can eliminated by choosing large gains in the proportional or derivative block gains. For $K_{pv} = K_{dv} = 10000$ the response is shown by curve b. The integral control makes the response worse as shown by curve c.

The corresponding rotor angle variations of the generator are plotted in Fig. 3.7. It can be seen that even though large K_{pv} or K_{dv} can eliminate voltage fluctuations (curve b, Fig. 3.6), they, virtually, have no impact on system damping.

Though the control in the voltage loop does not provide extra system damping, the role of the voltage loop should not be underestimated. The voltage loop is an essential component of the STATCOM controller from voltage regulation view point.

3.2.3 PID control in both voltage and speed loops

The PID controllers in both speed and voltage loops were next employed to investigate the damping improvement of the linearized 3rd order model. Various combinations of proportional, integral and derivative controls were used in both the speed as well as voltage loops. It was found in section 3.2.2 that a PID control in

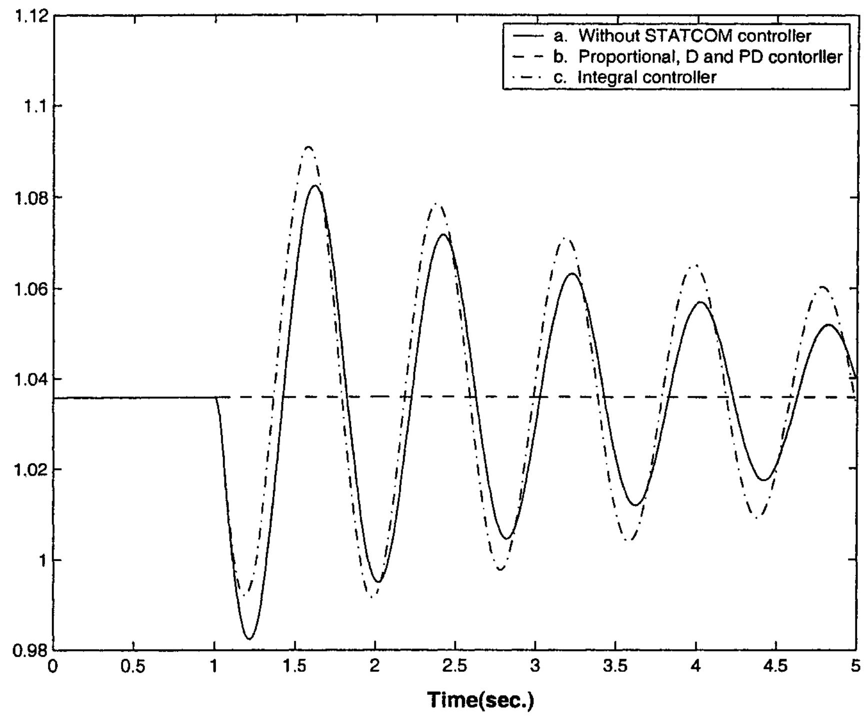

Figure 3.6: Comparative analysis of STATCOM bus voltage (voltage loop only)with Different PID controllers.

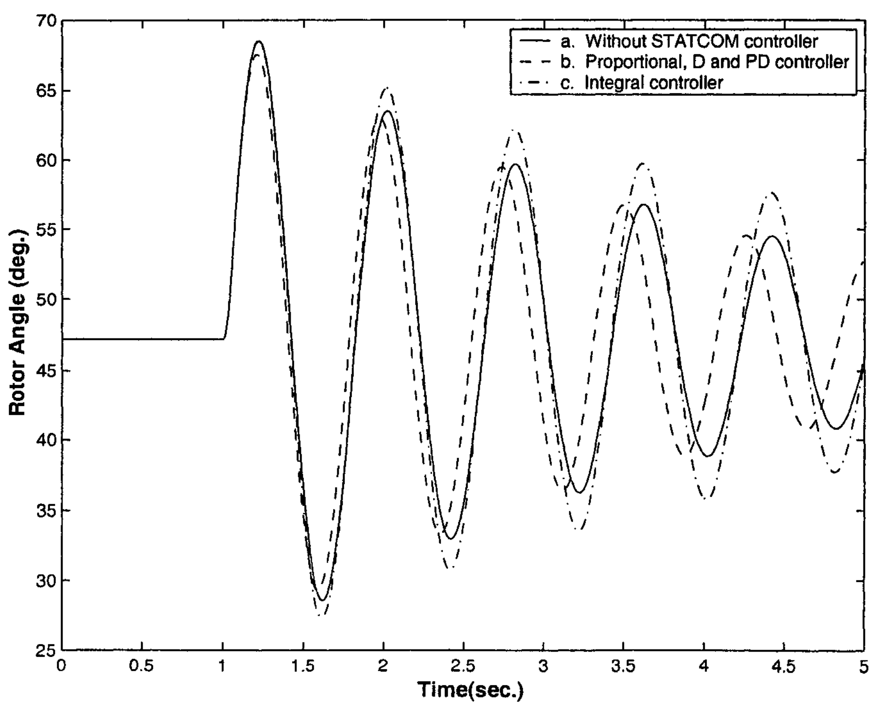

Figure 3.7: Rotor angle variation corresponding to Fig. 3.6.

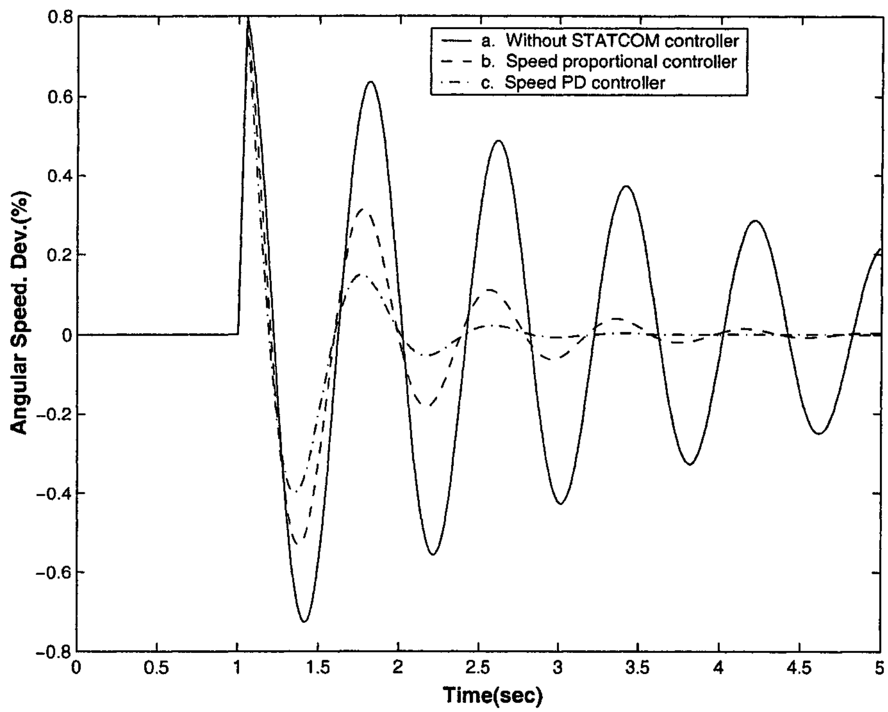

Figure 3.8: % Angular Speed Deviation with combined voltage-speed PID control.

the voltage loop does not provide extra damping. However, because of its role in the voltage regulation, a nominal value of $K_{pv} = 10$ was selected. The gains in the speed controller loop were retuned for this value of K_{pv}.

As in speed controller alone, K_{ps}=100 was again found to provide the best damping. For K_{ps}=100 and K_{pv} =10, various values of K_{ds} were tried. It was observed that for $K_{ds} = 10$ electromechanical damping was satisfactory, but the overshoot in STATCOM bus voltage and controller current were excessive. The generator angular speed deviation , the STATCOM bus voltage and controller currents variations

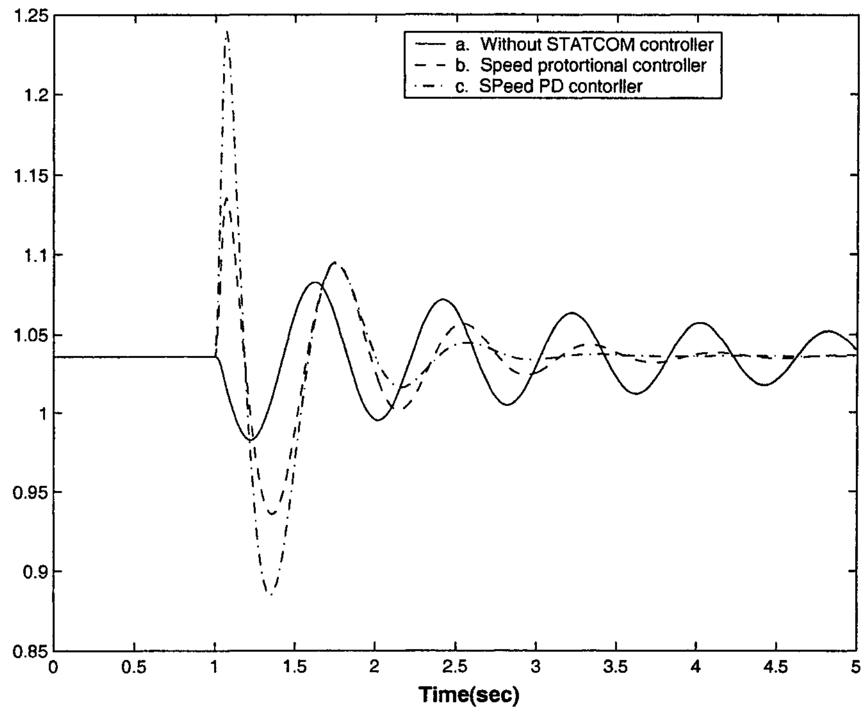

Figure 3.9: STATCOM Bus Voltage with combined voltage-speed PID control.

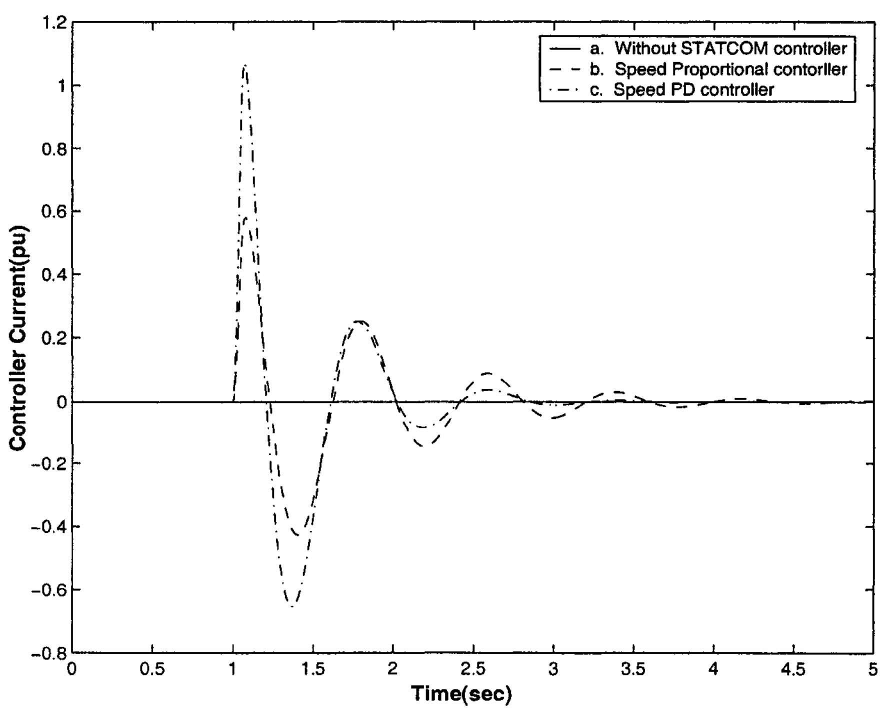

Figure 3.10: Controller current corresponding to Fig 3.9.

are presented in Figures 3.8 - 3.10 respectively for a 100 % input torque pulse disturbance for 5ms. In each figure, curve a represents the without controller. Response due to proportional control in the speed loop is shown by curve b and that due to PD control by curve c. It was observed that an integral control worsens the generator speed as well as STATCOM bus voltage response and the response has not been shown.

From this section, it is summarized that

a) A control in the voltage loop does not contribute to system damping.

b) A PD control in the speed loop provides a reasonable damping of electromechanical variables but the voltage variations are larger control.

c) A PD control in the speed loop and proportional control in the voltage loop provides a reasonable damping of electromechanical variables but the voltage variations are larger control in the case of combined speed-voltage system.

3.3 PID control with detailed model

The block diagram for the detailed model of the power system installed with the STATCOM is given in Fig. 3.11. The block diagrams for the phase angle and the magnitude control circuits are given in Figures 3.13 and 3.12. The following three PID controller configurations were examined,

- Controller in the phase angle control loop
- Controller in the voltage magnitude control loop

- Controller in both voltage and phase angle control loop

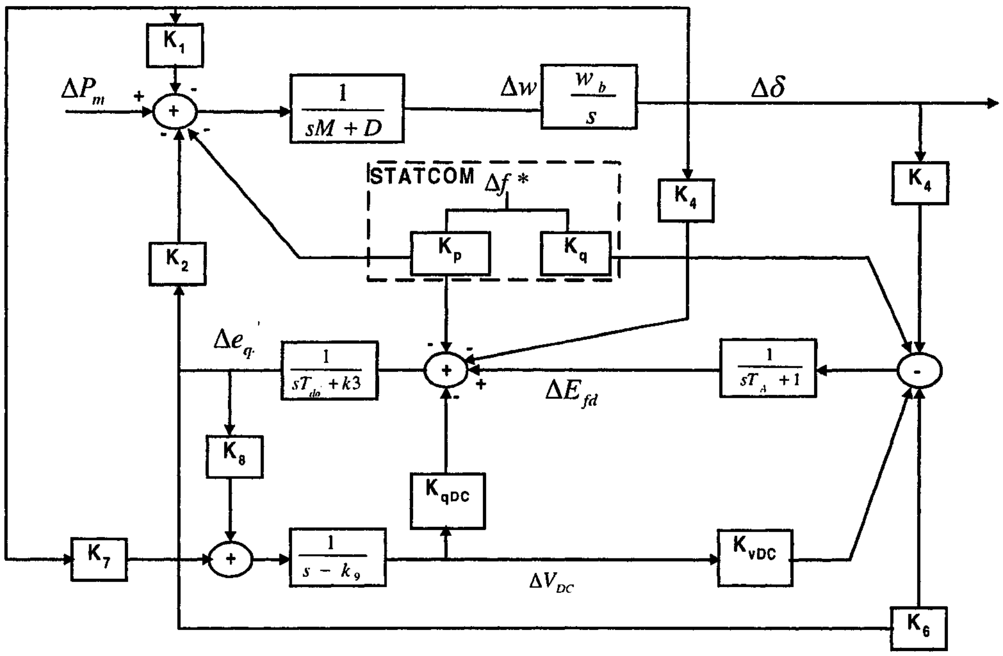

Figure 3.11: Block diagram of the linearized power system with STATCOM.

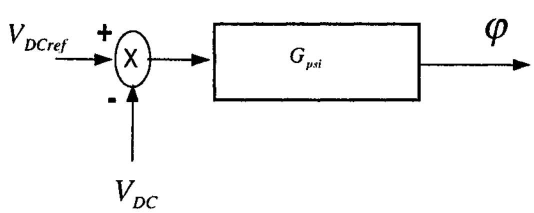

Figure 3.12: The phase conrol circuit blcok diagram.

In Figures 3.13 and 3.12 , the functions G_{psi} and G_c are considered to be the PID control functions. The system is simulated for a disturbance of 100 % torque pulse of 5 ms duration.

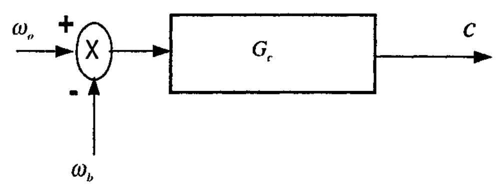

Figure 3.13: The Magnitude control blcok diagram.

3.3.1 PID control in the phase angle control loop

Different combinations of PID control in the phase angle control loop were attempted. It was observed that none of the P, PD, or PI control is effective in providing damping. The presence of these controllers even worsen the responses. Fig. 3.14 shows the rotor angle variation when proportional or proportional plus integral controllers were used in phase angle control loop. Here, curve a represent the response without STATCOM control, curve b gives the response with proportional control and curve c with PI control. The phase angle control in the detailed representation is similar to the voltage control in the approximate model. Though the phase controller does not play any part in providing damping, it is essential for voltage regulation. In the subsequent analysis the phase control has been set to a nominal value, and the only control discussed is the magnitude control.

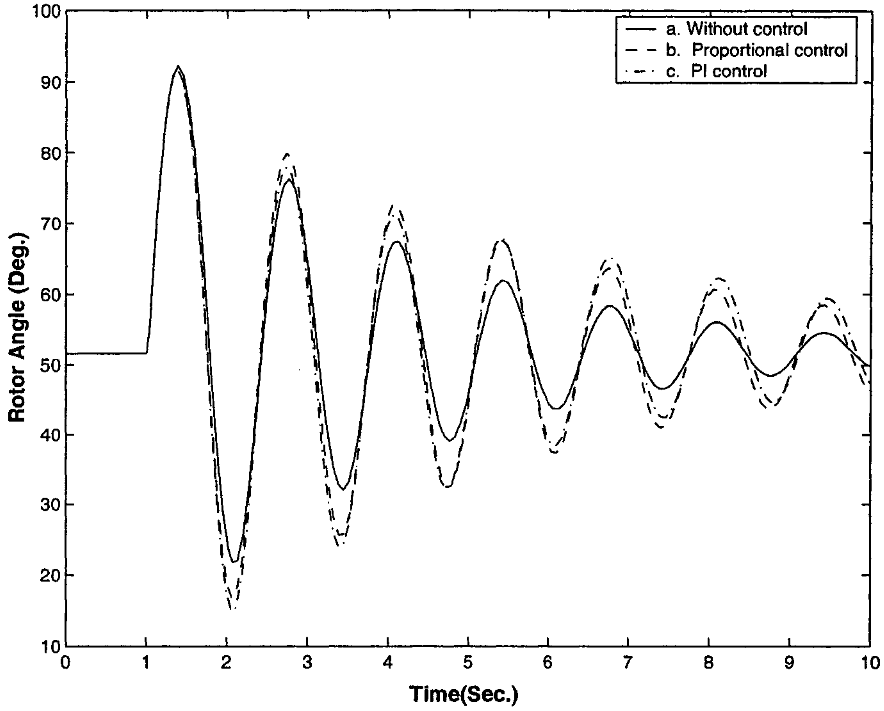

Figure 3.14: % Rotor angle (for phase angle control loop only) with different controllers.

3.3.2 PID control in the voltage magnitude loop for nominal phase angle control

For a nominal value of phase angle control if 1, different combinations of the PID controls in the magnitude control loop were investigated for the detailed model. Simulations carried out with the phase angle loop opened showed that PID controller in the voltage magnitude loop alone results in unstable system conditions.

For the 100 % torque pulse disturbance considered, the gains of the proportional controller (K_p) were varied between 0 - 30. It was observed that at very large gains the electromehanical damping improves but the STATCOM bus voltage excursions worsen. A reasonable damping of electromechanical and electrical transients is achieved for K_p of around 20.

It was observed that low K_I does not help in improving the damping. However some gain in damping is achieved for $K_I > 100$ at the cost of overshoot in the STATCOM bus voltage.

Simulation results for the 100 % torque pulse disturbance with and without PID controller are given in Figures 3.15 - 3.16. Fig. 3.15 shows the rotor angle variation of the generator for the following cases. a)with proportional control, b) with PD control, c) with PI control and d) with PID control. Fig. 3.16 shows the corresponding variations of the mid-bus voltage.

The study of the detailed model indicates that suitably designed PID controller can enhance electromechanical damping of the system. However, variations in the electrical transients such as STATCOM bus voltage, controller current output etc. may not be acceptable.

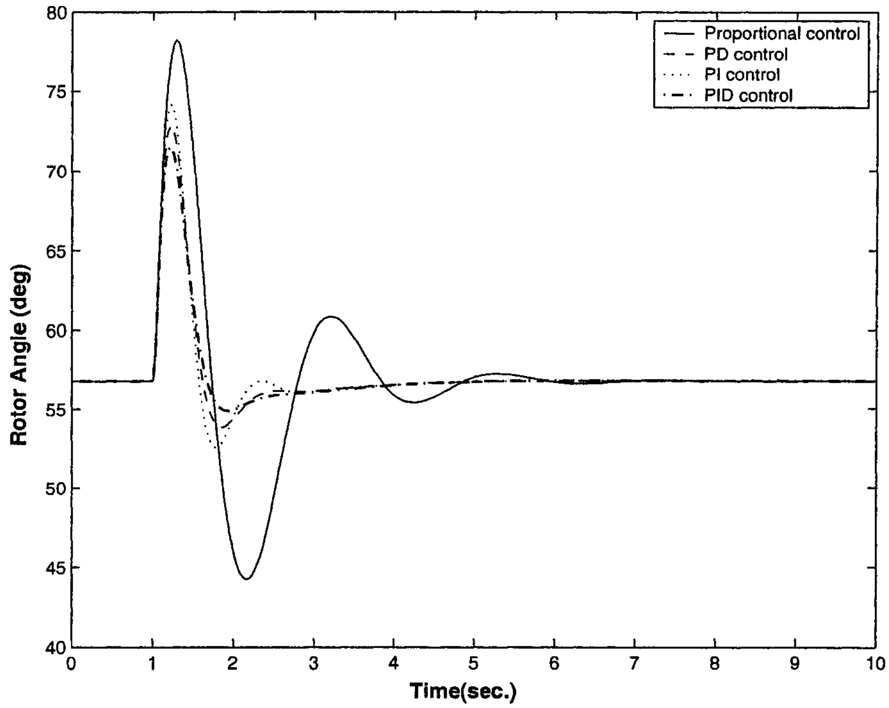

Figure 3.15: Comparative analysis of rotor angle with different gains of PID controller.

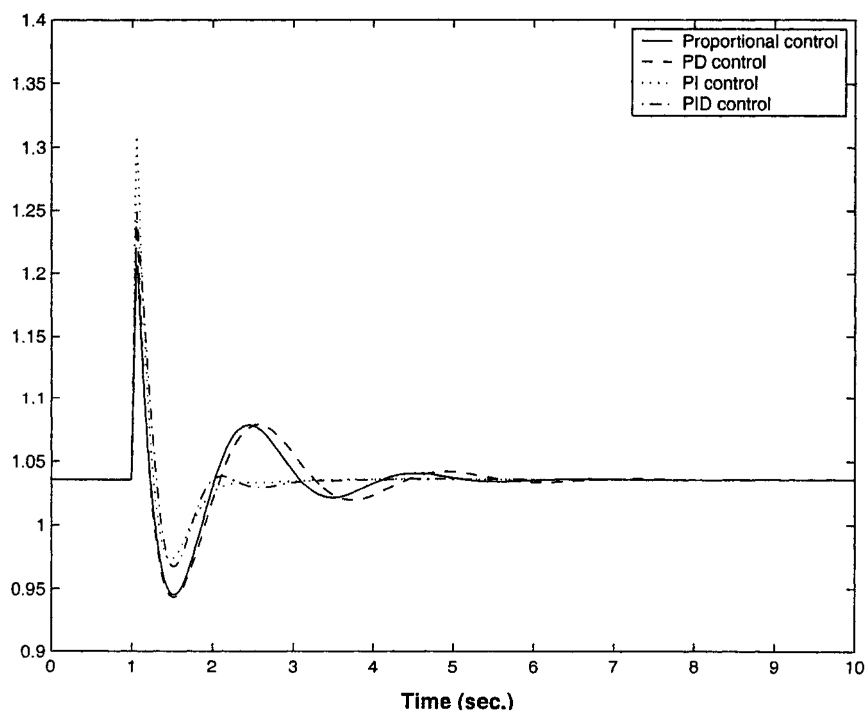

Figure 3.16: Bus voltage corresponding to Fig. 3.15.

Chapter 4

Introduction to Robust control and Loop-Shaping Technique

4.1 Introduction

Some of the STATCOM controllers presented in the previous chapter were observed to provide good damping properties. However, the voltage profiles in many of these designs were not satisfactory. Also, the PID design requires tuning of the gains for varying systems conditions.

This chapter presents the design of robust STATCOM controller. The design procedure starts by selecting a nominal operating point. The controller is designed so as to give satisfactory response over a set of perturbed plant. In the following a brief theory of the uncertainty model, the robust stability criteria, a graphical design technique termed as loop-shaping, which is employed to design the robust controller are presented. These are followed by an algorithm. The material on this robust design is available in the literature [40, 41] and is presented here for completness.

4.2 Uncertainty Modeling

Suppose that the nominal plant transfer function of a plant P belongs to a bounded set of transfer function $\mathbf{P}$ and consider the perturbed transfer function because of the variations of its parameters can be expressed in the form,

$$\hat{P} = [1 + \Delta W_2]P \tag{4.1}$$

where

$\hat{P}$= A perturbed Plant transfer function

Δ= A variable stable transfer function satisfying $\| \Delta \|_\infty \leq 1$

W_2= A fixed, stable and proper transfer function (also called the weight)

Note: The infinity norm (or ∞-norm) of a function is the least upper bound of its absolute value.

It is assumed that no unstable or imaginary axis poles of $P(s)$ are canceled in the formation of $\hat{P}(s)$. Thus $P(s)$ and $\hat{P}(s)$ have the same unstable poles.

Since Δ accounts for phase uncertainty and its magnitude varies between 0 and 1 at all frequencies (i.e. acts as a scaling factor on the magnitude of the perturbation), $\mathbf{P}$ is the set of the transfer functions whose magnitude bode plot lies in the envelope surrounding the magnitude plot of $P(s)$, as illustrated in Fig. 4.1. Thus, the size of the unstructured uncertainty is represented by the size of the envelope containing P

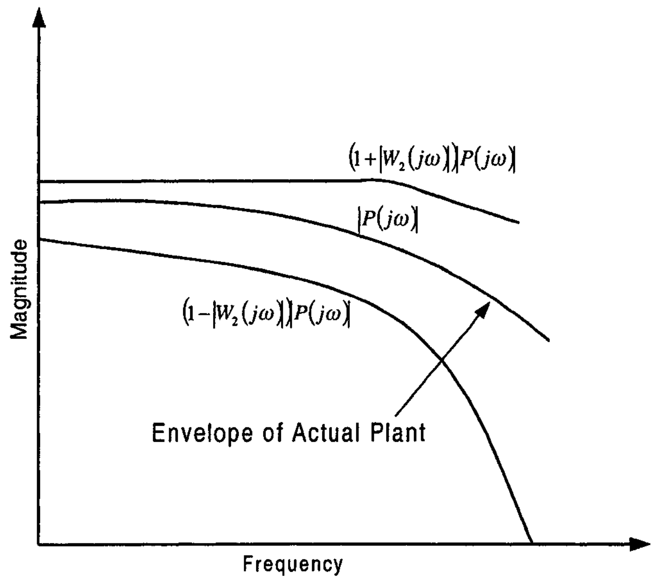

Figure 4.1: Bode plot interpretation of multiplicative uncertainty.

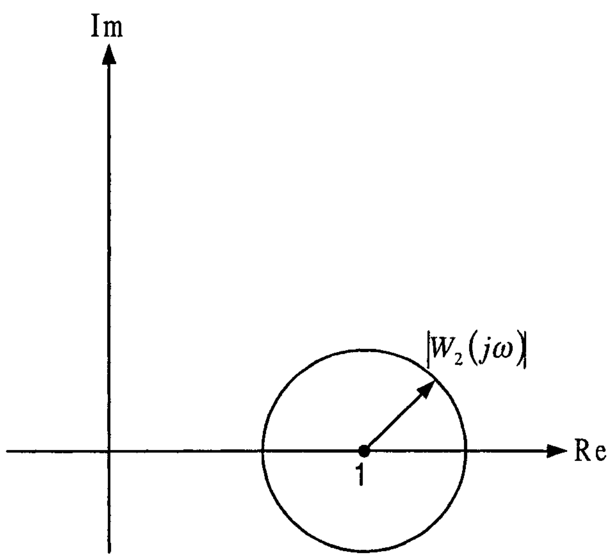

Figure 4.2: Multiplicative uncertainty in the complex plane.

and is found to increase with increasing frequency. The upper edge of the envelope confirms to the plot of $(1 + |W_2(j\omega)|)|P(j\omega)|$ while the lower edge of the envelope confirms to the plot of $(1 - |W_2(j\omega)|)|P(j\omega)|$.

In the multiplicative uncertainty model [40], ΔW_2 is the normalized plant perturbation away from 1. Hence, if $\| \Delta \|_\infty \leq 1$, then

$$|\frac{\hat{P}(j\omega)}{P(j\omega)} - 1| \leq |W_2(j\omega)| \tag{4.2}$$

for all frequencies, so $|W_2(j\omega)|$ provides the uncertainty profile. As shown in Fig. 4.2 this inequality describes a closed disk in the complex plane of radius $|W_2(j\omega)|$ and centered at 1, which contains the point $\frac{\hat{P}(j\omega)}{P(j\omega)}$ for each frequency. The unstructured uncertainty is then represented by the closed disk and therefore the direction and phase of the uncertainty is left arbitrary.

4.3 Robust Stability

Consider a multi-input control system given in Fig. 4.3. Suppose that P belongs to a set $\mathbf{P}$. The notion of robustness requires a controller, a set of plants and some characteristic of the system [40]. A controller C provides robust stability if it provides internal stability for every plant in the uncertainty set $\mathbf{P}$. Hence, a test for robust stability involves the controller and the uncertainty set. Let L denotes the open-loop transfer function (i.e. $L = PC$) and S denotes the sensitivity function or the error to reference transfer function given by the following relation,

$$S = \frac{1}{1+L} \tag{4.3}$$

Then the complimentary sensitivity function or the output to reference transfer function is given by

$$T = 1 - S = \frac{L}{1+L} = \frac{PC}{1+PC} \tag{4.4}$$

Furthermore, for a multiplicative perturbation model, the robust stability condition is met if and only if $\| \; W_2T \; \|_\infty \leq 1$ [40, 41]. A graphical interpretation of this condition is shown in Fig 4.4. Hence, the stability condition may be generalized as:

$$\begin{aligned} \| \;\; W_2T \;\; \|_\infty \leq 1 &\Leftrightarrow |\frac{W_2(j\omega)L(j\omega)}{1+L(j\omega)}| < 1, \quad for\ all\ \omega \\ &\Leftrightarrow \quad |W_2(j\omega)L(j\omega)| < |1 + L(j\omega)|, \quad for\ all\ \omega && (4.5) \\ &\Leftrightarrow \quad |\Delta(j\omega)W_2(j\omega)L(j\omega)| < |1 + L(j\omega)|, \quad for\ all\ \omega, \quad \| \; \Delta \; \|_\infty \leq 1 && (4.6) \end{aligned}$$

Therefore the critical point, -1 , lies outside the disk, which is centered at $L(j\omega)$ and radius $|W_2(j\omega)L(j\omega)|$.

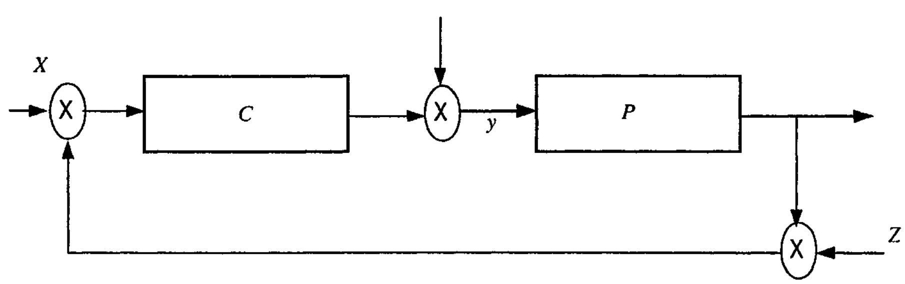

Figure 4.3: Unity feedback plant with controller.

The relevance of the condition $\| \; W_2T \; \|_\infty \leq 1$ can be seen in its relation to the small-gain theorem, which states that the feedback system is initially stable if all the transfer functions (i.e. The plant P, controller C and feedback gain F) are stable

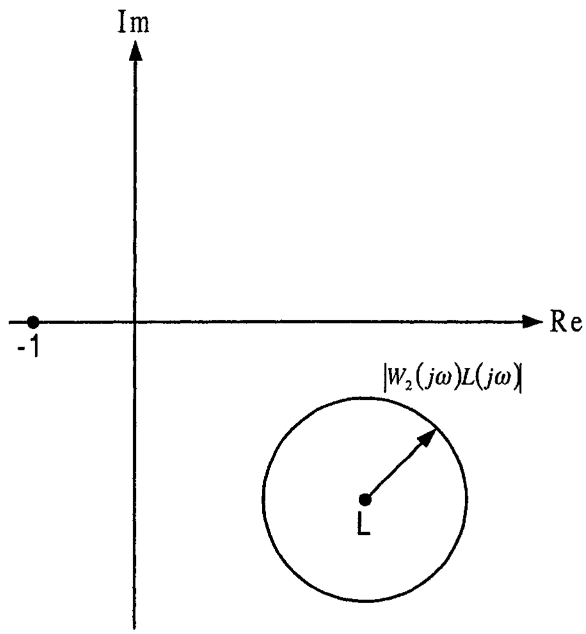

Figure 4.4: Robust stability condition in the complex plane

and $\| PCF \|_\infty \leq 1$. A block diagram of a typical perturbed system, ignoring all inputs, is shown in Fig 4.5. The transfer function from the output of Δ to the input of Δ equals $-W_2T$. The properties of the block diagram can be reduced to those of the configuration given in Fig 4.6. The maximum loop gain is $\| -\Delta W_2 T \|_\infty$, which is less than 1 for all allowable Δ if and only if the small-gain condition $\| W_2T \|_\infty \leq 1$ holds.

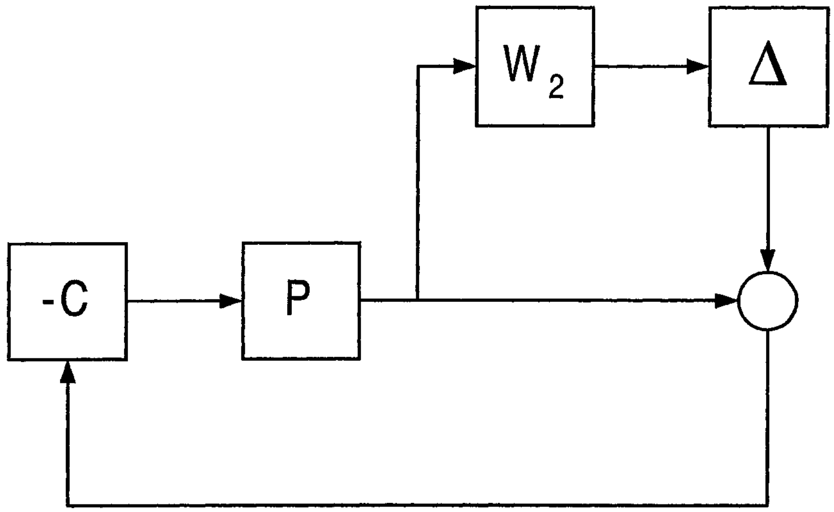

Figure 4.5: Perturbed feedback system

4.4 Robust Performance

Internal stability and performance should hold for all plants in the uncertainty set **P** according to the generalization of robust performance. The robust stability condition for an internally stable, nominal feedback system is $\| W_2 T \|_\infty \leq 1$, and the nominal performance condition is $\| W_1 S \|_\infty \leq 1$, where W_1 is a real-rational, stable, minimum-phase transfer function (also called the weighting function) such that

$$\begin{aligned} \| W_1 S \|_\infty \leq 1 &\Longleftrightarrow \left| \frac{W_1(j\omega)}{1 + L(j\omega)} \right| < 1, \text{ for all } \omega \\ &\Longleftrightarrow |W_1(j\omega)| < |1 + L(j\omega)|, \text{ for all } \omega \end{aligned} \tag{4.7}$$

If $\hat{P} = [1 + \Delta W_2]P$, then the perturbed sensitivity function is written as

$$\hat{S} = \frac{1}{1 + \hat{P}C} = \frac{1}{1 + (1 + \Delta W_2)PC} = \frac{1}{1 + (1 + \Delta W_2)L} = \frac{S}{1 + \Delta W_2 T} \tag{4.8}$$

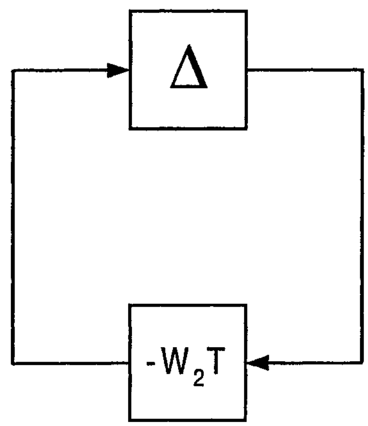

Figure 4.6: Reduced block diagram

Therefore, the robust performance condition is given by:

$$\| W_2T \|_\infty \leq 1 \text{ and } \| \frac{W_1S}{1+\Delta W_2T} \|_\infty \leq 1 \text{ ,for all allowlable } \Delta \tag{4.9}$$

Since $|\Delta| \leq 1$, then $|-\Delta W_2T| \leq |W_2T|$. Thus $|1+\Delta W_2T| \geq 1-|W_2T|$ for a fixed frequency, and it is then implied that

$$\| \frac{W_1S}{1+\Delta W_2T} \|_\infty \leq \| \frac{W_1S}{1-|W_2T|} \|_\infty \leq 1 \tag{4.10}$$

Hence Eq. (4.9) can be rewritten as a necessary and sufficient condition for robust performance, which is

$$\| \, |W_1S| + |W_2T| \, \|_\infty \leq 1 \tag{4.11}$$

Which is a stronger constraint than nominal performance or the robust stability condition alone. A graphical interpretation of this condition is shown in Fig. 4.7, whereby

$$\| \, |W_1S| + |W_2T| \, \|_\infty \leq 1 \Longleftrightarrow |\frac{W_1}{1+L}| + |\frac{W_2L}{1+L}| \leq 1, \; for \; all \; \omega$$

$$\Longleftrightarrow |W_1| + |W_2L| \leq 1 + L, \; for \; all \; \omega \tag{4.12}$$

At each frequency, there exist two closed disks, one disk centered at -1, radius $W_1(j\omega)$ and the other centered at $L(j\omega,)$, radius $|W_2(j\omega)L(j\omega)|$. The condition given by Eq. (4.11) then holds if and only if the two disks have no nontrivial intersection (i.e. they can touch, but They cannot overlap).

It should be noted that since the condition for simultaneously achieving nominal performance and robust stability is

$$\| \, max(|W_1S|, |W_2T)| \, \|_\infty \leq 1 \tag{4.13}$$

and the robust performance condition is tested by Eqn. (4.11), then the conditions in Eq.(4.11) and (4.13) differ at most by a factor of two, In other words,

$$\| \, max(|W_1S|, |W_2T)| \, \|_\infty \leq \| \, |W_1S| + |W_2T| \, \|_\infty \leq 2 \, \| \, max(|W_1S|, |W_2T)| \, \|_\infty \tag{4.14}$$

The choice of these norms is not crucial, even though they may vary by as much as a factor of two. The inherent trade-off in control problems between $|W_1S|$ and $|W_2T|$ allow for similar solutions to be achieved even when using different norms.

4.5 Loop-shaping Technique

Loop-shaping is a graphical design procedure for robust performance design, whereby P,W_1 and W_2 are the input data, and a proper controller C is designed to stabilize

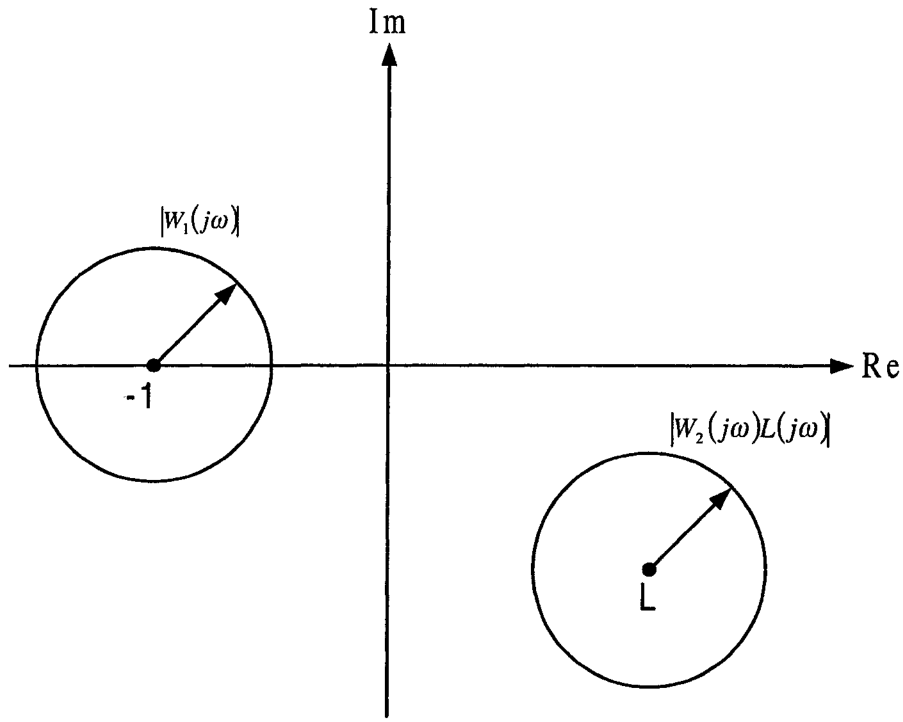

Figure 4.7: Robust performance condition in the complex plane

the plant and satisfy Eq. (4.11) [40]. The basic idea of this method is to construct the loop transfer function L to approximately satisfy Eqn.(4.11), and Then to attain C via $C = \frac{L}{P}$. Internal stability of the nominal feedback system and the properness of C constitute the constraints of this method. It is assumed that P and P^{-1} are both stable, otherwise L must contain P's unstable zeros and poles. Thus. the condition $L = PC$ must have no pole-zero cancellation. In terms of W_1,W_2, and L, Eq. (4.11) is given by

$$\Gamma(j\omega) = \left| \frac{W_1(j\omega)}{1 + L(j\omega)} \right| + \left| \frac{W_2(j\omega)L(j\omega)}{1 + L(j\omega)} \right| < 1 \tag{4.15}$$

which must hold for all frequencies. (Note that the argument $(j\omega)$ is dropped from this point onwards. The transfer functions are still functions of $(j\omega)$ unless otherwise stated.)

A necessary condition for robust performance is that at every frequency either $|W_1|$ or $|W_2|$ must be less than 1 [42]. Typically, $|W_1|$ is monotonically decreasing (for good tracking of low frequency signals) and $|W_2|$, is monotonically increasing (as uncertainty increases with increasing frequency). Hence, at each frequency, either $|W_1| < 1$ or $|W_2| < 1$. It is also the case when $|W_1| < 1$, $|W_2| \gg 1$. and when $|W_2| < 1$, $|W_1| \gg 1$. These properties can be used to determine the relationship between $|W_1|$, $|W_2|$, and $|L|$.

For the case $|W_1| \gg 1 > |W_2|$, Eq. (4.15) becomes

$$\Gamma < 1 \Longleftrightarrow |W_1| + |W_2||L| < |1 + L| \tag{4.16}$$

$$\Longrightarrow |W_1| + |W_2||L| < 1 + |L| \tag{4.17}$$

$$\Longrightarrow |L| > \frac{|W_1| - 1}{1 - |W_2|} \tag{4.18}$$

(a necessary condition), and because $|W_1| \gg 1$, it can be said that

$$|L| > \frac{|W_1| + 1}{1 - |W_2|} \Longleftrightarrow |W_1| + |W_2||L| < |L| - 1 \tag{4.19}$$

$$\Longrightarrow |W_1| + |W_2||L| < |L + 1| \tag{4.20}$$

$$\Longrightarrow \Gamma < 1$$

(a sufficient condition). Since $|W_1| \gg 1$, the condition $\Gamma < 1$ can be approximated by

$$|L| > \frac{|W_1|}{1 - |W_1|} \tag{4.21}$$

For the case $|W_1| < 1 \ll |W_2|$, Eq. (4.15)

$$\Gamma < 1 \Longleftrightarrow |W_1| + |W_2||L| < |1 + L| \tag{4.22}$$

$$\Longleftrightarrow |W_1| + |W_2||L| < 1 + |L| \tag{4.23}$$

$$\Longrightarrow |L| < \frac{1 - |W_1|}{|W_2| - 1} \tag{4.24}$$

(a necessary condition). Since $|W_2| \gg 1$, it can be said that

$$|L| > \frac{1 - |W_1|}{|W_2| + 1} \Longleftrightarrow |W_1| + |W_2||L| < 1 - |L| \tag{4.25}$$

$$\Longrightarrow |W_1| + |W_2||L| < |1 + L| \tag{4.26}$$

$$\Longrightarrow \Gamma < 1$$

(a sufficient condition). Since $|W_1| \gg 1$, the condition $\Gamma > 1$ can be approximated by

$$|L| < \frac{1 - |W_1|}{|W_2|} \tag{4.27}$$

Therefore, because $|W_1|$ is a decreasing function of frequency, and $|W_2|$ is an increasing function, then typically at low frequencies,

$$|W_1| > 1 > |W_2|$$

and at high frequencies

$$|W_1| < 1 < |W_2|$$

At very high frequencies, let $|L|$ roll off at least as quickly as $|P|$ does. This ensures that the controller is proper. The general features of the open-loop transfer function are that the gain in the low frequency region should be large enough, and in the high frequency region, the gain should be attenuated as much as possible. The gain at the intermediate frequencies typically controls the gain and phase margins. Near the gain crossover frequency ω_c, (where the magnitude equals 1), the slope of the log-magnitude curve in the Bode plot should be close to -20 dB/decade (i.e. the transition from low to high frequency should be smooth). If $|L|$ drops off too quickly through crossover, internal instability will result, so a gentle slope is crucial.

4.6 The Algorithm

The general algorithm for the loop-shaping design procedure can be outlined as [40]

- Obtain the db-magnitude plot for the nominal as well as perturbed plant transfer functions.
- Construct W_2 satisfying the constraint given in Eq. (4.2)
- On this plot, fit a graph of the magnitude of the open-loop transfer function L, whereby

  $|L| > \frac{|W_1|}{1-|W_2|}$ at low frequencies

  and

  $|L| < \frac{1-|W_1|}{|W_2|}$ at high frequencies.

- Obtain a stable minimum-phase open-loop transfer function L for the gain $|L|$ already constructed, normalizing so that $L(O) > 0$. The latter condition guarantees negative feedback

- Recover the controller C from the condition $L = PC$

- Verify nominal stability and the condition of Eq. (4.11), i.e.

  $\| \, |W_1 S| + |W_2 T| \, \|_\infty \leq 1$

- Test for the internal stability by direct simulation of the closed loop transfer function for pre-selected disturbances or inputs.

- Repeat the procedure until satisfactory L and C are obtained. Note that a robust controller may not exist for all nominal conditions, and if it does, it may not be unique.

Chapter 5

Application of Loop-shaping Technique for Design of Robust STATCOM Controller

The principles and technique of using multiplicative uncertainties for modeling a plant,the robust stability and performance criteria, loop-shaping technique, etc. which were presented in the previous chapter has been employed to design robust controllers for STATCOM.

5.1 Robust Controller design for the approximate model

For designing the robust controller for the approximate model, the two controller functions C_w and C_v in the speed and voltage loops respectively were considered individually and then both of them together [43], as done in the case of PID controllers

5.1.1 Robust Speed controller Design

The block diagram of the system in the absence of any control in the voltage feedback, and the absence of any input is shown in Fig. 5.1. Control in the speed loop alone is considered. The nominal operating point for the design was computed

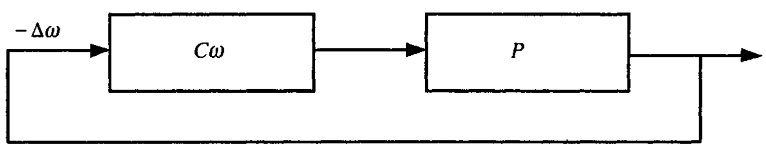

Figure 5.1: Collapsed block diagram for robust speed feedback system.

for delivered power of 0.9 per unit at unity power factor. Off-nominal power outputs between 0.2-1.4 p.u. and power factors ratings between 0.8 lag - 0.8 lead were considered for the perturbed plant transfer functions. The nominal plant transfer function for the selected operating point is computed as

$$P = \frac{1.0435s}{(s+50)(s^2+0.66s+60.72)} \tag{5.1}$$

The db-magnitude vs. frequency response for the nominal and the perturbed plants is plotted in Fig. 5.2.

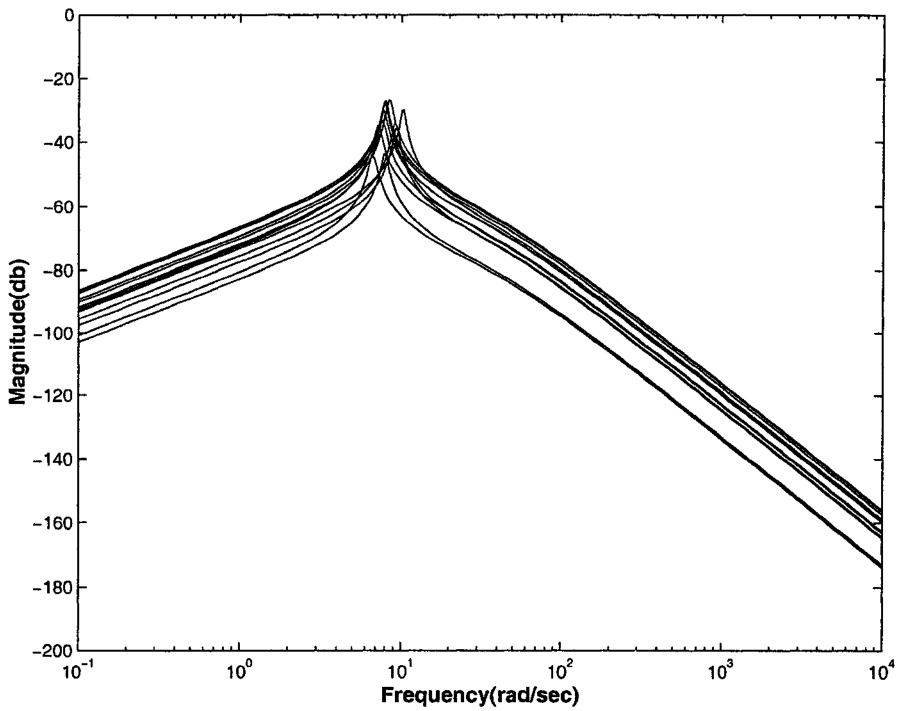

Figure 5.2: Nominal and perturbed plant transfer functions for robust speed feedback system.

From the relation $|\frac{\hat{P}(j\omega)}{P(j\omega)} - 1| \leq W_2$, the quantity $|\frac{\hat{P}(j\omega)}{P(j\omega)} - 1|$ for each purturbed plant is constructed and the uncertainty profile is fitted to the function

$$W_2(s) = \frac{0.8s^2 + 2.24s + 39.2}{(s^2 + 0.98s + 49)} \tag{5.2}$$

This is shown in Fig. 5.2

A butterworth filter satisfies all the properties of for $W_1(s)$ and is written as

$$W_1(s) = \frac{K_d f_c^2}{(s^3 + 2s^2 f_c + 2s f_c^2 + f_c^3)} \tag{5.3}$$

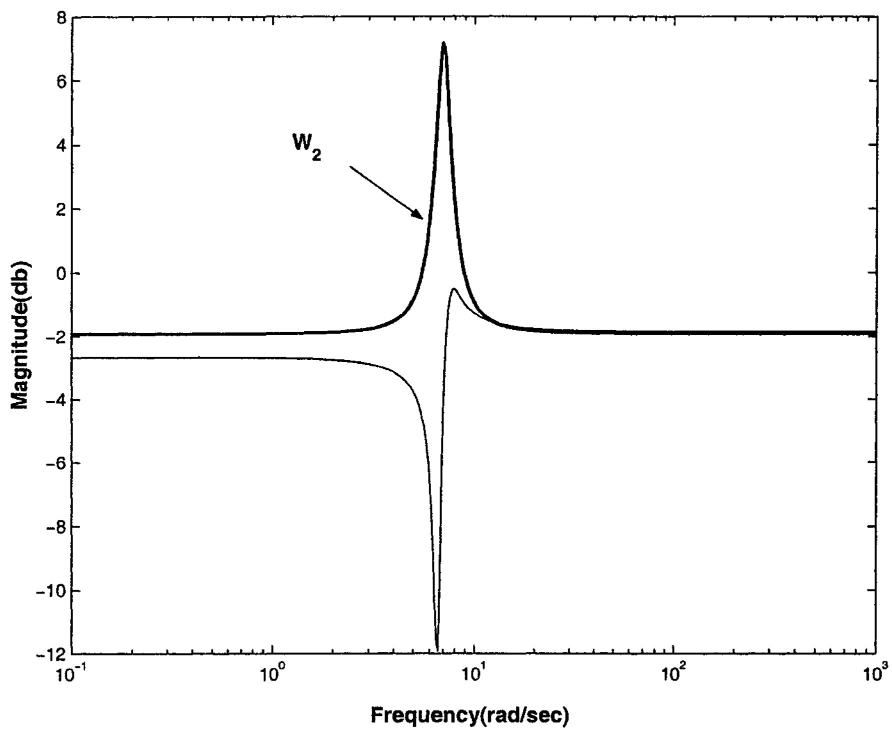

Figure 5.3: The uncertainty profile for the approximate model.

K_d and f_c are selected as 0.01 and 1 respectively.

For given W_1 and W_2, the open loop transfer function (L) is selected by trial and error to fit the relations that at low frequency $|L(s)| > \frac{|W_1|}{1-|W_2|}$, and for high frequency $|L(s)| < \frac{1}{|W_2|}$.It should also satisfies the robust stability criteria $||W_1S+W_2T||_\infty < 1$ and nominal performance criterion $||W_1S|_\infty|| < 1$. The open loop transfer function L that satisfies loop-shaping criteria has been obtained as

$$L(s) = \frac{208.75(s+1)(s+2)}{(s+0.01)(s+50)(s^2+0.66s+60.72)} \tag{5.4}$$

The db magnitude for L satisfying the conditions is shown Fig. 5.4. The plots for the nominal performance and robust performance criteria are shown in Fig. 5.5.As shown in the Figure, that the curve for $||W_1S + W_2T||$ is always less than 0 db

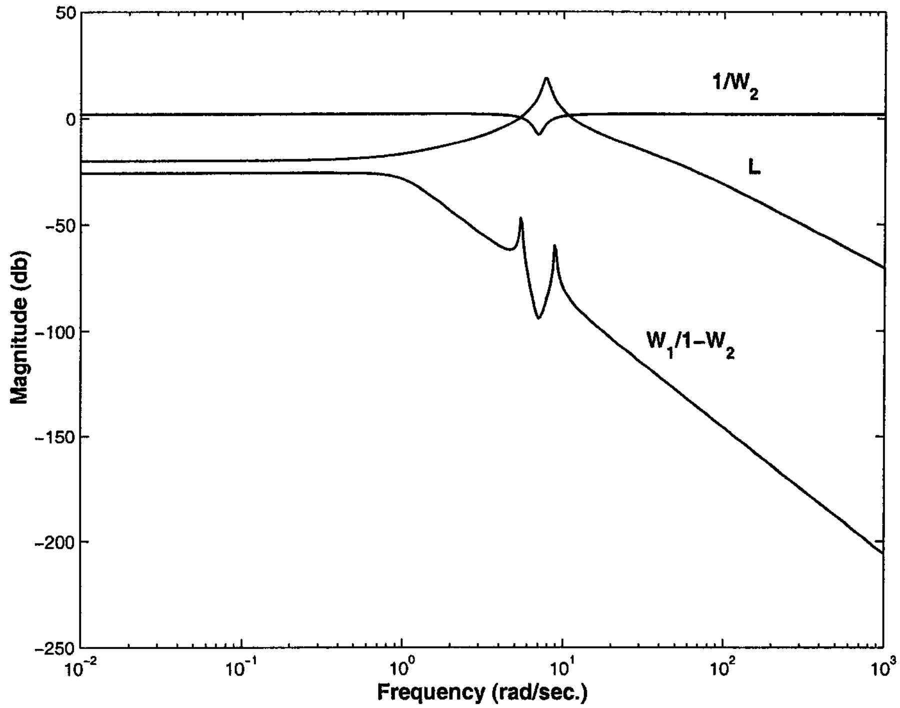

Figure 5.4: Loop shaping plots relating W_1, W_2 and L for robust speed controller.

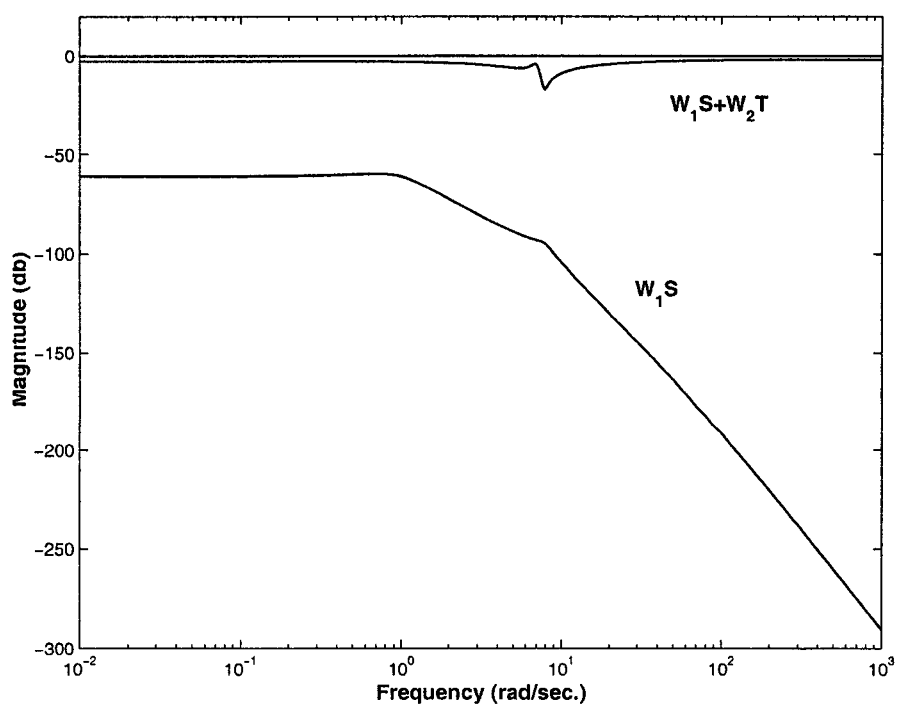

Figure 5.5: Robust and nominal performance criteria for robust speed controller.

and thus satisfying the relation robust stability and the performance criterion. The nominal performance criteria $\|W_1 S\|_\infty < 1$ is also satisfied.

For the above open loop transfer function, the controller function was found from the relation

$$C(s) = \frac{L(s)}{P(s)} \tag{5.5}$$

and is given as

$$C_w(s) = \frac{200(s+1)(s+2)}{s(s+0.01)} \tag{5.6}$$

The robust STATCOM speed controller was tested by applying an input torque pulse of 100% of 5 ms. duration to the generator shaft. For a number of operating conditions, simulation results for the STATCOM bus voltage and variation in the rotor angle are given in Fig. 5.6 - 5.7 respectively. Curve a represents the nominal operating condition.

Fig. 5.6 shows the STATCOM bus voltage variations for a) P_o= P_o= 0.9 p.u. at unity power factor, b) P_o= 1.0 p.u. at 0.95 lagging power factor, c) P_o= 1.1 p.u. at 0.95 leading power factor, d) 1.2 p.u. at 0.98 leading power factor, and e) P_o= 0.5 p.u. at 0.95 lagging power factor. The corresponding rotor angle variations are given in Fig. 5.7. From the figures, it can be observed that a very good damping properties can be obtained with the robust speed controller over a wide range of operating conditions.

Figures 5.8 and 5.9 shows the variations in the generator angular speed and the controller current output for even more largely varied operating conditions. Results

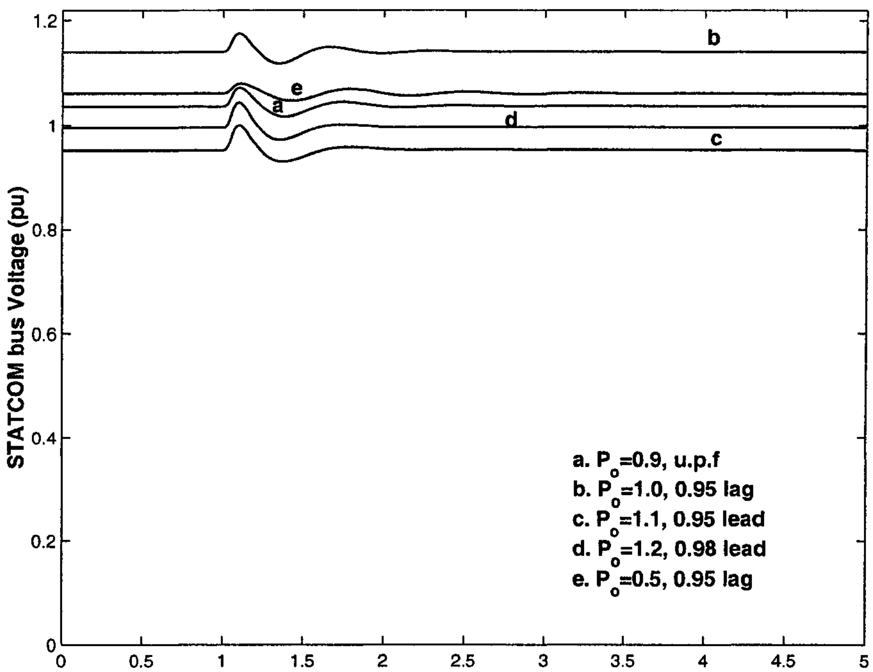

Figure 5.6: STATCOM bus voltage with robust speed controller.

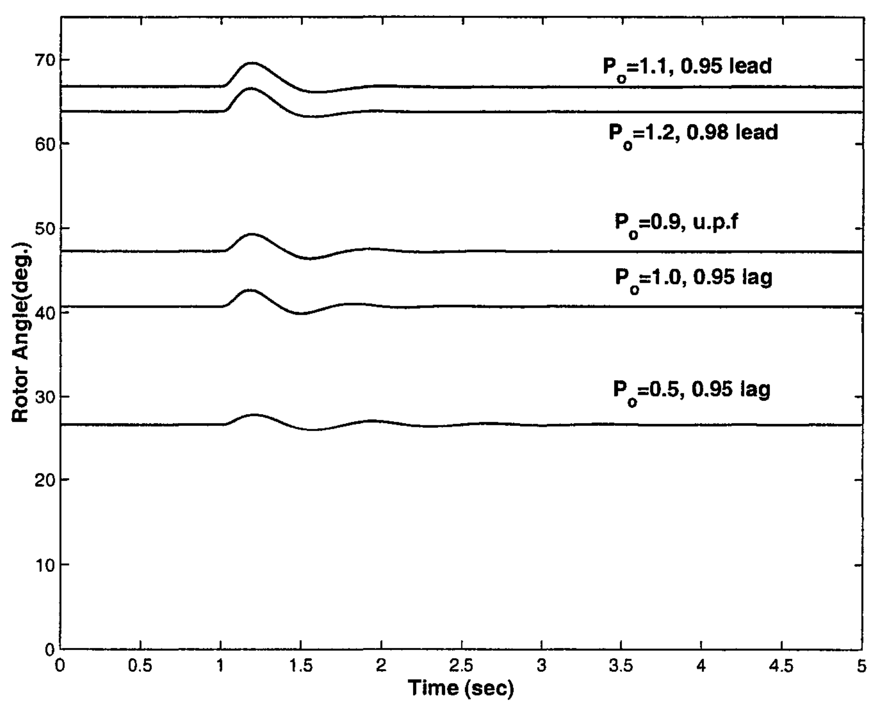

Figure 5.7: Rotor angle corresponding to Fig 5.6.

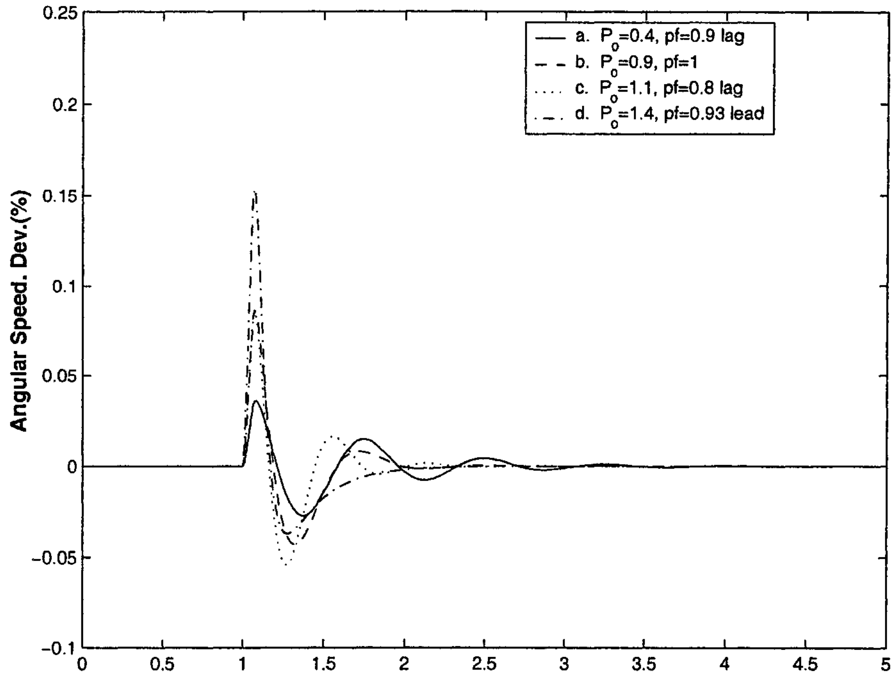

Figure 5.8: % Angular speed deviation with robust speed controller.

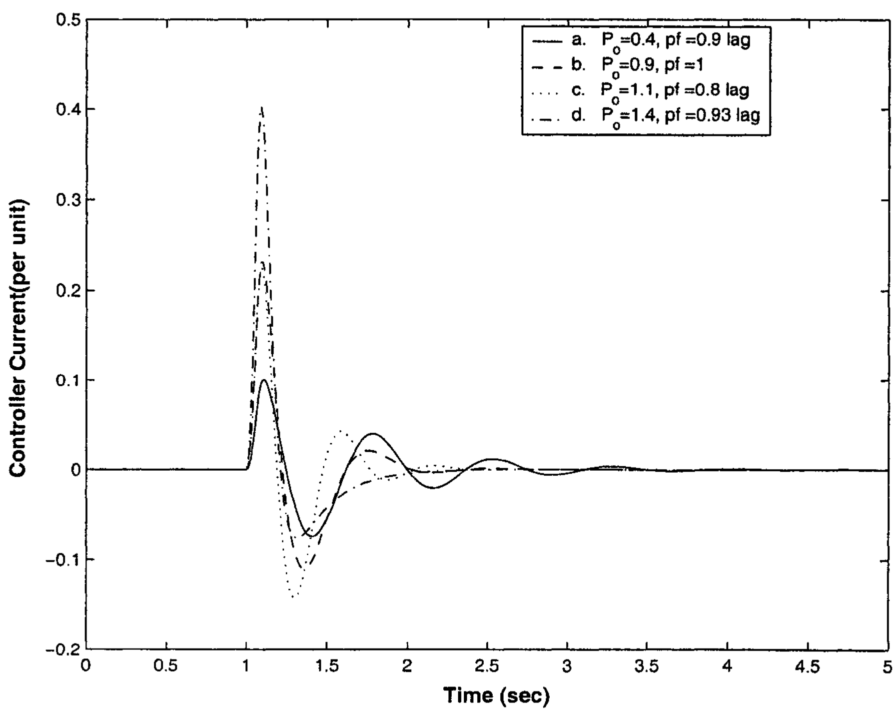

Figure 5.9: Controller output current corresponding to Fig.5.8

confirms that the designed STATCOM speed controller is robust to handle large variations in the system.

5.1.2 Robust controller in the voltage loop alone

The block diagram corresponding to Fig. 5.1. with the voltage loop controller is shown in Fig. 5.10. The nominal plant transfer function for this formulation is

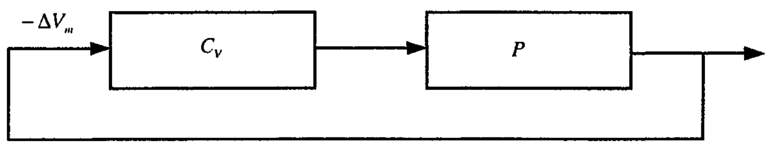

Figure 5.10: Collapsed block diagram with voltage controller.

$$P = \frac{-10.35(s^2 + 0.667s + 68.0233)}{(s + 50)(s^2 + 0.667s + 61.7585)} \tag{5.7}$$

Because of the sign of the P, the nominal plant is in a positive feedback loop. Such a system does not fall in the category of the internal stability [40] and robustness criterion cannot be applied as such. However, by forcing C_v to take the opposite polarity, a robust controller was designed following the procedure outlined in section 5.1.1. The controller does provide reasonable amount of damping over a range of operating conditions, but it is not as effective as the speed controller C_w. It is noted that earlier studies also revealed that the STATCOM voltage control loop does not provide enough damping [16, 37] and similar observation was found by the application of the PID controller in the voltage loop alone in section 3.2.2. PI controller design is often unsatisfactory, and may even may lead to unstable situation [37]. This can be attributed to the fact that there is a pair of poles and a pair of zeros is P on the imaginary axis, which are in close proximity. These pole-zero pairs are responsible for the oscillatory nature of the response in that voltage loop which is a desirable for voltage regulation purpose.

5.1.3 Voltage-speed Robust controller

In the following section, a robust design for a controller in the speed loops is presented which retains a nominal voltage feedback gain $C_v = 1$.

The nominal plant transfer function with robust controller in the speed loop and including the voltage feedback can be expressed as

$$P = \frac{1.1975s^2}{(s + 58.3475)(s^2 + 2.672s + 10.9579)} \tag{5.8}$$

Note that positive feedback situation disappears allowing a proper robust design. Continuing the same design procedure employed in section 5.1.1, considering the same transfer functions for W_1, W_2 as given in Eq. (5.3) and (5.2), a choice of the open loop transfer function,

$$L(s) = \frac{175(s + 6)(s + 0.8)}{(s + 58.3475)(s^2 + 5s + 49)} \tag{5.9}$$

with the resulting control function,

$$C_w(s) = \frac{146.13(s + 6)(s + 0.8)(s^2 + 2.672s + 10.9579)}{s^2(s^2 + 5s + 49)} \tag{5.10}$$

provides excellent damping control over a wide range of operating conditions. Fig. 5.11. shows the db-magnitude plot relating W_1, W_2 and L, which was employed to arrive at the controller of Eq. 5.10. The plots for the nominal and robust performance criteria are shown in Fig. 5.12.

The system model has been simulated for 100% mechanical torque pulse of 5 ms duration. Five different loading conditions have been considered to investigate the robustness of the designed controller. The variations in generator rotor angle and the bus voltage are shown in Figures 5.13 and 5.14 respectively. As can be observed, the robust controller provides excellent damping characteristics and keeping the bus voltage to an acceptable value. However for the operating condition away from the nominal operating point, an oscillatory response has been observed which damps with the time shown by curve e in Fig. 5.14 for 0.5 p.u power output at 0.95 lagging power factor.

5.2 Robust Controller design for detailed model

There are two possible controls in the detailed model of STATCOM as shown in Fig 2.9. These are the magnitude of the STATCOM voltage (c) and its phase (ψ). In chapter 3, it was shown that the controller in the phase angle control loop does not provide any extra damping. This is somewhat similar to the controller C_v in the approximate model.

Since the phase control does not provide extra damping, C_ψ was set to a nominal value of 1 for designing the robust magnitude controller. The nominal plant transfer function P is taken for power output of 0.9 at unity power factor load and is obtained

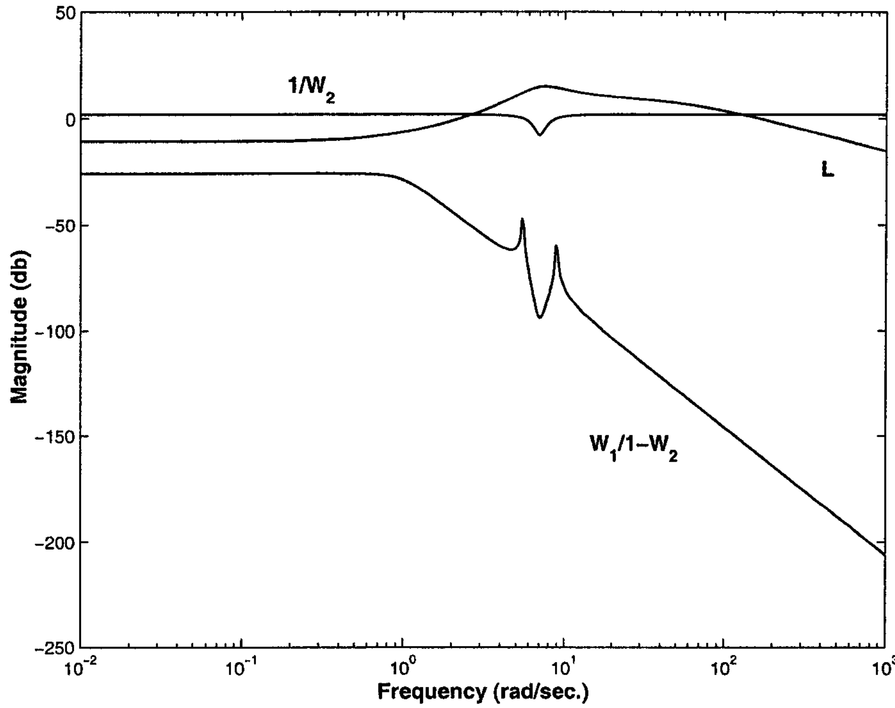

Figure 5.11: Loop shaping plots relating W_1, W_2 and L for voltage-speed robust controller.

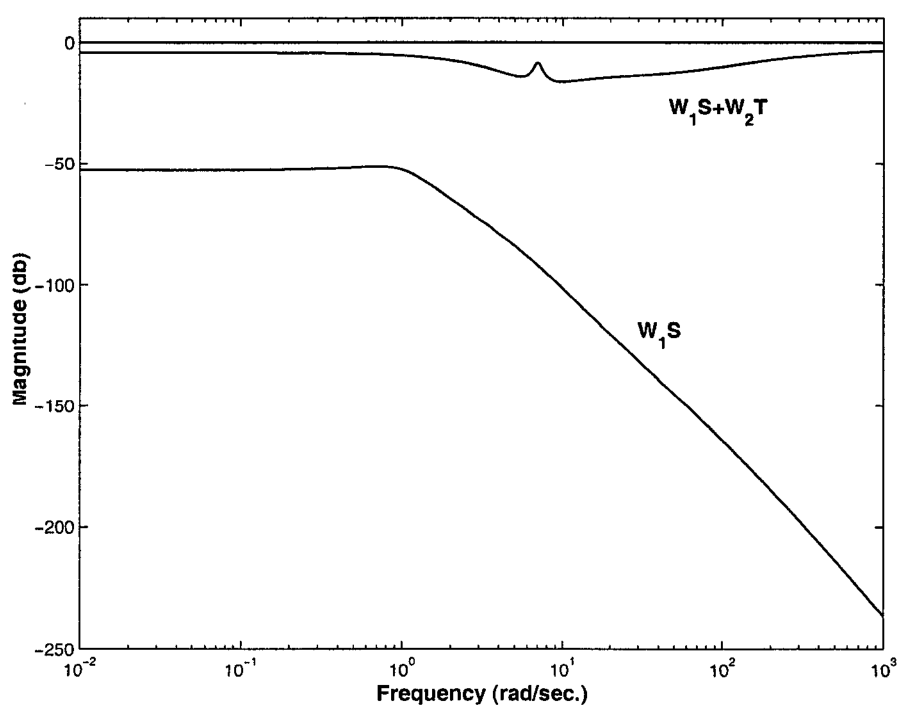

Figure 5.12: Robust and nominal performance criteria for voltage-speed robust controller.

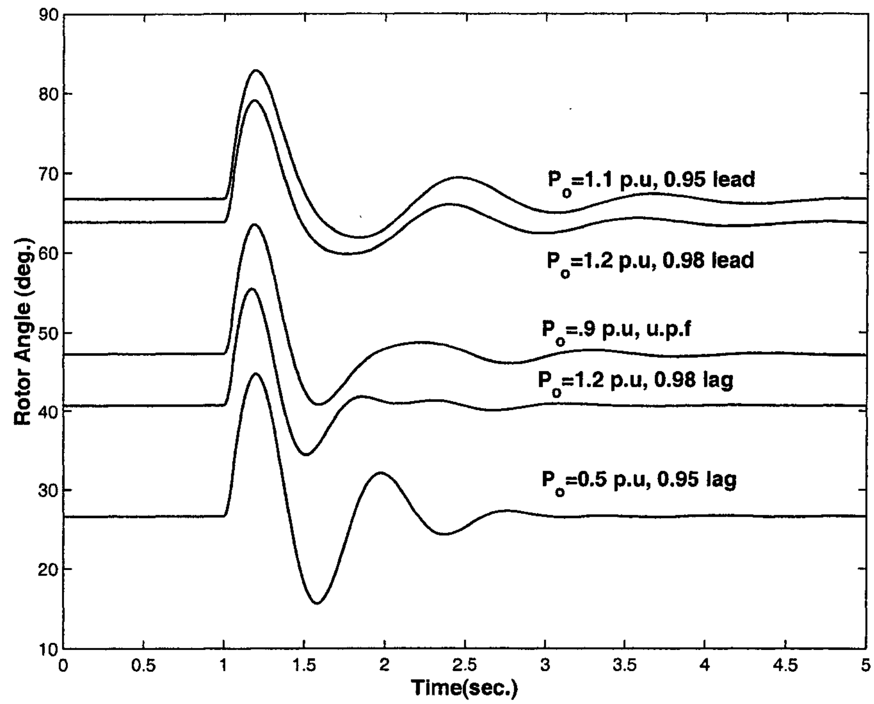

Figure 5.13: Rotor angle with robust controller for voltage-speed robust controller

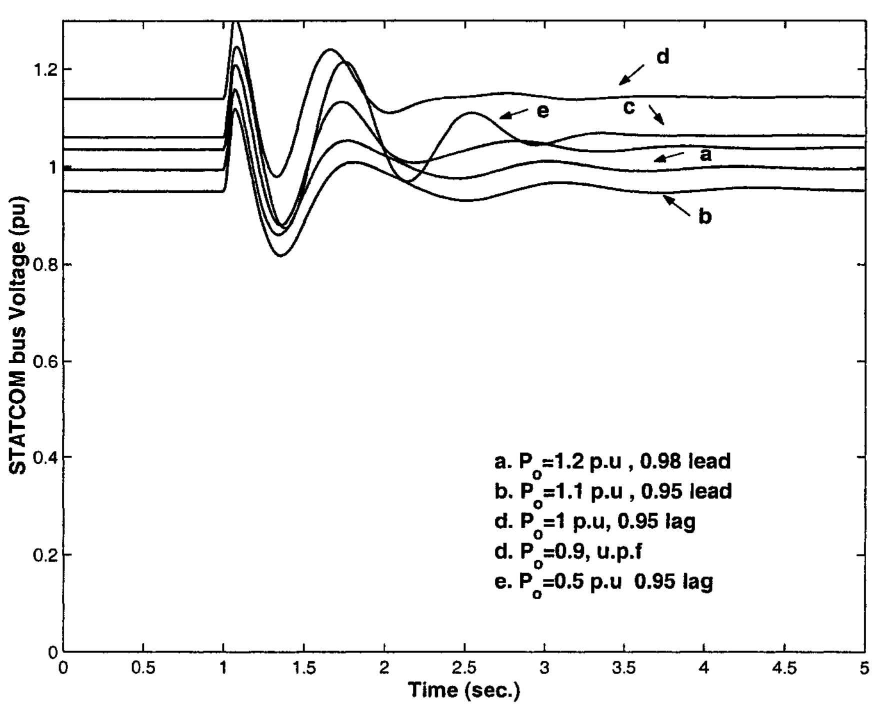

Figure 5.14: STATCOM bus voltage corresponding to Fig. 5.13

as,

$$P = \frac{0.2466s^2(s + 100.774)(s - 0.214309)}{(s + 99.1923)(s + 1.0901)(s + 0.0527)(s^2 + 0.65484s + 21.4956)} \tag{5.11}$$

The collapsed block diagram for only magnitude control is shown in Fig. 5.15. The db magnitude vs. frequency plot for the nominal and perturbed plants are shown in Fig. 5.16. From this plot the quantity $|\frac{\hat{P}(j\omega)}{P(j\omega)} - 1|$ is constructed and is shown in Fig 5.17. Off nominal operating points for output power ranges from 0.8 p.u to 1.4 p.u and power factor from 0.8 lagging to 0.8 leading were considered. The function W_2 fitting the relationship $|\frac{\hat{P}(j\omega)}{P(j\omega)} - 1| \leq |W_2(j\omega)|$ is constructed as

$$W_2(s) = \frac{2.165s^2 + 4.221s + 27.44}{(2.5s^2 + 2.436s + 18.92)} \tag{5.12}$$

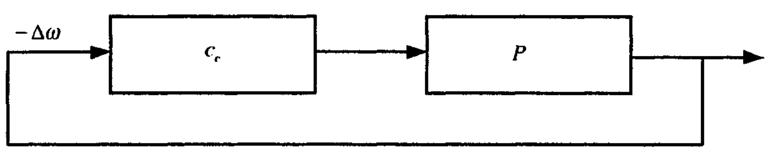

Figure 5.15: Collapsed block diagram for robust c controller.

The function W_1 was selected as,

$$W_1(s) = \frac{K_d f_c^2}{(s^3 + 2s^2 f_c + 2s f_c^2 + f_c^3)} \tag{5.13}$$

K_d and f_c were selected to 0.01 and 1 respectively. The open loop transfer function L which satisfies the loop-shaping criteria was found to be

$$L(s) = \frac{0.5(s + 0.009)(s + 100.774)(s - 0.214309)(s + 1)}{(s + 12)(s + 0.0901)(s + 0.01)()(s^2 + 0.65485s + 21.4956)} \tag{5.14}$$

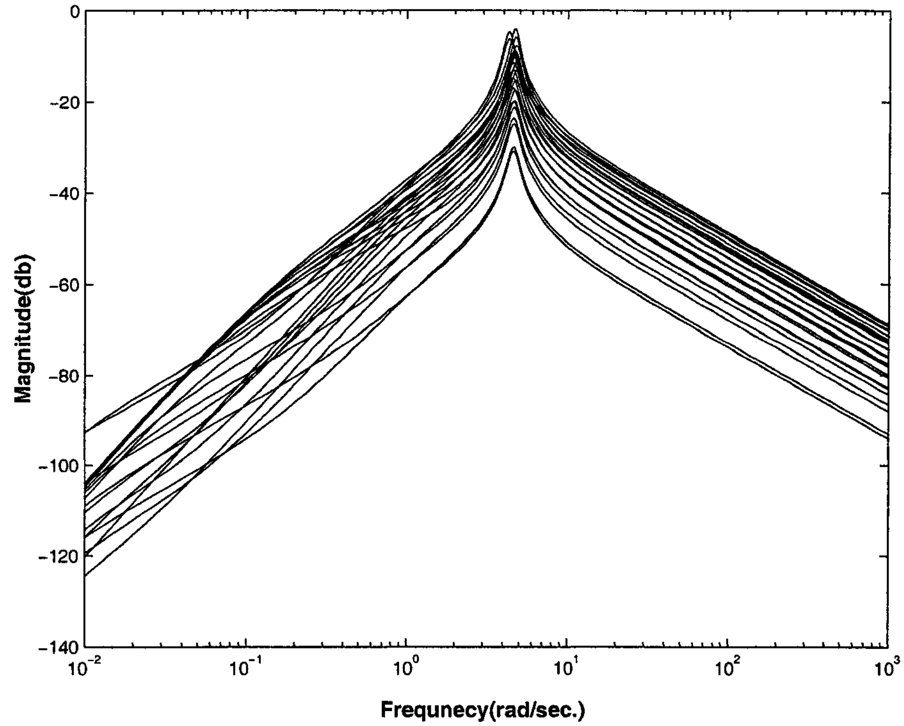

Figure 5.16: nominal and perturbed plant transfer functions for robust speed feedback system.

The db vs. frequency plots relating relating L, W_1 and W_2 is show in Fig. 5.18 . Fig. 5.19 shows the plots for the nominal and robust performance criterion. From the relation $L = PC$, the controller transfer function was constructed as

$$C_c(s) = \frac{2.0273(s+1)(s+1.0901)(s+0.0527)(s+99.19233)(s+0.009)}{s^2(s+12)(s+0.0901)(s+0.01)} \quad (5.15)$$

The controller was tested by simulating the detailed model for a disturbance of 100 % input torque pulse of 10 ms duration. The simulations results obtained for a number of operating conditions are given in Fig. 5.20 - 5.21. The responses recorded are the variations in the rotor angle and mid-bus respectively. Fig. 5.20 shows the rotor angle variation for the following operating conditions. a)Nominal operating

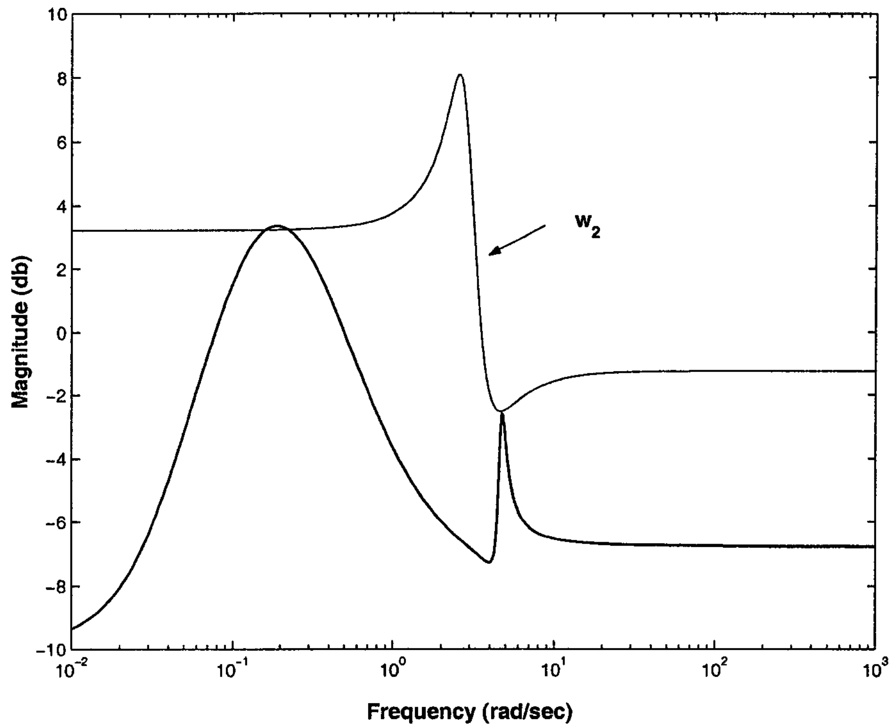

Figure 5.17: the uncertainty profile for detailed model.

condition, b) Unity power output at 0.95 lagging power factor. Curve c and d shows the responses at power output of 0.5 and 1.2 respectively with the corresponding power factors of 0.95 lagging and 0.98 leading. It was observed that the designed magnitude control provides damping for all the operating conditions. Expectedly, the response of the states farther away from the nominal are not as good. This is exhibited by a slightly oscillatory response for 0.5 p.u output shown by curve c.

Fig. 5.21 shows the corresponding variations in the mid bus voltage. The robust controller maintains the STATCOM bus voltage to its desired value faithfully. The maximum transient overshoot observed was about 10%

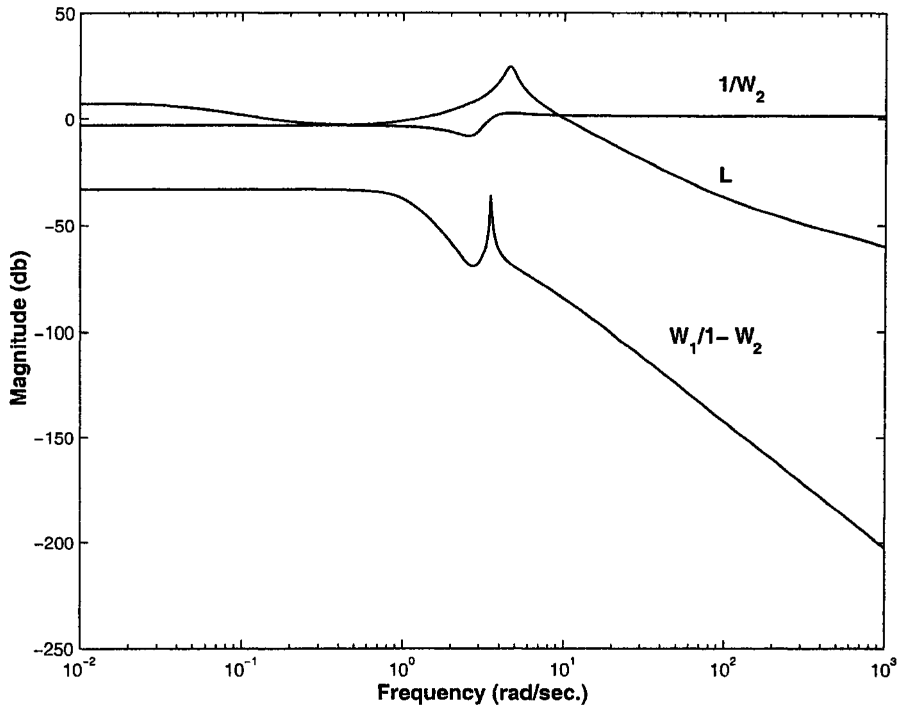

Figure 5.18: Loop shaping plots relating W_1, W_2 and L for detailed model Robust controller.

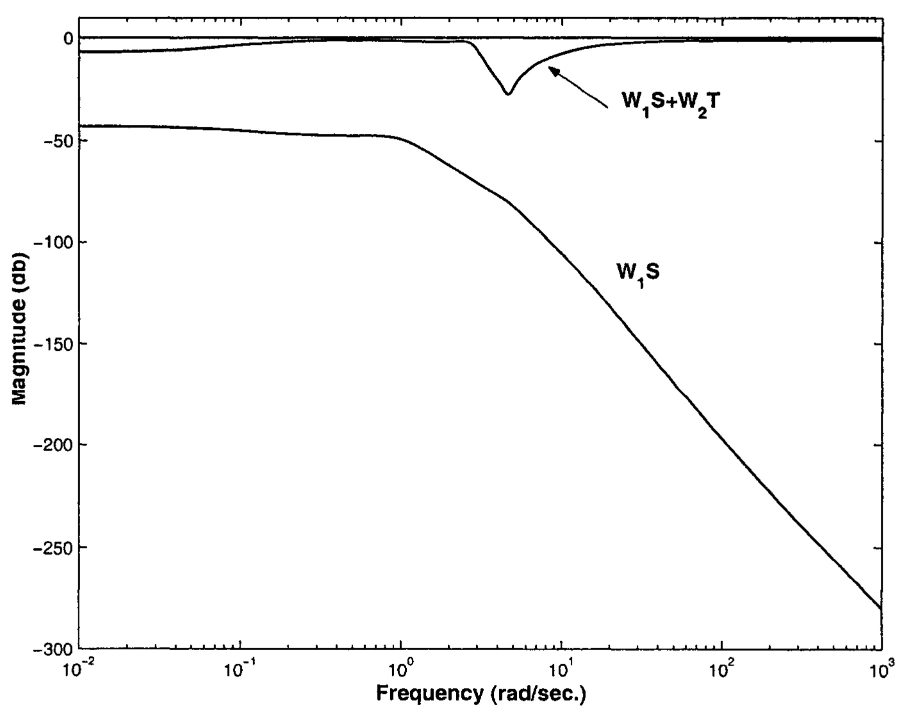

Figure 5.19: Robust and nominal performance criteria for detailed model Robust controller.

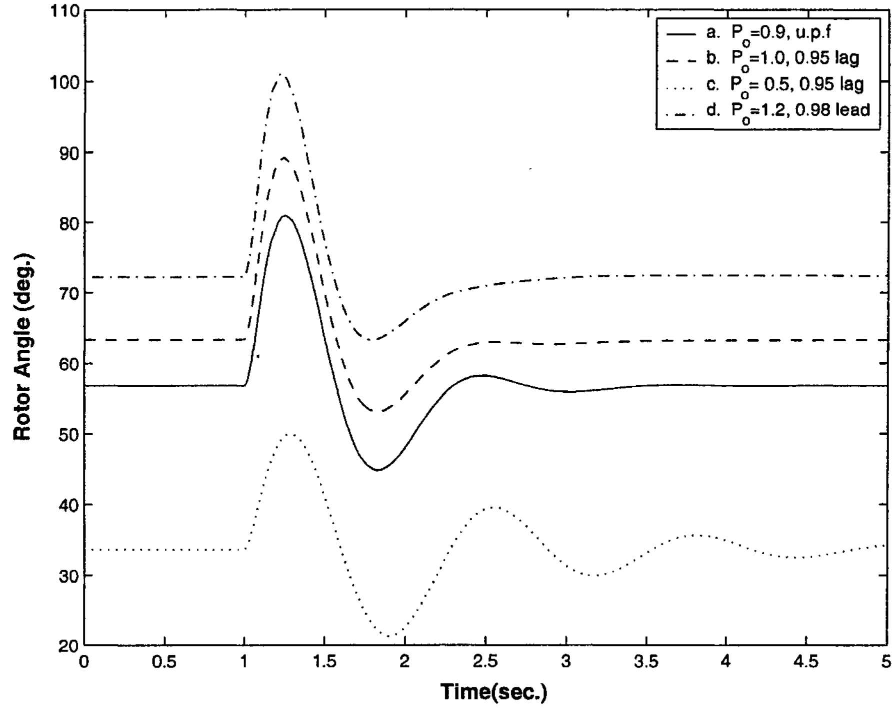

Figure 5.20: Rotor angle with robust controller for detailed model.

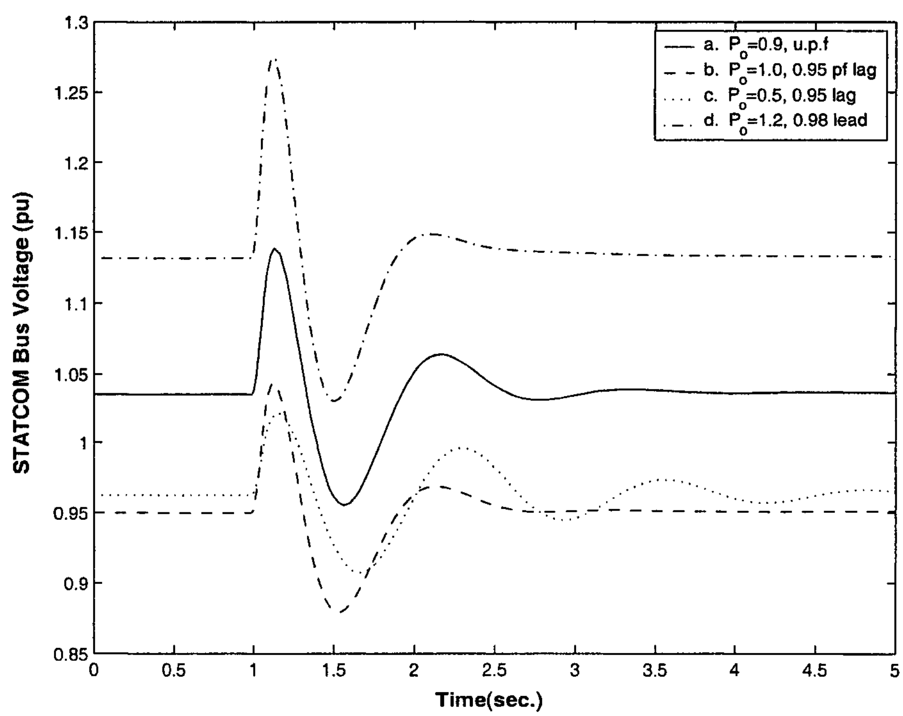

Figure 5.21: STATCOM bus voltage corresponding to Fig. 5.20.

5.2.1 Fault studies for the detailed model with Robust controller

The robust controller designed was tested for a three phase fault for 0.1 sec at the infinite bus of the power system. Figures 5.22 - 5.23 shows the generator rotor angle and STATCOM bus voltage variations for a wide range of power output conditions. The following cases has been considered. a) Nominal operating conditions, b) 1.0 p.u at 0.95 lagging power factor, c) 0.5 p.u. at 0.95 lagging power factor and d) 1.2 power output at 0.98 leading power factor.

The response shows that even for very heavily overloaded condition of $P_o = 1.2$ p.u. STATCOM bus voltage transient overshoot is less than 10 %. The electromechanical and electrical transients are controlled virtually in one or two oscillations with the robust controller. Even for large disturbances of 0.15 sec duration fault, the robust controller is able to stabilize the system . The voltage variations, however, are large.

The controller is designed to give robust performance for operating conditions near the nominal one. For operating conditions off the nominal one, the response may not be as good as depicted by curve c in Fig 5.22.

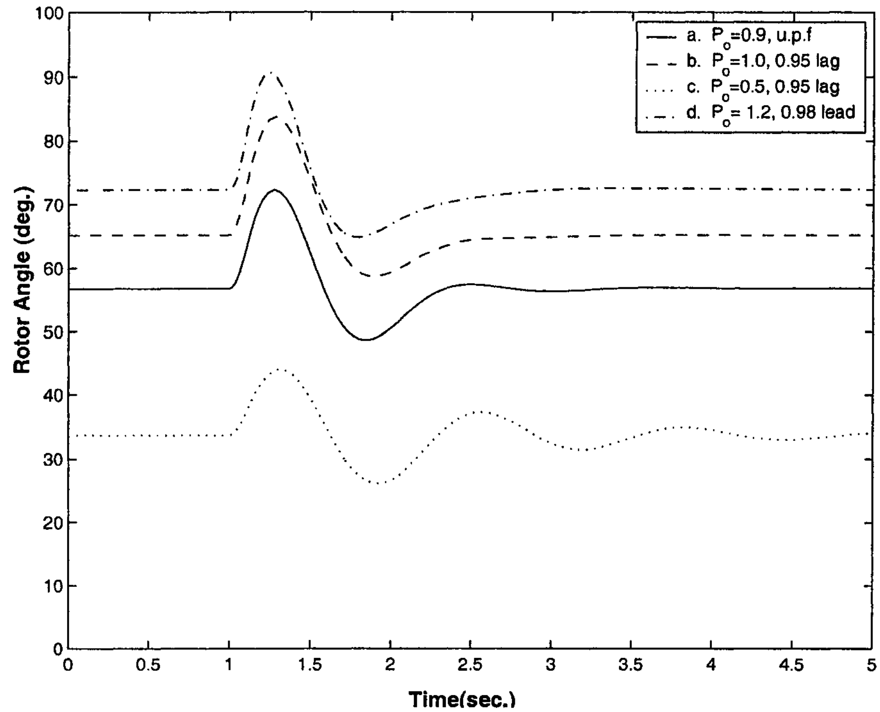

Figure 5.22: Rotor angle variation with robust controller for the detailed model (for three phase fault at infinite bus.)

model (for 3 phase fault at infinite bus.)

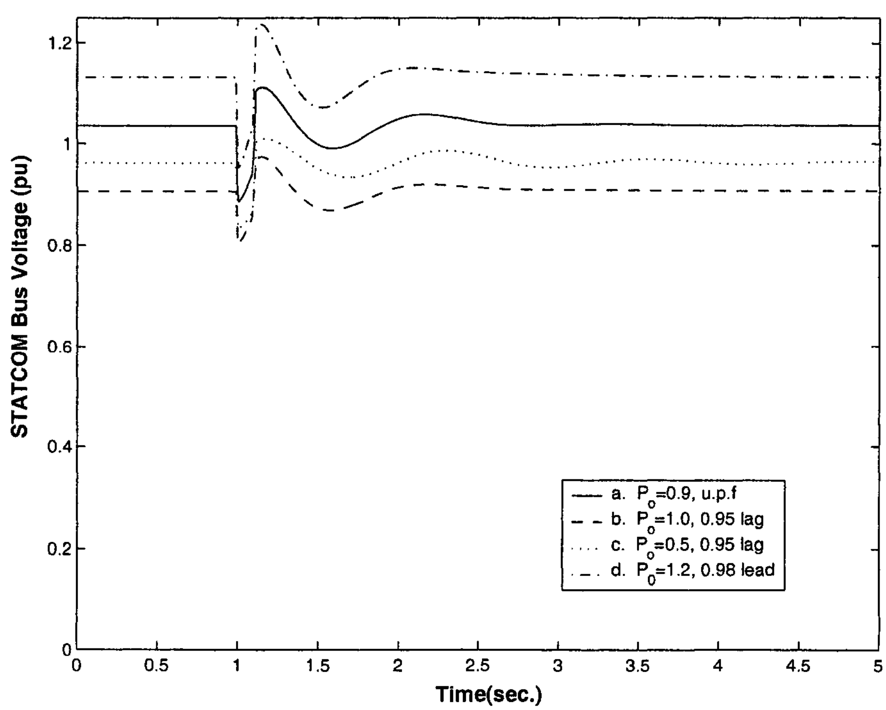

Figure 5.23: STATCOM bus voltage variation corresponding to Fig. 5.22.)

Chapter 6

Conclusions and Future Work

The dynamic behaviour of a single machine infinite bus power system installed with a STATCOM at the mid-point of the transmission line has been investigated in this thesis. Dynamic models has been derived for the approximate and the detailed representations of the power system. Comparative study for the different combinations of PID controller has been presented for both the models.

For the approximate model, two control inputs has been identified, one in the speed loop and the other in the voltage loop. It has been found that controller in the voltage loop alone is not effective in providing damping to the system but its presence is found to be necessary for the voltage regulation. A controller in the speed loop has effective control over the electrical and electro- mechanical transients. For a nominal unity gain in the voltage loop, a PD controller in the speed loop gave reasonably good damping characteristics.

For the detailed model also two control inputs to the STATCOM has been identified, one is the magnitude and the other is the phase for the STATCOM control voltage. It was observed that PID control for phase alone is not effective in providing damping. The proportional controller was observed to provide damping to the system but other transient indices were poor. The PID control was generally not found satisfactory in terms of both steady state and transient performance.

A novel method of designing robust damping control strategies for STATCOM controller is proposed for both the approximate and detailed models. The controller designed was tested for a number of disturbance conditions including symmetrical three-phase faults. The robust design has been found to be very effective for a range of operating conditions of the power system. The operating conditions for which the controller provides good performance depends on the spectrum of perturbed plants selected in the design process. The robust design has been found to be superior to the conventional PI controllers, where the controller coefficient normally need to be retuned for various operating conditions. The graphical loop-shaping method is simple and straightforward to implement.

The robust STATCOM controller designed through both the approximate and exact models did provide extra damping to the system. The design through the approximate model is simple in terms of the dimension, and was carried out as an initial study. Detailed study was more sensitive to variations of AVR and controller DC voltages.

6.1 Recommendations for future work

In the following, some recommendations are given for future research in the area.

- Further research is needed to evaluate the impact of phase angle (ψ) control of STATCOM voltage for the dynamic performance of the system.
- The effect of STATCOM on a multimachine system stability needs investigation. The location(s) of the STATCOM device(s) in a multimachine system requires careful study.
- In this study SMIB system with STATCOM located at the mid-point of the transmission line was considered. The impact of the location of the STATCOM other than mid-point of the transmission line on the dynamic performance can also be studied.
- The robust controller design of STATCOM for damping control with other FACTS devices such as unified power flow controller (UFPC) and static synchronous series compensator SSSC, etc. also needs investigation.

Appendix A

Derivation of the Simplified Dynamic Model of SMIB installed with STATCOM

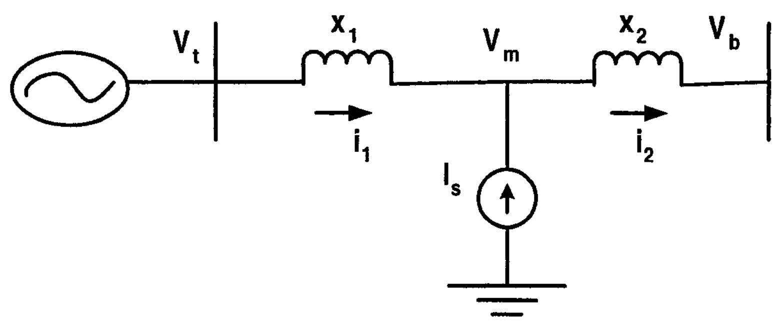

Figure A.1: Equivalent Circuit Diagram of the System of fig. 2.5

From Fig. A.1

$$i_2 = i_1 + I_S \tag{A.1}$$

Now

$$V_m = V_t - j i_1 X_1 \tag{A.2}$$

$$V_m = V_b + j i_2 X_2 \tag{A.3}$$

Equating equation A.2 and A.3 and substituting the value of i_2:

$$V_t - j i_1 X_1 = V_b + j X_2 (i_1 + i_S) \tag{A.4}$$

But

$$V_t = V_d + j V_q \tag{A.5}$$

$$V_t = x_q i_{1q} + j(e_q{}' - x_d{}' i_{1d}) \tag{A.6}$$

$$i_1 = i_{1d} + j i_{1q} \tag{A.7}$$

$$i_S = I_S \angle -\theta = I_S(\cos\theta - j\sin\theta) \tag{A.8}$$

where θ is the angle of the mid bus or STATCOM bus.

$$V_b = V\sin\delta + jV\cos\delta = V_{bd} + jV_{bq} \tag{A.9}$$

where δ = load angle.

Substituting all into equation A.4

$$x_q i_{1q} + j(e_q{}' - x_d{}' i_{1d}) - j(i_{1d} + j i_{1q}) X_1 =$$

$$V_{bd} + jV_{bq} + jX_2[i_{1d} + j i_{1q} + I_S\cos\theta - jI_S\sin\theta] \tag{A.10}$$

$$(X_1 + x_q)i_{1q} + j[e_q{}' - x_d{}' i_{1d} - X_1 i_{1d}] =$$

$$V_{bd} - X_2 i_{1q} + I_S \sin\theta + j[V_{bq} + X_2 i_{1d} + X_2 I_S \cos\theta] \quad \text{(A.11)}$$

Comparing the real and imaginary parts.

From Real part:

$$(x_q + X_1)i_{1q} = V_{bd} - X_2 i_{1q} + I_S \sin\theta \quad \text{(A.12)}$$

$$i_{1q} = \frac{V_{bd} + I_S \sin\theta}{X_1 + X_2 + x_q} \quad \text{(A.13)}$$

and from Imaginary part:

$$e_q{}' - (x_d{}' + X_1)i_{1d} = V_{bq} + X_2 i_{1d} + X_2 I_S \cos\theta \quad \text{(A.14)}$$

$$i_{1d} = \frac{e_q{}' - V_{bq} - X_2 I_S \cos\theta}{X_1 + X_2 + x_d{}'} \quad \text{(A.15)}$$

Expression for V_m:

from equation A.3

$$V_m = V_b + j i_2 X_2 \quad \text{(A.16)}$$

$$V_{md} + jV_{mq} = V_{bd} + jV_{bq} + j(i_{1d} + j i_{1q} + I_S \cos\theta - jI_S \sin\theta)X_2 \quad \text{(A.17)}$$

$$V_{md} + jV_{mq} = (V_{bd} - X_2 i_{1q} + X_2 I_S \sin\theta) +$$

$$j(V_{bq} + X_2 i_{1d} + X_2 I_S \cos\theta) \quad \text{(A.18)}$$

Comparing real and imaginary parts:

$$V_{md} = V_{bd} - (i_{1q} - I_S \sin\theta)X_2 \quad \text{(A.19)}$$

$$V_{mq} = V_{bq} + (i_{1d} + I_S \cos\theta)X_2 \quad \text{(A.20)}$$

Substituting the value of i_{1d} and i_{1q} from equation A.13 and A.15:

$$V_{md} = V_{bd} - \left[\frac{V_{bd} + I_S X_2 \sin\theta}{X_1 + X_2 + x_q} - I_S \sin\theta\right] X_2 \tag{A.21}$$

$$V_{md} = V_{bd} - \left[\frac{V_{bd} + I_S X_2 \sin\theta - (X_1 + X_2 + x_q) I_S \sin\theta}{X_1 + X_2 + x_q}\right] X_2 \tag{A.22}$$

$$V_{md} = V_{bd} - \left[\frac{V_{bd} - (X_1 + x_q) I_S \sin\theta}{X_1 + X_2 + x_q}\right] X_2 \tag{A.23}$$

$$V_{md} = \frac{(V_{bd} + X_2 I_S \sin\theta)(X_1 + x_q)}{X_1 + X_2 + x_q} \tag{A.24}$$

Similarly,

$$V_{mq} = V_{bq} + \left[\frac{e_q{}' - V_{bq} - X_2 I_S \cos\theta}{X_1 + X_2 + x_d{}'} + I_S \cos\theta\right] X_2 \tag{A.25}$$

$$V_{mq} = \frac{e_q{}' + V_{bq}(X_1 + x_d{}') + (X_1 + x_d{}') X_2 I_S \cos\theta}{X_1 + X_2 + x_d{}'} \tag{A.26}$$

The non-linear model is given by the following equations:

$$\dot{\delta} = \omega_b \omega \tag{A.27}$$

$$\dot{\omega} = \frac{1}{M}\left[P_m - P_e - D\omega\right] \tag{A.28}$$

$$\dot{I_S} = \frac{1}{T}\left[-I_S + Ku\right] \tag{A.29}$$

where

$$P_e = \frac{e_q{}' V_m}{x_d{}' + X_1} \sin\theta + \frac{V_m^2}{2} \frac{x_d{}' - x_q}{(x_d{}' + X_1)(x_q + X_1)} \sin 2\theta \tag{A.30}$$

$$V_{md} = \frac{(X_1 + x_q) V \sin\delta + I_S X_2 \sin\theta (X_1 + x_q)}{X_1 + X_2 + x_q} \tag{A.31}$$

$$V_{mq} = \frac{(X_1 + x_d{}') V \cos\delta + e_q{}' X_2 + I_S X_2 \cos\theta (X_1 + x_d{}')}{X_1 + X_2 + x_d{}'} \tag{A.32}$$

$$V_m = V_{md} + j V_{mq} \tag{A.33}$$

$$\theta = \tan^{-1}\left(\frac{V_{md}}{V_{mq}}\right) \tag{A.34}$$

For Linear Model:

$$\tan\theta = \frac{V_{md}}{V_{mq}} \tag{A.35}$$

$$\tan\theta = \left(\frac{X_1 + X_2 + x_d{'}}{X_1 + X_2 + x_q}\right) \times \tag{A.36}$$

$$\left(\frac{(X_1 + x_q)V\sin\delta + I_S X_2 \sin\theta(X_1 + x_q)}{(X_1 + x_d{'})V\cos\delta + e_q{'}X_2 + X_2(X_1 + x_d{'})I_S\cos\theta}\right) \tag{A.37}$$

Let

$$d_1 = \frac{X_1 + X_2 + x_d{'}}{X_1 + X_2 + x_q} \tag{A.38}$$

$$d_2 = (X_1 + x_q)V \tag{A.39}$$

$$d_3 = X_2(X_1 + x_q) \tag{A.40}$$

$$d_4 = e_q{'}X_2 \tag{A.41}$$

$$d_5 = (X_1 + x_d{'})V \tag{A.42}$$

$$d_6 = X_2(X_1 + x_d{'}) \tag{A.43}$$

$$\tan\theta = d_1 \frac{d_2\sin\delta + d_3 I_S \sin\theta}{d_4 + d_5\cos\delta + d_6 I_S\cos\theta} \tag{A.44}$$

(A.45)

By Cross multiplication:

$$d_4\tan\theta + d_5\tan\theta\cos\delta + d_6 I_S\sin\theta = d_1 d_2\sin\delta + d_1 d_3 I_S\sin\theta \tag{A.46}$$

$$d_4\tan\theta + d_5\tan\theta\cos\delta + (d_6 I_S - d_1 d_3 I_S)\sin\theta = d_1 d_2\sin\delta \tag{A.47}$$

Differentiating equation A.47 with respect to δ assuming θ depends on δ

$$d_4\sec^2\theta\frac{\partial\theta}{\partial\delta} + d_5\cos\delta\sec^2\theta\frac{\partial\theta}{\partial\delta} + d_5\tan\theta(-\sin\delta) +$$

$$(d_6 I_S - d_1 d_3 I_S)\cos\theta\frac{\partial\theta}{\partial\delta} = d_1 d_2\cos\delta \tag{A.48}$$

$$\left[d_4 \sec^2\theta + d_5 \cos\delta \sec^2\theta + (d_6 I_S - d_1 d_3 I_S)\cos\theta\right]\frac{\partial\theta}{\partial\delta} =$$

$$d_1 d_2 \cos\delta + d_5 \tan\theta \sin\delta \qquad \text{(A.49)}$$

Let

$$d_7 = d_4 \sec^2\theta + d_5 \cos\delta \sec^2\theta + (d_6 I_S - d_1 d_3 I_S)\cos\theta \qquad \text{(A.50)}$$

Therefore, equation A.50 becomes:

$$\frac{\partial\theta}{\partial\delta} = \frac{1}{d_7}\left[d_1 d_2 \cos\delta + d_5 \tan\theta \sin\delta\right] \qquad \text{(A.51)}$$

Similarly differentiating equation A.47 with respect to I_S assuming θ depends on I_S:

$$d_4 \sec^2\theta \frac{\partial\theta}{\partial I_S} + d_5 \cos\delta \sec^2\theta \frac{\partial\theta}{\partial I_S} + (d_6 I_S - d_1 d_3 I_S)\cos\theta \frac{\partial\theta}{\partial I_S} +$$

$$\sin\theta(d_6 - d_1 d_3) = 0 \qquad \text{(A.52)}$$

$$\left[d_4 \sec^2\theta + d_5 \cos\delta + (d_6 I_S - d_1 d_3 I_S)\cos\theta\right]\frac{\partial\theta}{\partial I_S} = \sin\theta(d_1 d_3 - d_6) \qquad \text{(A.53)}$$

$$\frac{\partial\theta}{\partial I_S} = \frac{1}{d_8}(d_1 d_3 - d_6) \qquad \text{(A.54)}$$

where

$$d_8 = d_4 \sec^2\theta + d_5 \cos\delta + (d_6 I_S - d_1 d_3 I_S)\cos\theta \qquad \text{(A.55)}$$

By linearizing equation A.31, A.32 and A.33, around equilibrium point. We got

$$\Delta V_m = K_{V_m\delta}\Delta\delta + K_{V_m I_S}\Delta I_S \qquad \text{(A.56)}$$

and

$$\Delta P_e = K_{P_e\delta}\Delta\delta + K_{P_eI_S}\Delta I_S \tag{A.57}$$

where

$$K_{V_m\delta} = \frac{\partial V_m}{\partial \delta} \tag{A.58}$$

$$K_{V_mI_S} = \frac{\partial V_m}{\partial I_S} \tag{A.59}$$

$$K_{P_e\delta} = \frac{\partial P_e}{\partial \delta} \tag{A.60}$$

$$K_{P_eI_S} = \frac{\partial P_e}{\partial I_S} \tag{A.61}$$

Calculating the coefficients

$$K_{P_e\delta} = \frac{\partial P_e}{\partial \delta} \tag{A.62}$$

$$K_{P_e\delta} = \frac{\partial P_e}{\partial \theta}\frac{\partial \theta}{\partial \delta} \tag{A.63}$$

$$K_{P_e\delta} = \frac{\partial}{\partial\theta}\left[\frac{e_q{}'V_m}{X_1 + x_d{}'}\sin\theta + \frac{V_m^2}{2}\frac{(x_d{}' - x_q)}{(x_d{}' + X_1)(x_q + X_1)}\sin 2\theta\right] \times \frac{1}{d_7}\left[d_5\tan\theta\sin\delta + d_1 d_2\cos\delta\right] \tag{A.64}$$

$$K_{P_e\delta} = \frac{1}{d_7}\left[\frac{e_q{}'V_m}{X_1 + x_d{}'}\cos\theta + \frac{V_m^2(x_d{}' - x_q)}{(x_d{}' + X_1)(x_q + X_1)}\cos 2\theta\right] \times \left[d_5\tan\theta\sin\delta + d_1 d_2\cos\delta\right] \tag{A.65}$$

Similarly,

$$K_{P_eI_S} = \frac{\partial P_e}{\partial I_S} \tag{A.66}$$

$$= \frac{\partial P_e}{\partial \theta}\frac{\partial \theta}{\partial I_S} \tag{A.67}$$

$$K_{P_eI_S} = \frac{1}{d_8}\left[\frac{e_q{}'V_m}{X_1 + x_d{}'}\cos\theta + \frac{V_m^2(x_d{}' - x_q)}{(x_d{}' + X_1)(x_q + X_1)}\cos 2\theta\right][d_1 d_3 - d_6]\sin\theta \quad \text{(A.68)}$$

In order to obtain $\frac{\partial V_m}{\partial \delta}$ and $\frac{\partial V_m}{\partial I_S}$, applying the relation for the magnitude of the mid bus voltage V_m:

$$V_m^2 = V_{md}^2 + V_{mq}^2 \quad \text{(A.69)}$$

Differentiating partially with respect to δ and I_S

$$V_m \frac{\partial V_m}{\partial \delta} = V_{md}\frac{\partial V_{md}}{\partial \delta} + V_{mq}\frac{\partial V_{mq}}{\partial \delta} \quad \text{(A.70)}$$

$$V_m \frac{\partial V_m}{\partial I_S} = V_{md}\frac{\partial V_{md}}{\partial I_S} + V_{mq}\frac{\partial V_{mq}}{\partial I_S} \quad \text{(A.71)}$$

where

$$\frac{\partial V_{md}}{\partial \delta} = \left(\frac{X_1 + x_q}{X_1 + X_2 + x_q}\right) V\cos\delta + \frac{I_S X_2 (X_1 + x_q)}{X_1 + X_2 + x_q}\cos\theta\frac{\partial \theta}{\partial \delta} \quad \text{(A.72)}$$

$$\frac{\partial V_{md}}{\partial \delta} = \left(\frac{X_1 + x_q}{X_1 + X_2 + x_q}\right) V\cos\delta + \frac{I_S X_2 (X_1 + x_q)}{X_1 + X_2 + x_q} \times \cos\theta\frac{1}{d_7}[d_5\tan\theta\sin\delta + d_1 d_2\cos\delta] \quad \text{(A.73)}$$

and

$$\frac{\partial V_{mq}}{\partial \delta} = \frac{1}{X_1 + X_2 + x_d{}'}[-(X_1 + x_d{}')V\sin\delta - I_S X_2\left(X_1 + x_d{}'\right)\sin\theta \times \frac{1}{d_7}\left(d_5\tan\theta\sin\delta + d_1 d_2\cos\delta\right)] \quad \text{(A.74)}$$

$$\frac{\partial V_{mq}}{\partial \delta} = -\frac{(X_1 + x_d{}')}{(X_1 + X_2 + x_d{}')}\left[V\sin\delta + \frac{I_S X_2\sin\theta}{d_7}\cdot\left(d_5\tan\theta\sin\delta + d_1 d_2\cos\delta\right)\right] \quad \text{(A.75)}$$

$$\frac{\partial V_{md}}{\partial I_S} = \frac{1}{X_1+X_2+x_q}\left[X_2(X_1+x_q)\sin\theta + I_S X_2\left(X_1+x_q\right)\cos\theta\cdot\frac{\partial\theta}{\partial I_S}\right] \quad (A.76)$$

$$= \frac{(X_1+x_q)X_2}{X_1+X_2+x_q}\left[\sin\theta + \frac{I_S}{d_8}\cdot\cos\theta\cdot(d_1d_3-d_6)\sin\theta\right] \quad (A.77)$$

Similarly

$$\frac{\partial V_{mq}}{\partial I_S} = \frac{1}{X_1+X_2+x_d'}\left[X_2(X_1+x_d')\cos\theta - I_S X_2\left(X_1+x_d'\right)\sin\theta\cdot\frac{\partial\theta}{\partial I_S}\right] \quad (A.78)$$

$$= \frac{(X_1+x_d')X_2}{X_1+X_2+x_d'}\left[\cos\theta - \frac{I_S}{d_8}\cdot\sin\theta\cdot(d_1d_3-d_6)\sin\theta\right] \quad (A.79)$$

Substituting back into equation A.70 and A.71

$$K_{V_m\delta} = \frac{\partial V_m}{\partial\delta} \quad (A.80)$$

$$K_{V_m\delta} = \frac{V_{md}}{V_m}\cdot\frac{(X_1+x_q)}{(X_1+X_2+x_q)}\left[V\cos\delta + \frac{1}{d_7}I_S X_2\cos\theta\left(d_5\tan\theta\sin\delta + d_1d_2\cos\delta\right)\right]$$
$$-\frac{V_{mq}}{V_m}\cdot\frac{(X_1+x_d')}{(X_1+X_2+x_d')}\left[V\sin\delta + \frac{1}{d_7}I_S X_2\sin\theta\left(d_5\tan\theta\sin\delta + d_1d_2\cos\delta\right)\right] \quad (A.81)$$

$$K_{V_mI_S} = \frac{\partial V_m}{\partial I_S} \quad (A.82)$$

$$K_{V_mI_S} = \frac{V_{md}}{V_m}\cdot\frac{(X_1+x_q)X_2}{(X_1+X_2+x_q)}\left[\sin\theta + \frac{1}{d_8}I_S\cos\theta\left(d_1d_3-d_6\right)\sin\theta\right]$$
$$+\frac{V_{mq}}{V_m}\cdot\frac{(X_1+x_d')X_2}{(X_1+X_2+x_d')}\left[\cos\theta - \frac{1}{d_8}I_S\sin\theta\left(d_1d_3-d_6\right)\sin\theta\right] \quad (A.83)$$

Appendix B

Derivation of the Detailed Dynamic Model of SMIB installed with STATCOM

The voltage and current relationship for the power system with STATCOM shown in Fig. B.1 are expressed as

$$\bar{I}_{Lo} = \bar{I}_{Lod} + j\bar{I}_{Loq}$$

$$V_o = cV_{DC}(\cos\psi + j\sin\psi) = cV_{DC}\angle\psi \tag{B.1}$$

$$\frac{dV_{DC}}{dt} = \frac{I_{DC}}{C_{DC}} = \frac{c}{C_{DC}}(I_{Lod}\cos\psi + I_{Loq}\sin\psi) \tag{B.2}$$

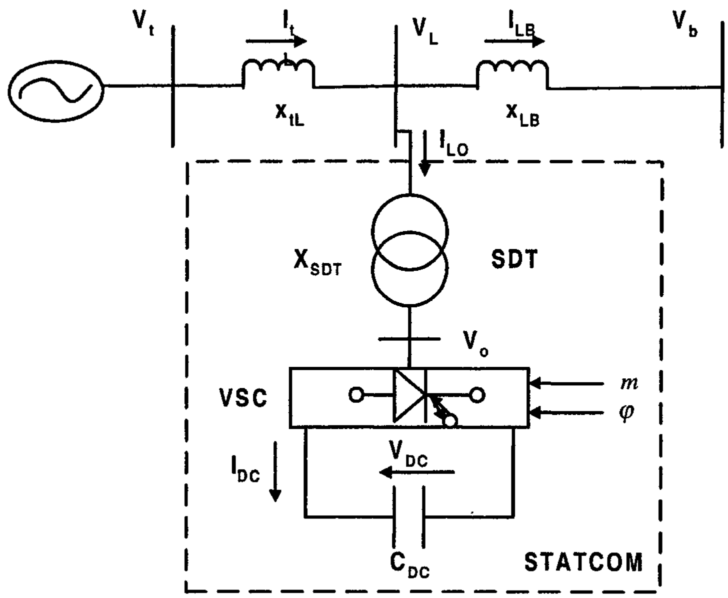

Figure B.1: STATCOM installed in a single machine infinite bus power system.

where

$$
\begin{aligned}
c &= mk \\
k &= \frac{\text{AC Voltage}}{DCVoltage} \\
m &= \text{modulation ratio defined by PWM} \\
\psi &= \text{defined by PWM}
\end{aligned}
$$

From Fig. B.1,

$$\bar{V}_t = jX_{tL}\bar{I}_{tL} + jX_{LB}\bar{I}_{LB} + \bar{V}_B \tag{B.3}$$

Now

$$\bar{I}_{LB} = \bar{I}_{tL} - \bar{I}_{Lo} \tag{B.4}$$

$$\bar{I}_{Lo} = \frac{\bar{V}_L - \bar{V}_o}{jX_{SDT}} \tag{B.5}$$

$$\bar{V}_L = \bar{V}_t - X_{tL}\bar{I}_{tL} \tag{B.6}$$

Substituting in the expression for I_{LB}

$$\bar{I}_{LB} = \bar{I}_{tL} - \frac{V_t - jX_{tL}\bar{I}_{tL} - V_o}{jX_{SDT}} = \frac{jX_{SDT}\bar{I}_{tL} - V_t + jX_{tL}\bar{I}_{tL}}{jX_{SDT}} \tag{B.7}$$

Eq. B.4 becomes

$$V_t = jX_{tL}\bar{I}_{tL} + \frac{jX_{LB}}{jX_{SDT}}(j\bar{I}_{tL}X_{SDT} - \bar{V}_t + jX_{tL}\bar{I}_{tL} + V_o) \tag{B.8}$$

$$V_t = jX_{tL}\bar{I}_{tL} + jX_{LB}\bar{I}_{tL} - \frac{X_{LB}}{X_{SDT}}\bar{V}_t + \frac{jX_{tL}X_{LB}}{X_{SDT}}\bar{I}_{tL} + \frac{X_{LB}}{X_{SDT}} + V_B \tag{B.9}$$

$$\left(1 + \frac{X_{LB}}{X_{SDT}}\right)\bar{V}_t - \frac{X_{LB}}{X_{SDT}}V_o - \bar{V}_B = j\left(X_{tL} + X_{LB} + \frac{X_{tL}}{X_{SDT}}\right)\bar{I}_{tL} \tag{B.10}$$

Let

$$Z = \left(1 + \frac{X_{LB}}{X_{SDT}}\right) \tag{B.11}$$

$$A = \left(X_{tL} + X_{LB} + \frac{X_{tL}}{X_{SDT}}\right) \tag{B.12}$$

$$Z\bar{V}_t - \frac{X_{LB}}{X_{SDT}}V_o - \bar{V}_B = jA\bar{I}_{tL} \tag{B.13}$$

Now

$$\bar{V}_t = V_d + jV_q = x_q I_{tLq} + j(eq' - x_d' I_{tLd}) \tag{B.14}$$

$$\bar{V}_o = cV_{DC}\cos\psi + jcV_{DC}\sin\psi \tag{B.15}$$

$$\bar{V}_B = V_B\sin\delta + jV_B\cos\delta \tag{B.16}$$

$$\bar{I}_{tL} = I_{tLd} + jItLq \tag{B.17}$$

Substituting all in B.13

$$Z\left[x_q I_{tLq} + j(eq' - x_d' I_{tLd})\right] - \frac{X_{LB}}{X_{XSD}}\left(cV_{DC}\cos\psi + jcV_{DC}\sin\psi\right)$$
$$-(V_B \sin\delta + jV_B\cos\delta) = jA(I_{tLd} + jI_{tLq})$$

$$\left[Zx_q I_{tLq} - \frac{X_{LB}}{X_{SDT}} cV_{DC}\cos\psi - V_B\sin\delta\right] + j\left[Z(eq' - x_d' I_{tLd})\right.$$
$$\left. - \frac{X_{LB}}{X_{SDT}} cV_{DC}\sin\psi - V_B\cos\delta\right] = -AI_{tLq} + jAI_{tLd}$$

Comparing the real and imaginary parts,

for real part

$$Zx_q I_{tLq} - \frac{X_{LB}}{X_{SDT}} cV_{DC}\cos\psi - V_B\sin\delta = -AI_{tLq} \tag{B.18}$$

$$(Zx_q + A)I_{tLq} = \frac{X_{LB}}{X_{SDT}} cV_{DC}\cos\psi \tag{B.19}$$

$$I_{tLq} = \frac{\frac{X_{LB}}{X_{SDT}} cV_{DC}\cos\psi + V_B\sin\delta}{(Zx_q + A)} \tag{B.20}$$

$$I_{tLq} = \frac{\frac{X_{LB}}{X_{SDT}} cV_{DC}\cos\psi + V_B\sin\delta}{X_{tL} + X_{LB} + \frac{X_{tL}}{X_{SDT}} + \left(1 + \frac{X_{LB}}{X_{SDT}}\right) x_q} \tag{B.21}$$

Similarly from imaginary part

$$Z(eq' - x_d' I_{tLd}) - \frac{X_{LB}}{X_{SDT}} cV_{DC}\sin\psi - V_B\cos\delta = AI_{tLd} \tag{B.22}$$

$$(A + Zx_d')I_{tLd} = Zeq' - \frac{X_{LB}}{X_{SDT}} cV_{DC}\sin\psi - V_B\cos\delta \tag{B.23}$$

$$I_{tLd} = \frac{Zeq' - \frac{X_{LB}}{X_{SDT}} cV_{DC}\sin\psi - V_B\cos\delta}{A + Zx'_d} \tag{B.24}$$

$$I_{tLd} = \frac{\left(1 + \frac{X_{LB}}{X_{SDT}}\right) eq' - \frac{X_{LB}}{X_{SDT}} cV_{DC}\sin\psi - V_B\cos\delta}{X_{tL} + X_{LB} + \frac{X_{tL}}{X_{SDT}} + \left(1 + \frac{X_{LB}}{X_{SDT}}\right) x'_d} \tag{B.25}$$

Therefore the nonlinear model is given as:

$$\dot{\delta} = \omega_b \omega \tag{B.26}$$

$$\dot{\omega} = \frac{1}{M}\left[P_m - P_e - D\omega\right] \tag{B.27}$$

$$\dot{eq'} = \frac{1}{T_{do'}}\left[E_{fd} - eq' - (x_d - x'_d)I_{tLd}\right] \tag{B.28}$$

$$\dot{E}_{fd} = -\frac{1}{T_A}\left(E_{fd} - E_{fdo}\right) + \frac{K_A}{T_A}\left(V_{to} - V_t\right) \tag{B.29}$$

$$\dot{V}_{dc} = \frac{c}{C_{DC}}\left[I_{lod}\cos\psi + I_{loq}\sin\psi\right] \tag{B.30}$$

where

$$\begin{aligned} P_e &= v_d I_{tLd} + v_q I_{tLq} \\ &= eq' I_{tLd} + (x_d - x'_d) I_{tLd} I_{tLq} \\ V_t &= \sqrt{v_d^2 + v_q^2} = \sqrt{(eq' - x'_d I_{tLd})^2 + x'_q I_{tLq}^2} \end{aligned}$$

For Linear Model

$$I_{tLd} = \frac{\left(1 + \frac{X_{LB}}{X_{SDT}}\right) eq' - \frac{X_{LB}}{X_{SDT}} cV_{DC}\sin\psi - V_B\cos\delta}{X_{tL} + X_{LB} + \frac{X_{tL}}{X_{SDT}} + \left(1 + \frac{X_{LB}}{X_{SDT}}\right) x'_d} \tag{B.31}$$

$$I_{tLd} = \frac{1}{[A]}\left[Zeq' - \frac{X_{LB}}{X_{SDT}} cV_{DC}\sin\psi - V_B\cos\delta\right] \tag{B.32}$$

where

$$[A] = X_{tL} + X_{LB} + \frac{X_{tL}}{X_{SDT}} + \left(1 + \frac{X_{LB}}{X_{SDT}}\right) x_d^{'} \tag{B.33}$$

&

$$Z = 1 + \frac{X_{LB}}{X_{SDT}} \tag{B.34}$$

Linearizing

$$\Delta I_{tLd} = \frac{1}{[A]}[Z\Delta eq^{'} - \frac{X_{LB}}{X_{SDT}} c_o V_{DCo} \cos\psi_o \Delta\psi - \frac{X_{LB}}{X_{SDT}} c_o \sin\psi_o \Delta V_{DC} \\ - \frac{X_{LB}}{X_{SDT}} V_{DCo} \sin\psi_o \Delta c + V_B \sin\delta_o \Delta\delta] \tag{B.35}$$

$$\begin{aligned} \Delta I_{tLd} &= \frac{Z}{[A]}\Delta eq^{'} + \frac{V_B \sin\delta_o}{[A]}\Delta\delta + \left(-\frac{X_{LB}}{X_{SDT}[A]} V_{DCo}\sin\psi_o\right)\Delta c \times \\ &\quad \left(-\frac{X_{LB}}{X_{SDT}[A]} c_o V_{DCo}\cos\psi_o\right)\Delta\psi + \\ &\quad \left(-\frac{X_{LB}}{X_{SDT}[A]} c_o \sin\psi_o\right)\Delta V_{DC} && \text{(B.36)} \\ \Delta I_{tLd} &= C_5\Delta eq^{'} + C_6\Delta\delta + C_7\Delta\psi + C_8\Delta c + C_9\Delta V_{DC} && \text{(B.37)} \end{aligned}$$

Where

$$C_5 = \frac{Z}{[A]}, \qquad C_6 = \frac{V_B \sin\delta_o}{[A]}, \qquad C_7 = -\frac{X_{LB} c_o V_{DCo} \cos\psi_o}{X_{SDT}[A]}$$

$$C_8 = \frac{X_{LB} V_{DCo} \sin\psi_o}{X_{SDT}[A]}, \qquad C_9 = -\frac{X_{LB} c_o \sin\psi_o}{X_{SDT}[A]}$$

Similarly

$$I_{tLq} = \frac{V_B \sin\delta + \frac{X_{LB}}{X_{SDT}} c V_{DC} \cos\psi}{X_{tL} + X_{LB} + \frac{X_{tL} X_{LB}}{X_{SDT}} + \left(1 + \frac{X_{LB}}{X_{SDT}}\right) x_q} \tag{B.38}$$

$$I_{tLq} = \frac{1}{[B]} \left[V_B \sin\delta + \frac{X_{LB}}{X_{SDT}} c V_{DC} \cos\psi \right] \tag{B.39}$$

Linearizing

$$\begin{aligned} \Delta I_{tLq} &= \frac{1}{[B]} \left[V_B \cos\delta_o \Delta\delta - \frac{X_{LB}}{X_{SDT}} c_o V_{DCo} \sin\psi_o \Delta\psi \right. \\ &\quad \left. + \frac{X_{LB}}{X_{SDT}} c_o \sin\psi_o \Delta V_{DC} + \frac{X_{LB}}{X_{SDT}} V_{DCo} \sin\psi_o \Delta c_o \right] \end{aligned} \tag{B.40}$$

$$\begin{aligned} \Delta I_{tLq} &= \frac{V_B \cos\delta_o}{[B]} \Delta\delta + \left(-\frac{X_{LB}}{X_{SDT}[B]} c_o V_{DCo} \sin\psi_o \right) \Delta\psi \\ &+ \left(\frac{X_{LB}}{X_{SDT}[A]} V_{DCo} \cos\psi_o \right) \Delta c \\ &+ \left(\frac{x_{LB}}{X_{SDT}[A]} c_o \cos\psi_o \right) \Delta V_{DC} \end{aligned} \tag{B.41}$$

$$\Delta I_{tLq} = C_1 \Delta\delta + C_2 \Delta\psi + C_3 \Delta c + C_4 \Delta V_{DC} \tag{B.42}$$

where

$$C_1 = \frac{V_B \cos\delta_o}{[B]}, \qquad C_2 = -\frac{X_{LB}}{X_{SDT}[B]} c_o V_{DCo} \sin\psi_o$$

$$C_3 = \frac{X_{LB} V_{DCo} \cos\psi_o}{X_{SDT}[A]}, \qquad C_4 = \frac{X_{LB} c_o \cos\psi_o}{X_{SDT}[A]}$$

The linearized model of (B.27) to (B.30) is

$$\Delta\dot{\delta} = \omega_b \Delta\omega \tag{B.43}$$

$$\Delta\dot{\omega} = -\frac{1}{M}\left[\Delta P_e + D\Delta\omega\right] \tag{B.44}$$

$$\Delta\dot{eq}' = \frac{1}{T_{do}}\left[-\Delta eq' + \Delta E_{fd}\right] \tag{B.45}$$

$$\Delta\dot{E}_{fd} = -\frac{1}{T_A}\Delta E_{fd} - \frac{K_A}{T_A}\Delta V_t \tag{B.46}$$

$$\tag{B.47}$$

$$Delta\dot{V}_{dc} = \frac{c}{C_{DC}}\left[I_{lod}\cos\psi + I_{loq}\sin\psi\right] \tag{B.48}$$

Since

$$eq = eq' + (x_d - x_d')I_{tld}$$

Therefore by linearizing

$$\Delta eq = \Delta eq' + (x_d - x_d')\Delta I_{tld}$$

Calculation of ΔP_e

$$P_e = eq' I_{tlq} + (x_q - x_d')I_{tld}I_{tlq} \tag{B.49}$$

linearizing

$$\Delta P_e = eq_o'\Delta I_{tlq} + I_{tlqo}\Delta eq' + (x_q - x_d')I_{tldo}\Delta I_{tlq} + (x_q - x_d')I_{tlqo}\Delta I_{tld} \tag{B.50}$$

$$= \left[eq_o' + (x_q - x_d')I_{tldo}\right]\Delta I_{tlq} + I_{tlqo}\Delta eq' + (x_q - x_d')I_{tlqo}\Delta I_{tld} \tag{B.51}$$

Substituting the value of ΔI_{tld} & ΔI_{tlq}

$$\Delta P_e = \left[eq_o' + (x_q - x_d')I_{tldo}\right]\{C_1\Delta\delta + C_2\Delta\psi + C_3\Delta c + C_4\Delta V_{DC}\} + I_{tlqo}\Delta eq'$$
$$+ (x_q - x_d')I_{tlqo}\left\{C_5\Delta eq' + C_6\Delta\delta + C_7\Delta\psi + C_8\Delta c + C_9\Delta V_{DC}\right\} \quad \text{(B.52)}$$
$$= \left\{eq_o' + (x_q - x_d')I_{tldo}\, C_1 + (x_q - x_d')I_{tldo}\, C_6\right\}\Delta\delta + \left[I_{tlqo}\left\{1 + (x_q - x_d')C_5\right\}\right]\Delta eq'$$
$$+ \left[\left\{eq_o' + (x_q - x_d')I_{tldo}\right\}C_4 + (x_q - x_d')I_{tlqo}C_9\right]\Delta V_{DC}$$
$$+ \left[\left\{eq_o' + (x_q - x_d')I_{tldo}\right\}C_3 + (x_q - x_d')I_{tlqo}C_8\right]\Delta c$$
$$+ \left[\left\{eq_o' + (x_q - x_d')I_{tldo}\right\}C_2 + (x_q - x_d')I_{tlqo}C_7\right]\Delta\psi \quad \text{(B.53)}$$

Let

$$C_{111} = eq_o' + (x_q - x_d')I_{tldo}$$
$$C_{112} = (x_q - x_d')I_{tlqo}$$

Therefore

$$\Delta P_e = (C_{111}\, C_1 + C_{112}\, C_6)\Delta\delta + \left[I_{tlqo}\left\{1 + (x_q - x_d')C_5\right\}\right]\Delta eq'$$
$$+ (C_{111}C_4 + C_{112}C_9)\Delta V_{DC} + (C_{111}C_3 + C_{112}C_8)\Delta c$$
$$+ (C_{111}C_2 + C_{112}C_7)\Delta\psi \quad \text{(B.54)}$$
$$\Delta P_e = K_1\Delta\delta + K_2\Delta eq' + K_{pDC}\Delta V_{DC} + K_{pc}\Delta c + K_{p\psi}\Delta\psi \quad \text{(B.55)}$$

where

$$K_1 = C_{111}\, C_1 + C_{112}\, C_6, \qquad K_2 = I_{tlqo}\left\{1 + (x_q - x_d')C_5\right\}$$
$$K_{pDC} = C_{111}C_4 + C_{112}C_9, \qquad K_{pc} = C_{111}C_3 + C_{112}C_8$$
$$K_{p\psi} = C_{111}C_2 + C_{112}C_7$$

Calculation of Δeq

$$\begin{aligned}
\Delta eq &= \Delta eq' + (x_d - x_d')\Delta I_{tld} \\
&= \Delta eq' + (x_d - x_d')\left(C_5\Delta eq' + C_6\Delta\delta + C_7\Delta\psi + C_8\Delta c + C_9\Delta V_{DC}\right) \\
&= \left\{1 + (x_d - x_d')C_5\right\}\Delta eq' + (x_d - x_d')C_6\Delta\delta + (x_d - x_d')C_7\Delta\psi \\
&\qquad + (x_d - x_d')C_8\Delta c + (x_d - x_d')C_9\Delta V_{DC}
\end{aligned}$$

Let

$$(x_d - x_d') = J \tag{B.56}$$

$$\begin{aligned}
\Delta eq &= (1 + JC_5)\Delta eq' + JC_6\Delta\delta + JC_7\Delta\psi + JC_8\Delta c + JC_9\Delta V_{DC} \\
&= K_3\Delta eq' + K_4\Delta\delta + K_{q\psi}\Delta\psi + K_{qc}\Delta c + K_{qDC}\Delta V_{DC}
\end{aligned}$$

where

$$K_3 = 1 + JC_5, \qquad K_4 = JC_6, \qquad K_{q\psi} = JC_7$$

$$K_{qc} = JC_8, \qquad K_{qDC} = JC_9$$

Calculation of ΔV_t

$$\Delta V_t = \frac{V_{qo}}{V_{to}}\Delta V_d + \frac{V_{qo}}{V_{to}}\Delta V_q \tag{B.57}$$

$$= \frac{V_{qo}}{V_{to}}(x_q\Delta I_{tlq}) + \frac{V_{qo}}{V_{to}}(\Delta eq' - x_d'\Delta I_{tld}) \tag{B.58}$$

$$= \frac{V_{qo}}{V_{to}}(x_qC_5\Delta eq' + C_6\Delta\delta + C_7\Delta\psi + C_8\Delta c + C_9\Delta V_{DC}) + \frac{V_{qo}}{V_{to}}(\Delta eq' - x_d'\Delta I_{tld}) \tag{B.59}$$

Let $L = \frac{1}{V_{to}}$

therefore

$$\Delta V_t = L(V_{do}x_qC_1 - V_{qo}x_d^{'}C_6)\Delta\delta + LV_{qo}(1 - x_d^{'}C_5)\Delta eq^{'}$$

$$+L(V_{do}x_qC_4 - V_{qo}x_d^{'}C_9)\Delta V_{DC} + L(V_{do}x_qC_3 - V_{qo}x_d^{'}C_8)\Delta c \tag{B.60}$$

$$+L(V_{do}x_qC_2 - V_{qo}x_d^{'}C_7)\Delta\psi$$

$$\Delta V_t = K_5\Delta\delta + K_6\Delta eq^{'} + K_{VDC}\Delta V_{DC} + K_{Vc}\Delta c + K_{V\psi}\Delta\psi \tag{B.61}$$

where

$$K_5 = L(V_{do}x_qC_1 - V_{qo}x_d^{'}C_6),$$

$$K_6 = LV_{qo}(1 - x_d^{'}C_5), \qquad K_{V\psi} = L(V_{do}x_qC_2 - V_{qo}x_d^{'}C_7)$$

$$K_{Vc} = L(V_{do}x_qC_3 - V_{qo}x_d^{'}C_8), \qquad K_{VDC} = L(V_{do}x_qC_4 - V_{qo}x_d^{'}C_9)$$

Substituting all values in the linearized model given by equations (B.44) to (B.48)

$$\dot{\Delta\delta} = \omega_b\Delta\omega \tag{B.62}$$

$$\begin{aligned}\dot{\Delta\omega} &= -\frac{1}{M}[\{K_1\Delta\delta + K_2\Delta_{eq'} + K_{pDC}\Delta V_{DC} + K_{pc}\Delta c + K_{p\psi}\Delta\psi\} + D\Delta\omega] \\ &= -\frac{K_1}{M}\Delta\delta - \frac{K_2}{M}\Delta_eq^{'} - \frac{K_{pDC}}{M}\Delta V_{DC} - \frac{K_{pc}}{M}\Delta c - \frac{K_{p\psi}}{M}\Delta\psi - \frac{D}{M}\Delta\omega \\ &= -\frac{K_1}{M}\Delta\delta - \frac{D}{M}\Delta\omega - \frac{K_2}{M}\Delta_eq^{'} - \frac{K_{pDC}}{M}\Delta V_{DC} - \frac{K_{pc}}{M}\Delta c - \frac{K_{p\psi}}{M}\Delta\psi \end{aligned} \tag{B.63}$$

$$\Delta \dot{eq'} = \frac{1}{T_{do'}}(-\Delta eq + \Delta E_{fd}) \tag{B.64}$$

$$\begin{aligned}
\Delta \dot{eq'} &= \frac{1}{T_{do'}}[-(K_3 \Delta eq^{'} + K_4 \Delta\delta + K_{q\psi}\Delta\psi + K_{qc}\Delta c + K_{qDC}\Delta V_{DC}) + \Delta E_{fd}] \\
&= -\frac{K_4}{T_{do'}}\Delta\delta - \frac{K_3}{T_{do'}}\Delta eq^{'} + \frac{1}{T_{do'}}\Delta E_{fd} - \frac{K_{qDC}}{T_{do'}}\Delta V_{DC} - \frac{k_{qc}}{T_{do'}}\Delta c \\
&\quad -\frac{k_{q\psi}}{T_{do'}}\Delta\psi
\end{aligned} \tag{B.65}$$

$$\Delta E_{fd} = -\frac{1}{T_A}\Delta E_{fd} - \frac{K_A}{T_A}\Delta V_t \tag{B.66}$$

$$\begin{aligned}
&= -\frac{1}{T_A}\Delta E_{fd} - \frac{K_A}{T_A} \\
&\quad [K_5\Delta\delta + K_6\Delta eq^{'} + K_{VDC}\Delta V_{DC} + k_{Vc}\Delta c + K_{v\psi}\Delta\psi]
\end{aligned} \tag{B.67}$$

$$\begin{aligned}
&= -\frac{K_A k_5}{T_A}\Delta\delta - \frac{K_A K_6}{T_A}\Delta eq^{'} - \frac{1}{T_A}\Delta E_{fd} - \frac{K_A k_{VDC}}{T_A}\Delta V_{DC} \\
&\quad -\frac{K_{Vc}K_A}{T_A}\Delta c - \frac{K_{V\psi}K_A}{T_A}\Delta\psi
\end{aligned} \tag{B.68}$$

In Matrix form

$$\begin{bmatrix} \dot{\Delta\delta} \\ \dot{\Delta\omega} \\ \dot{\Delta eq'} \\ \Delta\dot{E}_{fd} \end{bmatrix} = \begin{bmatrix} 0 & \omega_b & 0 & 0 \\ -K_1/M & -D/M & -K_2/M & 0 \\ -K_4/T_{do'} & 0 & -K_3/T_{do'} & 1/T_{do'} \\ -k_AK_5/T_A & 0 & -K_AK_6/T_A & -1/T_A \end{bmatrix} \begin{bmatrix} \Delta\delta \\ \Delta\omega \\ \Delta eq' \\ \Delta E_{fd} \end{bmatrix} +$$

$$\begin{bmatrix} 0 \\ -K_{pDC}/M \\ -K_{qDC}/T_{do'} \\ -K_AK_{VDC}/T_A \end{bmatrix} \Delta V_{DC} +$$

$$\begin{bmatrix} 0 & 0 \\ -K_{pc}/M & -K_{p\psi}/M \\ -K_{qc}/T_{do'} & -K_{q\psi}/T_{do'} \\ -K_AK_{Vc}/T_A & -K_AK_{V\psi}/T_A \end{bmatrix} \begin{bmatrix} \Delta c \\ \Delta\psi \end{bmatrix} \tag{B.69}$$

Now,

$$\bar{I_{Lo}} = \frac{\bar{V_L} - \bar{V_0}}{jX_{SDT}} \tag{B.70}$$

$$\bar{I_{Lo}} = \frac{\bar{V_t} - jX_{tL}\bar{I_{tL}} - V_0}{jX_{SDT}} \tag{B.71}$$

Substituting values of $\bar{I_{Lo}}$, $\bar{V_t}$, $\bar{I_{tL}}$, $\bar{V_0}$

$$I_{lod} + j\overline{I}_{loq} = \frac{1}{jX_{SDT}}[X_q I_{tLq} + j(eq' - X_d' I_{tLd}) - jX_{tL}(I_{tLd} + jI_{tLq}) - cV_{DC}(cos\psi + jsin\psi)] \quad (B.72)$$

$$I_{lod} + j\overline{I}_{loq} = \frac{1}{jX_{SDT}}[x_q I_{tLq} + j(eq' - x_d' I_{tLd}) - jX_{tL}I_{tLd} + X_{tL}I_{tLq} - cV_{DC}cos\psi - jcV_{DC}sin\psi] \quad (B.73)$$

$$I_{lod} + j\overline{I}_{loq} = \frac{1}{jX_{SDT}}[\{(x_q + X_{tL})I_{tLq} - cV_{DC}\ cos\psi\} + j\{eq' - (x_d' + X_{tL})I_{tLq} - cV_{DC}\ sin\psi\}] \quad (B.74)$$

$$I_{lod} + j\overline{I}_{loq} = \frac{eq' - (x_d' + X_{tL})I_{tLq} - cV_{DC}sin\psi}{X_{SDT}} + j\frac{\{cV_{DC}\ cos\psi - (x_d' + X_{tL})I_{tLq}\}}{X_{SDT}} \quad (B.75)$$

Comparing real & Imaginary Parts

$$\overline{I}_{lod} = \frac{eq'}{X_{SDT}} - \frac{(x_d' + X_{tL})I_{tLq}}{X_{SDT}} - \frac{cV_{DC}\ sin\psi}{X_{SDT}} \quad (B.76)$$

$$\overline{I}_{loq} = \frac{cV_{DC}\ cos\psi}{X_{SDT}} - \frac{(x_q' + x_{tL})I_{tLq}}{X_{SDT}} \quad (B.77)$$

linearizing equation B.76 and B.77

$$\Delta\overline{I}_{lod} = \frac{1}{x_{SDT}}\Delta eq' - \frac{(x_d' + X_{tL})}{X_{SDT}}\Delta I_{tLd} - \frac{c_o V_{DCo}}{X_{SDT}}\cos\psi_o\Delta\psi - \frac{c_o\sin\psi_o}{X_{SDT}}\Delta V_{DC} - \frac{V_{DCo}\sin\psi_o}{X_{SDT}}\Delta c \quad (B.78)$$

$$\Delta\overline{I}_{lod} = \frac{1}{X_{SDT}}\Delta eq' - \frac{(x_d' + X_{tL})}{X_{SDT}}\{C_5\Delta eq' + C_6\Delta\delta + C_7\Delta\psi + C_8\Delta c + C_9\Delta V_{\Delta V_{DC}}\} - \frac{c_o V_{DCo}}{X_{SDT}}\cos\psi_o\Delta\psi - \frac{c_o\sin\psi_o}{X_{SDT}}\Delta V_{DC} - \frac{V_{DCo}\sin\psi_o}{X_{SDT}}\Delta c \quad (B.79)$$

$$\Delta\overline{I}_{lod} = \frac{1}{x_{SDT}}\{1 - (x_d' + X_{tL})C_5\}\Delta eq' - \frac{(x_d' + X_{tL})}{x_{SDT}}C_6\Delta\delta - \frac{(x_d' + X_{tL})}{X_{SDT}}C_7\Delta\psi - \frac{(x_d' + X_{tL})}{X_{SDT}}C_8\Delta c - \frac{(x_d' + X_{tL})}{X_{SDT}}C_9\Delta V_{DC} - \frac{c_o V_{DCo}\cos\psi_o}{X_{SDT}}\Delta\psi - \frac{c_o\sin\psi_o}{X_{SDT}}\Delta V_{DC} - \frac{V_{DCo}\sin\psi_o}{X_{SDT}}\Delta c \quad (B.80)$$

Let

$\frac{x'_d + X_{tL}}{X_{SDT}} = E$ and $\frac{sin\psi_o}{X_{SDT}} = G$

$$\begin{aligned}\Delta \bar{I}_{lod} &= \frac{1}{X_{SDT}}\{1-(x'_d + X_{tL}C_5)\}\Delta eq' - EC_6\Delta\delta - EC_7\Delta\psi - EC_8\Delta c \\ &\quad -EC_9\Delta V_{DC} - \frac{c_o V_{DCo} cos\psi_o}{X_{SDT}}\Delta\psi - Gc_o\Delta V_{DC} - GV_{DCo}\Delta c \qquad \text{(B.81)}\\ \Delta \bar{I}_{lod} &= C_{10}\Delta eq' + C_{11}\Delta\delta + C_{12}\Delta\psi + C_{13}\Delta c + C_{14}\Delta V_{DC} \qquad \text{(B.82)}\end{aligned}$$

where $C_{10} = \frac{1}{X_{SDT}}\{1-(x'_d + X_{tL}C_5)\}$, $C_{11} = -EC_6$

$C_{12} = -\{EC_7 + \frac{c_o V_{DCo} Cos\psi_o}{X_{SDT}}\}$, $C_{13} = -\{EC_8 + GV_{DCo}\}$

$C_{14} = -\{EC_9 + Gc_o\}$

Similarly

$$\begin{aligned}\Delta \bar{I}_{loq} &= -\frac{c_o V_{DCo}\sin\psi_o}{X_{SDT}}\Delta\psi + \frac{c_o\cos\psi_o}{X_{SDT}}\Delta V_{DC} + \frac{V_{DCo}\cos\psi}{X_{SDT}}\Delta c \\ &\quad -\frac{(x_q + x_{tL})}{X_{SDT}}\Delta I_{tLq} \qquad \text{(B.83)}\\ \Delta \bar{I}_{loq} &= -\frac{c_o V_{DCo}\sin\psi_o}{X_{SDT}}\Delta\psi + \frac{c_o\cos\psi_o}{X_{SDT}}\Delta V_{DC} + \frac{V_{DCo}\cos\psi}{X_{SDT}}\Delta c - \\ &\quad \frac{(x_q + X_{tL})}{X_{SDT}}\{C_1\Delta\delta + C_2\Delta\psi + C_3\Delta c + C_4\Delta V_{DC}\} \qquad \text{(B.84)}\\ \Delta \bar{I}_{loq} &= -\frac{(x_q + X_{tL})}{X_{SDT}}C_1\Delta\delta - \{c_o V_{DCo} G + (\frac{x_q + X_{tL}}{X_{SDT}})C_2\}\Delta\psi + \\ &\quad \left\{\frac{c_o\cos\psi_o}{X_{SDT}} - (\frac{x_q + X_{tL}}{x_{SDT}})C_4\right\}\Delta V_{DC} + \\ &\quad \left\{\frac{V_{DCo}\cos\psi_o}{X_{SDT}} + (\frac{x_q + X_{tL}}{X_{SDT}})C_3\right\}\Delta c \qquad \text{(B.85)}\end{aligned}$$

Let

$$\left(\frac{x_q + x_{tL}}{X_{SDT}}\right) = W$$

$$\begin{aligned}\Delta\bar{I}_{loq} &= -WC_1\Delta\delta - \{c_oV_{DCo}G + WC_2\}\Delta\psi + \{\frac{c_ocos\psi_o}{X_{SDT}} - WC_4\}\Delta V_{DC} + \\ &\{\frac{V_{DCo}cos\psi_o}{X_{SDT}} - WC_3\}\Delta c \qquad (B.86)\\ \Delta\bar{I}_{loq} &= C_{15}\Delta\delta + C_{16}\Delta\psi + C_{17}\Delta V_{DC} + C_{18}\Delta c \qquad (B.87)\end{aligned}$$

where $C_{15} = -WC_1$, $C_{16} = -\{c_oV_{DCo}G + WC_2\}$
$C_{17} = \left\{\frac{c_ocos\psi_o}{X_{SDT}} - WC_4\right\}$, $C_{18} = \left\{\frac{V_{DCo}cos\psi_o}{X_{SDT}} - WC_3\right\}$
Now since the expression for $\dot{V_{DC}}$ is given as

$$\dot{V_{DC}} = \frac{c}{C_{DC}}(I_{lod}cos\psi + I_{loq}sin\psi) \qquad (B.88)$$

linearizing with $\frac{1}{C_{DC}} = N$

$$\begin{aligned}\Delta\dot{V_{DC}} &= N[(I_{lod_o}\ cos\psi_o + I_{loq_o}\ sin\psi_0)\Delta c + c_o(-I_{lod_o}\ sin\psi_o + I_{loq_o}\ cos\psi_o)\Delta\psi + \\ &c_o\ (cos\psi_o\Delta I_{lod} + sin\psi_o\Delta I_{lod})] \qquad (B.89)\end{aligned}$$

Substituting the value of ΔI_{lod} and ΔI_{loq}

$$\begin{aligned}\Delta\dot{V_{DC}} &= N[(I_{lod_o}cos\psi_o + I_{loq_o}sino)\Delta c + c_o(-I_{lod_o}sin\psi_o + I_{loq_o}cos\psi_o)\Delta\psi + \\ &c_o\{cos\psi_o(C_{10}\Delta eq' + C_{11}\Delta\delta + C_{12}\Delta\psi + C_{13}\Delta c + C_{14}\Delta V_{DC}) + \\ &sin\psi_o(C_{15}\Delta\delta + C_{16}\Delta\psi + C_{17}\Delta V_{DC} + C_{18}\Delta c)\}] \qquad (B.90)\\ \Delta\dot{V_{DC}} &= Nc_o(cos\psi_oC_{11} + sin\psi_oC_{15})\Delta\delta + (NC_oCos\psi_oC_{10})\Delta eq' + \\ &Nc_o(cos\psi_oC_{14} + Sin\psi_oC_{17})\Delta V_{DC} + N(I_{lod_o}Cos\psi_o + \\ &I_{loq_o}Sin\psi_o + c_ocos\psi_oC_{13} + c_0sin\psi_oC_{18})\Delta c + \\ &Nc_o(-I_{lod_o}sin\psi_o + I_{loq_o}cos\psi_o + cos\psi_oC_{12} + sin\psi_oC_{16})\Delta\psi \qquad (B.91)\\ \Delta\dot{V_{DC}} &= K_7\Delta\delta + K_8\Delta eq' + k_9\Delta V_{DC} + K_{DC}\Delta c + K_{d\psi}\Delta\psi \qquad (B.92)\end{aligned}$$

where

$K_7 = Nc_o(\cos\psi_o C_{11} + \sin\psi_o C_{15})$

$K_8 = Nc_o \cos\psi_o C_{10}$

$K_9 = Nc_o(\cos\psi_o C_{14} + \sin\psi_o C_{17})$

$K_{DC} = N(I_{lod_o}\cos\psi_o + I_{loq_o}\sin\psi_o + c_o\cos\psi_o C_{13} + c_o\sin\psi_o C_{18})$

$k_{d\psi} = Nc_o(-I_{lod_o}\sin\psi_o + I_{loq_o}\cos\psi_o + \cos\psi_o C_{12} + \sin\psi_o C_{16})$

In Matrix form

$$\begin{bmatrix} \dot{\Delta\delta} \\ \dot{\Delta\omega} \\ \Delta\dot{eq'} \\ \Delta\dot{E}_{fd} \\ \Delta\dot{V}_{DC} \end{bmatrix} = \begin{bmatrix} 0 & \omega_b & 0 & 0 & 0 \\ -K_1/M & -D/M & -K_2/M & 0 & -K_{pDC}/M \\ -K_4/T_{do'} & 0 & -K_3/T_{do'} & 1/T_{do'} & -K_{qDC}/T_{do'} \\ -K_AK_5/T_A & 0 & -K_AK_6/T_A & -1/T_A & -K_AK_{VDC}/T_A \\ K_7 & 0 & K_8 0 & K_9 & 0 \end{bmatrix} \begin{bmatrix} \Delta\delta \\ \Delta\omega \\ \Delta eq' \\ \Delta E_{fd} \\ \Delta V_{DC} \end{bmatrix} +$$

$$\begin{bmatrix} 0 & 0 \\ -K_{pc}/M & -K_{p\psi}/M \\ -K_{qc}/T_{do'} & -K_{q\psi}/T_{do'} \\ -K_AK_{Vc}/T_A & -K_AK_{V\psi}/T_A \\ K_{DC} & K_{d\psi} \end{bmatrix} \begin{bmatrix} \Delta c \\ \Delta\psi \end{bmatrix} \tag{B.93}$$

Appendix C

STATCOM and Controller Data

- Parameters for the approximate model (in p.u. except indicated)

  $H = 3s.$, $D = 4.0$, $K = 1.0$, $x_1 = 0.3$, $x_2 = 0.3$, $x_d' = 0.3$, $x_d = 1.0$, $T = 0.02$, $I_{so} = 0$.

- Parameters for the Detailed model (in p.u. except indicated)

  $H = 3s.$, $T_{do}' = 6.3$, $x_d = 1.0$,$x_d' = 0.3$, $x_q = 0.6$. $D = 4.0$, $x_{TL} = 0.3$, $x_{LB} = 0.3$, $x_{SDT} = 0.15$, $K_A = 10.0$,$T_A = 0.01s.$, $T_C = 0.05s.$, $C_{DC} = 1.0$, $c_o = 0.25$, $\psi_o = 46.52°$

- Nominal Plant Operating condition :

  $P_{eo} = 0.9$,$V_{to} = 1.0$,p.f. $= 1.0$

Bibliography

[1] Laszlo Gyugyi. Converter based facts controller. *IEE colloquim on FACTS*, pages 1–11, November 23 1998.

[2] N.G. Hingorani. Power electronics in electrical utilitie: Role of power electronics in future power system. *Proceedings of IEEE*, 76(4):481–482, April 1988.

[3] N.G. Hingorani. Facts-flexible ac transmission system. *Fifth IEE Int. conference on AC and Dc transmission*, (IEE Pub. No. 345):1–7, September 1991.

[4] N.G. Hingorani. Flexible ac transmission systems. *IEEE Spectrum*, (40-45), April 1993.

[5] N.G. Hingorani. Facts technology and opportunities. *IEEE Colloquium, " FACTS the key to increased utilization of the power system"*, June 12, 1994.

[6] Laszlo Gyugi. Dynamic cpmensation of ac transmission line by soild state synchronous voltage sources. *IEEE transaction on power deilvery*, 9(2):904–911, April 1994.

[7] D.R. Trainber, Tenakoon S.B., and R.E. Morrison. Analysis of gto based statci var compensators. *IEEE Proceedings -Elecrtical Power Application*, 141(6):293–302, Nov. 1994.

[8] C. W. Edwards, P. R. Nannery, and K. E. Mattern. Advanced static var generator employing gto thyristors. *IEEE Transactions on power delivery*, 11(1):1622–1627, October 1988.

[9] J.B. Ekanayake and N. Jenkins. A three level advanced static var compensator. *IEEE transaction on power delivery*, 11(1):540–545, Jan 1996.

[10] R. W. Menzies and Y. Zhuang. Advanced static compensation using multilevel gto inverter. *IEEE transaction on power delivery*, 9(4):732–737, April 1995.

[11] C. Schauder and H. Mehta. Vector analysis and control of advanced static var compensators. *IEE proceedings on generation, transmission and distribution*, 140(4):299–306, July 1993.

[12] K.R.Padiyar and A.M. Kulkarni. Analysis and design of voltage control of static condenser. *IEEE Conf. On power electronics, derives and energy system for industrial growth*, 1:393–398, 1996.

[13] P. Petitclair, S. Bacha, and J. Prognon. Averaged modelling and nonlinear control of an asvc (advanced static var compensator). *IEEE power electronics specialist conference*, 1:753–758, 1996.

[14] Z. Yao, P. Kesimar, Nicolas Lechevin, and V. Rajagopalan. Nonlinear control for statcom based on differential algebra. *IEEE power electronics specialist conference,*, 1:323–334, 1998.

[15] Y. Ni and S. Chen. Application of a nonlinear pid controller on statcom with a differential tracker. *IEEE power energy management and power delivery conference*, 1:29–34, 1998.

[16] Chun Li, Qirong Jiang, Z. Wang, and D. Retzmann. Design of rule-based controller for statcom. " *IEEE industrial electronics society conference*, 1:467–472, 1998.

[17] Yu David C. and Liu Haijun. Simulation of the static condenser for the prevention of transient voltage instability due to induction motor load. *Proceedings of the American Power Conference*, 59(2):1076–1081, 1997.

[18] P.W. Lehn and M.R. Iravani. Experimental evaluation of statcom closed loop dynamics. *IEEE transaction on power delivery*, 13(4):1378–1384, Oct. 1998.

[19] In gyu Park, J. T. Yoon, and I.S. Kim. Thyrister controlled static condenser with new double firing phase control. *IEEE Industry Applications society conference*, 2:999–1006, 1996.

[20] M. Moaddes, A.M. Gole, and P.G. McLaren. Neural network controlled optimal pwm statcom. *IEEE Transaction on power delivery*, 14(2):481– 488., April 1999.

[21] Yixin Ni and L.O. Mak. Fuzzy login damping controller for facts devices in interconnected power systems. *Proceedings of IEEE Intl. Symposium on circuits and systems*, 5:591–594, 1999.

[22] M.Parnaini and M.R. Iravani. Optimal robust control desgin of static var compensators. *IEE Proc. Gener. Transm. Distrib*, 145(3):301–306, May 1998.

[23] Sami Ammari, Yvon Besanger, Nourdine Hadjsaid, and Didier Georges. Robust solutions for the interaction phenomena between dynamic loads and facts controllers. *IEEE Power Engineering society summer meeting*, 1:401–406, July 2000.

[24] M.M. Farsangi, Y.H.Song, and Y.Z.Sun. Supplementary control design of svc and statcom using h_{infty} optimal robust control. *International conference on Electric Utility Deragulation and Restructring and power technologies*, pages 355–360, April 2000.

[25] H.Chen, R.Zhou, and Y.Wang. Analysis of voltage stability enhancement by robust nonlinear statcom control. *IEEE*, pages 1924–1929, 2000.

[26] B.T. Ooi, M. Kazerani, R. Marceau, and Z. Wolanski. Mid-point sitting of facts devices in transmission lines. *IEEE transaction on power delivery,*, 12(4):1717–1722, Oct. 1997.

[27] R.J. Nelson, J. Bian, and Miklos Sarkozi. Increasing the capability of voltage-limited distribution feeders with distribution static condensers. " *Proceedings of the American Power Conference*, 57(2):1524–1529, 1995.

[28] J.E Hill, C.M. Chileshe, S.M Boardman, and M.P. Westrick. Experimental model of a harmonic neutralized statcon. *Proceedings of the 29th universities power engineering conference*, 1:338–341, 1994.

[29] D. A. Pastos and N.A. Vovos. Influence of the real power modulation provided by the shunt ompensator on damping power swings. *Proceedings of IEEE Intl. Conference on electronics, circuits and systems*, 2:884–887, 1996.

[30] Li Wang and Zon-Yan Tsai. Stabilization of generator oscillations using a pid statcon damping controllers and pid power system stabilizers. *IEEE Engineering society, winter meeting*, 1:616–621, 1999.

[31] J.C. Passelergue, N. Hadjsaid, and Y. Basanger. Low frequency oscillations damping by facts and power system stabilizers. *Proceedings of 32nd universities power engineering conference*, 1:9–12, 1997.

[32] Li Wang and Zon-Yan Tsai. Dynamic stability enhancement of nuclear plants of taiwan power systems using statcon. *IEEE Engineering society, winter meeting*, 1:604–609, 1999.

[33] K.V. Patil, J. Senthil, J. Jiang, and R.M. Mathur. Application of stactom for damping torsional oscillations in series compensated ac systems. *IEEE Transaction on Energy Conversion*, 3:237–243, Sep. 1998.

[34] Z. Saad-Saoud, M. L. Libosa, J. B. Ekanayake, and N. Jenkins. Application of statcoms to wind farms. *IEE Proceedings on Generation, transmission and Distribution*, 145(5):511–518, Sep. 1998.

[35] Narain G. Hingorani and Laszlo Gyugyi. *Understanding FACTS Concepts and Technology of Flexible AC Transmission Systems.* IEEE Press, 2000.

[36] Einar V. Larsen, Juan J. Sanchez-Gasca, and Joe H. Chow. Concepts for design of facts controllers to damp powerr swings. *IEEE Trans. Power Systems*, 10(2):948–955, 1995.

[37] H.F.Wang. Phillips-heffron model of power systems installed with statcom and applicatons. *IEE Proc.-Geer, Transm. Distrib.,*, 146(5):521–527, 1999.

[38] www.engin.umich.edu/group/ctm/PID/PID.html. Control tutorials for matlab. Technical report, college of Engineering, university of Michigan, 2001.

[39] M.F. Kandlawala and A.H.M.A Rahim. Power system dynamic performance with statcom controller. *8th Annual IEEE technical exchange meeting*, April 2001.

[40] J. C. Doyle, B. A. Francis, and A. R. Tannenbaum. *Feedback Control Theory.* Macmillan Publishing Co., 1992.

[41] Neil M. Cumbria. Robust controlled flux estimation for indirect field oriented control induction motor drives. Master's thesis, University of Calgary, Alberta Canada, April 1998.

[42] M. Green and D. J. N. Limebeer. *Linear Robust Control.* Prentice Hall, 1995.

[43] A.H.M.A.Rahim, S.A.Al-Baiyat, and F.M. Kandlawala. A robust controller for power system dnamic performance enhancement. *2001 IEEE Power Engineering Society Summer Meeting, Vancouver, Canada*, July 2001.

Vita

- Muhammad Fareed Kandlawala.
- Born in Karachi, Pakistan on January 12, 1972.
- Received Bachelor of Engineering (B.E) degree in Electrical Engineering from N.E.D University of Engineering and Technology, Karachi, Pakistan in 1997.
- Joined King Fahd University of Petroleum and Minerals in January 1998.
- Email: mfareed@kfupm.edu.sa

Publications

- M. F. Kandlawala, and A. H. M. A. Rahim , Power System Dynamic Performance with STATCOM Controller, Proceedings of 8th IEEE Technical exchange meeting, KFUPM, Dhahran, Saudi Arabia, April 16-17, 2001.
- A. H. M. A. Rahim and M. F. Kandlawala, A robust STATCOM controller for power system dynamic performance enhancement, 2001 IEEE Power system Engineering society summer meeting, Vancouver, Canada, July 2001.
- A. H. M. A. Rahim and M. F. Kandlawala, Robust Design of a Power System STATCOM Controller using Loop-Shaping Technique. Accepted to appear in Saudi Engineering society conference, June 2002.